

**STUDIES ON THE UNIVERSAL PARAMETERS
AND
ONSET OF CHAOS IN DISSIPATIVE SYSTEMS**

G. AMBIKA

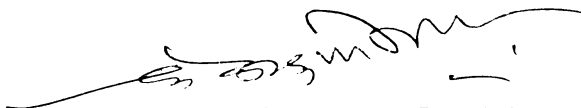
**THESIS SUBMITTED IN
PARTIAL FULFILMENT OF THE REQUIREMENTS
FOR THE DEGREE OF
DOCTOR OF PHILOSOPHY**

**DEPARTMENT OF PHYSICS
Cochin University of Science and Technology
COCHIN - 682 022**

1988

C E R T I F I C A T E

Certified that the work reported in the present thesis is based on the bonafide work done by Ms. G Ambika under my guidance in the Department of Physics, Cochin University of Science and Technology and has not been included in any other thesis submitted previously for the award of any degree.

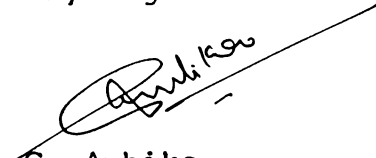


K Babu Joséph
(Supervising Teacher)
Professor and Head of
the Department of
Physics
Cochin University of
Science and Technology
Cochin-682 022

D E C L A R A T I O N

Certified that the work presented in this thesis is based on the original work done by me under the guidance of Dr K Babu Joseph, Prof. and Head of the Department of Physics, Cochin University of Science and Technology and has not been included in any other thesis submitted previously for the award of any degree.

Cochin 682 022


G Ambika

29.3.1988.

ACKNOWLEDGEMENTS

I express my sincere thanks to

Dr. K.Babu Joseph, Professor and Head of the Department of Physics, Cochin University of Science and Technology, for his guidance and encouragement throughout the period of this work;

Dr. M.G. Krishna Pillai, former Head of the Department of Physics, for providing all facilities for research in the department of Physics;

Prof. M.K. Prasad, former Principal, Maharaja's College, Cochin for his encouragement and interest in my work;

Dr. V.M. Nandakumaran, Dr. R. Pratap and Dr. C.S. Sreedhar for various informative discussions;

Mr. A.V. Ravikumar, Mr. A.T. Raghunath, Mr. N.K. Narayanan and all the research students of theory group for help and cooperation and Ms. P.R. Rajalakshmi for her excellent typing.

'My life is spent in one long effort to escape from the common places of existence. These little problems help me to do so'.

- Sir Arthur Conan Doyle

C O N T E N T S

	Page No.
Preface	i
Synopsis	iv
1. INTRODUCTION	
1.1 General concepts and definitions	2
1.2 Conservative systems	7
1.3 Dissipative systems	11
1.4 Routes to chaos in dissipative systems	17
1.5 Characterisation of chaos	21
1.6 Relevance of chaos in related fields	35
2. ONE DIMENSIONAL MAPS AND UNIVERSALITY	
2.1 The universality theory	39
2.2 The renormalisation group equations and the calculation of α and δ	46
2.3 Perturbative scheme for evaluation of universal parameters	47
2.4 Universal relations for general z	53
3. UNIVERSAL PARAMETERS FOR ONE-HUMP MAPS	
3.1 The universal constant δ for a quadratic map	61

3.2	Solutions of renormalisation group equations for a cubic map	64
3.3	Universal parameters of a quartic map	71
3.4	Universal constants of nonpolynomial maps	80
3.5	Comments and discussion	88
4.	FRACTAL DIMENSIONS OF THE FEIGENBAUM ATTRACTOR	
4.1	Self-similarity of the Feigenbaum attractor	90
4.2	The capacity dimension D_0	94
4.3	The information dimension D_1	97
4.4	The correlation dimension D_2	104
4.5	Discussion	105
5.	ONSET OF CHAOS IN DISSIPATIVE SYSTEMS	
5.1	The Melnikov-Holmes method	110
5.2	Transition to chaos in a driven pendulum with nonlinear dissipation	118
5.3	Numerical Analysis	123
5.4	Effects of external noise	145
	REFERENCES	153

PREFACE

This is a report of the investigations carried out on the universal parameters associated with the transition to chaos in nonlinear dissipative systems. It essentially deals with an analytic perturbative procedure developed to solve the renormalisation group equations and its application to specific one-hump maps. The universal function obtained is used to compute the fractal dimensions of the Feigenbaum attractor. The Melnikov-Holmes method of predicting the onset of chaos is applied to a driven pendulum with nonlinear damping followed by a detailed numerical analysis.

Chapter 1 gives an introduction to deterministic chaos, surveying briefly the nature of onset of chaos in conservative and dissipative systems. The different routes to chaos in dynamical systems along with the existing methods of characterising them are touched upon. The Chapter ends with an attempt to reveal the relevance of chaos in related fields.

In Chapter 2, the universality theory as developed by Feigenbaum in the context of one-dimensional maps

is presented, with special emphasis on the two renormalisation group equations involving the universal parameters α and δ and the function $g(x)$. The solution of these equations using the perturbative scheme is developed. A universal relation characterising any 1-d map for a specified z is derived.

The perturbative procedure is applied to specific cases in Chapter 3. Thus the α and δ values as well as the function $g(x)$ for quadratic, cubic and quartic maps are computed analytically. For nonpolynomial maps, an expansion about the nearest integer value is also discussed.

Chapter 4 begins with a brief discussion of the self-similar property of the Feigenbaum attractor at the accumulation point of the bifurcations. The iterates of $g(x)$ form a Cantor set. Here the function $g(x)$ is obtained using the perturbative analysis and expressions for the first three dimensions D_0, D_1 and D_2 are derived. These are computed for a range of z values and the variation of these dimensions with z is studied.

The last Chapter forms a separate section of the thesis. It deals with the onset of chaos in

near-integrable systems. The Melnikov-Holmes criterion which forms the lowest threshold for chaos is described. It is then applied to a specific system, namely, a driven pendulum with a small nonlinear x -dependent dissipation. The dissipation is chosen to be of the van der Pol type. This analytic treatment is supported by a detailed numerical analysis involving phase portraits, Poincaré sections, Lyapunov exponent, power spectra etc. The last section deals with the effect of an external random noise on the dynamical behaviour of the above system.

Part of the investigations presented in this thesis has provided material for the following papers.

1. 'Perturbative evaluation of universal constants for a quartic map' - Pramana (J. Phys.) 26 (1986) 465.
2. 'Calculation of universal parameters of one hump maps' - Communicated to Physica D.
3. 'Transition to chaos in a driven pendulum with nonlinear dissipation' - Communicated to Pramana (J. Phys.)

SYNOPSIS

The thesis work is mainly centered on the asymptotic behaviour of nonlinear and nonintegrable dissipative dynamical systems. It is found that completely deterministic nonlinear differential equations describing such systems can exhibit random or chaotic behaviour. Theoretical studies on this chaotic behaviour can enhance our understanding of various phenomena such as turbulence, nonlinear electronic circuits, erratic behaviour of heart and brain, fundamental molecular reactions involving DNA, meteorological phenomena, fluctuations in the cost of materials and so on.

Chaos is studied mainly under two different approaches - the nature of the onset of chaos and the statistical description of the chaotic state. Successive period doubling bifurcations constitute one of the most common mechanisms for the onset of chaos in many systems representing a wide variety of physical phenomena. Irrespective of the differences

in the underlying physics, such systems are found to have some common behaviour as far as onset of chaos is considered. This universal behaviour was reported by M. J. Feigenbaum in the case of one dimensional maps that represent the Poincaré sections of higher dimensional flows [26]. He found that the period doubling route to chaos is characterised by two universal constants, the bifurcation rate δ and the scaling factor α . The computation of α and δ for any map is usually done numerically [51].

We have developed an analytic algorithm involving a perturbative scheme, which provides fairly accurate values for α and δ . This is given in the first section of the thesis. We consider maps of the form $x_{n+1} = 1 - \lambda |x_n|^z$, where z is the order of the local maximum of the map. The universality theory is based on two renormalisation group (RG) equations for the fixed point function $g(x)$ at the accumulation point λ_∞ of the period-doubling bifurcations [49]. Expanding $g(x)$ into a general power series in $|x|^z$ and substituting in one of the RG equations, an infinite set of coupled nonlinear

equations for the coefficients of expansion S_n are obtained. To solve them, S_n are expanded into a perturbative series in inverse powers of α . The equations can then be successively solved for the coefficients S_{nm} . Thus α as well as $g(x)$ can be expressed explicitly in terms of S_{nm} and therefore computed analytically. Using the other RG equation, δ can be computed in a similar way. We find that the equations for δ can be cast in the form of a matrix eigenvalue equation and the highest positive and real eigenvalue furnishes δ .

In general for any z value, the first three coefficients S_{nm} can be written down explicitly. Using them and using the technique of Padé approximants to sum the series, we get $\alpha(z)$ and $\delta(z)$ for any z value. These equations define the different universality classes and a universal relation connecting α , δ and z is also derived.

For a given z , it is possible to carry out the calculations to any order of accuracy. Thus for a quartic map and a cubic map, we computed α and δ to different orders and found that the agreement with the numerical values is excellent. However, the perturbation series is not highly convergent but

asymptotic in nature and therefore the truncation of the series is crucial in giving good results.

When z is not an integer, the above method is rather cumbersome to apply. In such cases we find that the general method can be side stepped and the expressions for α and δ can be expanded in ϵ , where $0 < |\epsilon| < 1$. Any noninteger z value can be written as $z = z' \pm \epsilon$, where z' is the integer nearest to z . Then the ϵ -expansions can be used to compute α and δ . We observe that this expansion procedure does not affect the accuracy of the values much. Using the iterates of the computed universal function and some scaling arguments, we have derived expressions for the important dimensions characterising the attractor at λ_∞ in one dimensional maps [31]. The agreement with available numerical values is good. The behaviour of D_0 and D_1 with z is different for large z values. $D_1(z)$ shows a dip as z increases while $D_0(z)$ shows saturation.

The second section of the thesis deals with investigations on the onset of stochastic behaviour in a driven pendulum with van der Pol like dissipation. Such a system with some modifications can model nonlinear

electronic circuits, Josephson junction with interference of tunnelling currents, and laser systems. Predicting the exact transition point where chaos sets in, in such systems is still a challenging problem. Till now, the only analytic method available for this has been the Melnikov criterion [4]. The Melnikov analysis gives the distance between the stable and unstable manifolds of the perturbed system based on calculations involving trajectories of the unperturbed system. We have derived this function for the above system, followed by a detailed numerical analysis including phase portraits, Poincaré sections and power spectra.

The system we considered has essentially three control parameters, the damping constant β , the driving amplitude A and the driving frequency ω . In our numerical computations, we mostly kept β at 0.2. Then the behaviour of the system as A is varied was studied at three different frequencies. We found the following interesting results.

i) At very low frequencies ie $\omega = 0.04$, the transition to chaos is quite obvious. Just as the Melnikov criterion is crossed, the invariant curve in phase space loses its smoothness. As A is increased, it develops distortions and twists and finally reaches the strange attractor.

- ii) At medium frequencies, $\omega = 0.4$, we found that as A increases, the limit cycle develops a stochastic band of increasing thickness.
- iii) At frequencies $\omega \approx 1$, the behaviour is qualitatively similar. However as A increases, the stochastic band splits again into periodic trajectories.
- iv) Because of the nature of the dissipation, the centre $(0,0)$ of the perturbed system is no longer stable. Numerical studies reveal that the centre becomes unstable through a bifurcation and for sufficient perturbations, orbits near $(0,0)$ spiral away to the limit cycle.

The effect of an additive white noise in the above system is interesting from a practical point of view [86]. We made a numerical analysis of the influence of noise especially near the transition point. We find that for low noise amplitudes, the presence of noise smooths out the stochasticity to some extent although the approach to chaos is accelerated by noise.

1. INTRODUCTION

It has become clear over the last few years that many deterministic dynamical systems described by simple but nonlinear equations with only a few variables can behave in an irregular or random fashion. This phenomenon, commonly called deterministic chaos, is essentially due to the fact that we cannot deal with infinitely precise numbers. In these systems trajectories emerging from nearby initial conditions diverge exponentially as time evolves, and therefore, any small error in the initial measurement spreads with time considerably, leading to unpredictable and chaotic behaviour. It is interesting to note that this unpredictability cannot be avoided by just making the observation more precise. If we use a measuring device having an accuracy $\pm \epsilon$, the same device can be used later with the same accuracy, but the equations of motion fail to predict the outcome of the observation with the same degree of accuracy. This accounts for the

apparent stochastic behaviour in deterministic systems. The analysis of the development of chaos has attained considerable sophistication by now and we shall now describe the technical background for the later chapters.

1.1 General concepts and definitions

A dynamical system is a time evolution defined by the system of first order differential equations,

$$\frac{dx}{dt} = f(x) \quad \dots (1.1)$$

where $x = x(t) \in \mathbb{R}^n$, is a vector valued function and $f : U \rightarrow \mathbb{R}^n$ is a smooth function, nonlinear in general [1]. f generates a flow $\varphi_t : U \rightarrow \mathbb{R}^n$, where $U \subseteq \mathbb{R}^n$ and $\varphi_t(x) = \varphi(x,t)$ is a smooth function defined for all x in U and t in some interval $I = (a,b) \subseteq \mathbb{R}$, and φ satisfies (1.1). If f does not contain time explicitly, the system is called autonomous; otherwise it is called non-autonomous.

The continuous time evolution equation (1.1) can be abstracted by a discrete map:

$$x_{n+1} = F(x_n) \quad \dots (1.2)$$

This can be done in one of the following ways.

i) If $x(t)$ is a solution of (1.1), we define

$x_{n+1} = x(n+1)$. Then F is the time-one map associated to the flow defined by f . This is called the stroboscopic method [2].

ii) We approximate $\frac{dx}{dt} = x(t+1) - x(t)$ so that

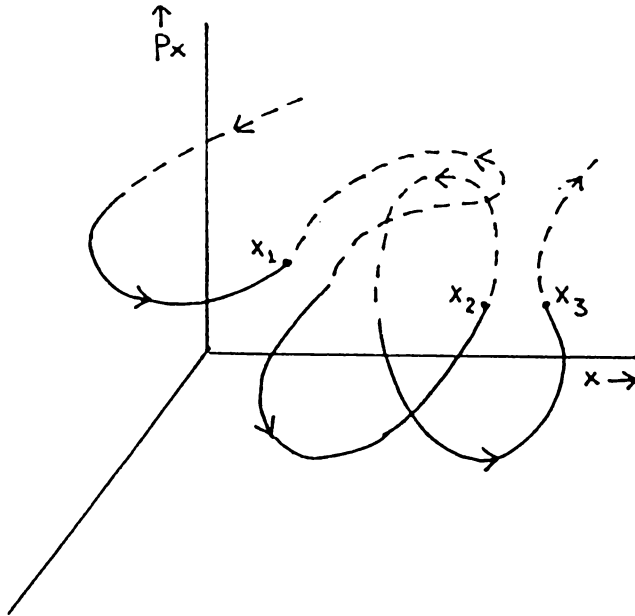
$x_{n+1} = f(x_n) + x_n = F(x_n)$, and this is the difference equation corresponding to (1.1). This method is applicable when the problem is one dimensional.

iii) F may be viewed as the Poincaré map of the flow φ_t , with respect to a chosen surface [3]. Thus

for a 2-dimensional problem, the phase space (q,p) is 4-dimensional and the energy surface is three-dimensional. If we consider the surface S_x with $y = 0$, p_y is determined from the condition

$H(x, y = 0, p_x, p_y) = E$. p_x and x are the variables and the position of the system on S_x completely

specifies the state of the system. The system starting out on S_x will cross it repeatedly at



$x_1, x_2, x_3 \dots$. Each crossing is a map of the plane into itself. Qualitatively different trajectories can be distinguished by their Poincaré sections. Thus a regular periodic orbit gives points lying on a closed curve while a chaotic trajectory yields an irregular set of points.

Fixed points form an important class of solutions of equation (1.2). A period k fixed

point is defined by

$$F^k(x_0) = x_0 \quad \dots \quad (1.3)$$

where $F^k = F(F(F(\dots k \text{ times } (x))) \dots)$. A fixed point x_0 is said to be stable if iterates of points x_n in its neighbourhood remain close to x_0 all the time. If $x_n \rightarrow x_0$ as $n \rightarrow \infty$, x_0 is asymptotically stable and is called a sink. Saddle points or sources are unstable fixed points. To examine the stability of fixed points, we expand x around x_0 :

$$x = x_0 + \Delta x \quad \dots \quad (1.4)$$

so that

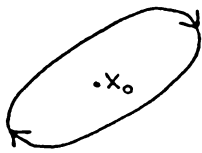
$$\Delta x_{n+k} = A \Delta x_n \quad \dots \quad (1.5)$$

where A is the ordered product of the k matrices $M_i = M(x_{0i})$ evaluated at the successive fixed points with

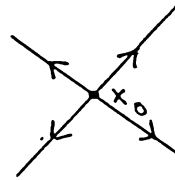
$$M(x) = \frac{\partial x_{n+1}}{\partial x_n} \quad \dots \quad (1.6)$$

If the eigenvalues of A are complex, then the fixed point is elliptic or stable, with trajectories forming ellipses around it. If the eigenvalues

are real, the trajectories are hyperbolae and thus move away from the fixed point. This type is therefore unstable or hyperbolic. If the eigenvalues are unity, the fixed point is parabolic [4].



elliptic fixed point



hyperbolic fixed point

If (1.2) has a hyperbolic fixed point, then there exist local stable and unstable manifolds which are defined as follows [1]:

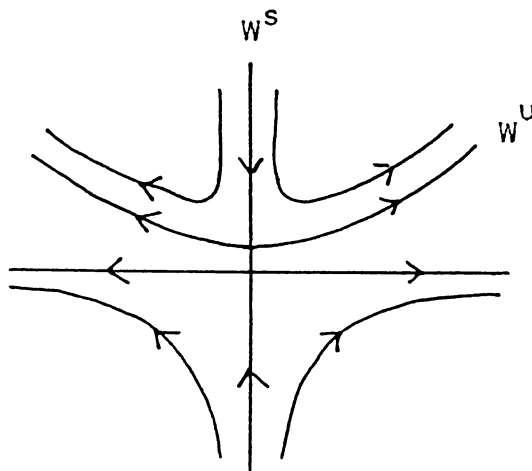
$$W_{loc}^S(x) = \left\{ x \in U \mid F^n(x) \rightarrow x \text{ as } n \rightarrow \infty \right. \\ \left. \text{and } F^n(x) \in U, \forall n \geq 0 \right\} \dots (1.7)$$

$$W_{loc}^U(x) = \left\{ x \in U \mid F^{-n}(x) \rightarrow x \text{ as } n \rightarrow \infty \right. \\ \left. \text{and } F^{-n}(x) \in U, \forall n \geq 0 \right\} \dots (1.8)$$

Here $U \subset \mathbb{R}^n$ is a neighbourhood of x . The global manifolds are obtained by taking unions of backward or forward iterates of the local manifolds:

$$W^s(x) = \bigcup_{n \geq 0} F^{-n}(W_{loc}^s(x)) \quad \dots (1.9)$$

$$W^u(x) = \bigcup_{n \geq 0} F^n(W_{loc}^u(x)) \quad \dots (1.10)$$



The stable and unstable manifolds may intersect at points which are called homoclinic, if they belong to the same hyperbolic fixed point and heteroclinic, if they belong to different fixed points.

1.2 Conservative systems

For a conservative system, Liouville's theorem says that the volume in phase space is conserved

by the time evolution. The equations of motion for a system with N degrees of freedom are obtained from the hamiltonian H as

$$\dot{q}_k = \frac{\partial H}{\partial p_k} : \dot{p}_k = - \frac{\partial H}{\partial q_k}, \quad k = 1, 2, \dots, N \quad \dots(1.11)$$

These equations can be transformed to a set of action and angle variables, by a **canonical transformation** giving

$$\dot{I}_k = - \frac{\partial \mathcal{H}}{\partial \theta_k} : \dot{\theta}_k = \frac{\partial \mathcal{H}}{\partial I_k} \quad \dots(1.12)$$

If the transformed hamiltonian is independent of θ_k , then $I_k(t) = I_k(o)$ and $\theta_k(t) = \omega_k t + \theta_k(o)$ so that we get 2N constants of motion I_k and $\theta_k(o)$. If we can find a transformation that will execute this, the system is called integrable. For nonlinear systems, this is possible by expanding the variables q_k and p_k in power series in I_k and θ_k and substituting into the equations of motion to solve for the coefficients of expansion. This is the subject of canonical perturbation theory. Whenever the series obtained converge, we have an integrable system.

When no such convergent series exist, the system is nonintegrable. The Toda chain [5], the KdV equation (6), the Calogero fluid system (7) etc. are examples of nonlinear integrable systems. An N -degree of freedom integrable system has orbits lying on an N -torus; the actions I_k measure the N radii of the torus and θ_k , the N angles of a point on the torus. When $N \geq 2$, each bounded orbit cannot come arbitrarily close to every point on the $(2N-1)$ energy surface. Hence an integrable system cannot be ergodic.

In a nonintegrable system, the series diverge due to a singularity in one of the integrals I_k [8]. Thus two orbits with initial conditions arbitrarily close to each other, but on either side of such a singularity can have entirely different behaviour. Such a sensitive dependence on initial conditions makes it impossible to calculate the orbit for any time interval of interest, resulting in unpredictability and chaos. As examples of nonintegrable systems, we quote the Henon-Heiles system [9], the motion of protons in the intersecting storage rings [10], the celestial three body problem [11],

wave-particle interaction [12] and Fermi acceleration [13]. If the system is near-integrable, one can write

$$H(I, \theta) = H_0(I) + \epsilon H_1(I, \theta) \quad (1.13)$$

where $|\epsilon| \ll 1$.

The equation of motion for such a system can be expressed through a perturbed area-preserving twist map on the I - θ surface of section [4]. For sufficiently small perturbation and moderate non-linearity, the celebrated KAM theorem [14,15] states that most of the tori of the unperturbed system persist albeit in distorted form. Some are destroyed and these form a finite measure which grows with the perturbation. The destroyed tori generate stochastic regions in the gaps between the KAM tori. The tori corresponding to rational winding number break up into alternate elliptic and hyperbolic fixed points. Near every elliptic fixed point, there are closed invariant curves and a new structure of elliptic and hyperbolic fixed points. It is fascinating to observe that this structure is repeated down to arbitrarily small scales. In the neighbourhood of a hyperbolic

fixed point, the stable and unstable manifolds intersect each other infinitely many times forming a kind of web or complex network. This occurs near every hyperbolic fixed point even to small scales resulting in a selfsimilar 'lace work of intimate intermixing of integrable and stochastic regions' [3].

As the strength of the perturbation increases more and more tori are destroyed with the accompanying growth of stochastic regions and the last torus to disappear is the one for which the winding number is the Golden Mean, $\frac{\sqrt{5}-1}{2}$ [16]. If $N \gg 3$, the gaps between the tori form a single connected region and there can be leakage from one stochastic region to another. This leads to Arnold diffusion [17]. Because of this the existence of invariant tori cannot guarantee stability of motion. The transition to global stochasticity in conservative systems is understood to be through the overlap of resonances [18].

1.3 Dissipative systems

Dissipative systems are those in which the volume of the phase space shrinks to zero as $t \rightarrow \infty$, and

hence are represented by dissipative or area-contracting maps. Thus the long time behaviour of the dissipative system is easier to predict than that of a conservative system. The local rate of change of volume is

$$\Lambda(x) = \ln|\det M(x)| \quad \dots \quad (1.14)$$

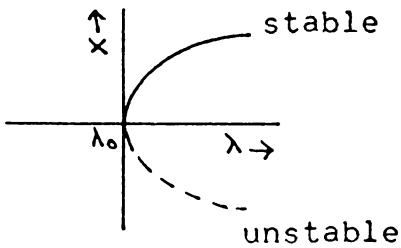
where M is the Jacobian of the discrete map given in (1.2). The average rate of contraction is

$$\Lambda_0(x_0) = \lim_{n \rightarrow \infty} \frac{1}{n} \ln|\det M^n(x)| \quad \dots \quad (1.15)$$

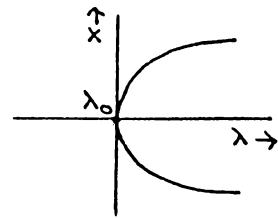
For dissipative systems, there is a contraction of volume so that $\Lambda_0 = -C[4]$.

Since the phase space volume contracts, the steady state motion for an N -dimensional system lies on a surface of lower dimensionality. Such a surface is called an attractor. For one dimensional flows the only possible attractors are fixed points or sinks, while for two dimensional flows, there can be two kinds of attractors, sinks and limit cycles. As the control parameter λ of the system changes, the stable attractor becomes unstable and undergoes bifurcation to pairs of attractors. The creation of two fixed points as $\lambda = \lambda_0$

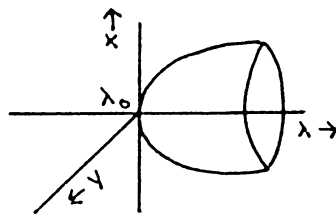
with no fixed points for $\lambda < \lambda_0$ is called a tangent bifurcation. If a fixed point is destroyed and two new sinks are produced, we have a pitch fork bifurcation. In higher dimensional systems, we have a fixed point bifurcating into a limit cycle. This is called a Hopf bifurcation.



tangent bifurcation



pitchfork bifurcation



Hopf bifurcation

When the bifurcation repeats successively and reaches a limit, the attractor changes character and becomes chaotic. On the chaotic attractor, nearby orbits, though bounded, diverge exponentially. This leads to sensitive dependence on initial conditions resulting in random or chaotic behaviour. Such an attractor is called a strange attractor. This has an infinitely leaved structure with the peculiarity that on finer and finer scales the basic pattern reappears. The strange attractor is a complicated manifold in phase space which is defined as an 'infinitely folded sheet of infinite extent located in a bounded region of phase space' [19]. The Hausdorff dimension of such an attractor is a non-integer or fraction.

In Hamiltonian systems, the stochastic region does not occupy the whole of the phase space, but is bordered by regions of regular behaviour. But in dissipative systems in the place of islands of stability, there appear stable limit cycles to which sooner or later all the initial points are attracted. When dissipation is large, a point wanders for infinite time over the stochastic region before reaching

the limit cycle, thus producing foliation characteristic of the strange attractor.

The greatest interest has been in the study of simple models; for example, a continuous map defined by

$$x_{n+1} = f(x_n, \lambda), \quad \dots \quad (1.16)$$

$$\text{with } f = \lambda x_n (1 - x_n), \quad \dots \quad (1.17)$$

is called the logistic map and this turns out to be the most widely studied system [20]. This occurs in the population studies of certain biological species [21].

The investigation of stochasticity by reduction to one dimensional map has been used extensively in the Lorenz system [22] described by,

$$\begin{aligned} \dot{x} &= -\sigma x + \sigma y \\ \dot{y} &= -xz + rx - y \\ \dot{z} &= xy - bz, \quad \dots \quad (1.18) \end{aligned}$$

with $\sigma = 10$, $r > 0$ and $b = 8/3$.

This arises from a three-mode truncation of the

Navier - Stokes equation describing Rayleigh-Bénard convection in hydrodynamics. Here x is the amplitude of the convective motion, y , the temperature difference between ascending and descending currents and z is the distortion of the vertical temperature profile from linearity. σ, r and b are dimensionless real parameters. It is interesting to note that the same system of equations can be obtained for single-mode lasers by truncating the Maxwell-Bloch equations[23]. A reduction to one dimension is possible because the instability of the trajectories occurs in the same direction everywhere. There are systems for which the unstable direction is multidimensional, for example the Rössler system given by [24]

$$\begin{aligned}\dot{x} &= -(y+z) \\ \dot{y} &= x + \frac{1}{5} y \\ \dot{z} &= \frac{1}{5} + z(x-\mu) \quad \dots \quad (1.19)\end{aligned}$$

The Henon-Heiles dissipative map is another example where the existence of the strange attractor as well as its self-similar structure has been proved conclusively by numerical experiments [25]. This is a two dimensional map

$$\begin{aligned}x_{n+1} &= y_n + 1 - ax_n^2 \\ y_{n+1} &= bx_n ; \quad b < 1 \quad \dots \quad (1.20)\end{aligned}$$

For $b = 0.3$, it is found that at $a = 0.3675$, the point attractor at x_0 undergoes a cascade of period doublings and a strange attractor exists for $1.06 < a < 1.55$.

1.4 Routes to chaos in dissipative systems

We have seen that in dissipative systems the topological nature of the attractor may change as the control parameter λ crosses a point λ_B . The first bifurcation is often followed by further bifurcations and this sequence is called a transition scenario. We consider three important scenarios which have had theoretical and experimental success.

The Feigenbaum Scenario

This is the most commonly occurring and consequently the most widely explored route to chaos. In this, the mechanism is a pitch fork bifurcation, an infinite cascade of such period-doublings leading

to chaotic behaviour. This has been observed in Bénard experiments, Taylor experiments, driven nonlinear oscillator, chemical reactions and optical instabilities. At the accumulation point λ_∞ of the period-doublings, an aperiodic attractor exists. There are two universal constants associated with the scenario [26],

i) the scale factor α ;

$$\alpha = \lim_{n \rightarrow \infty} \frac{\Delta x_n}{\Delta x_{n+1}} \quad \dots (1.21)$$

where Δx_n is half the separation between the fixed points in the 2^n cycle

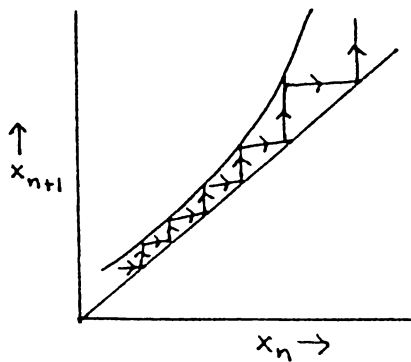
ii) the rate of accumulation of bifurcations

$$\delta = \lim_{n \rightarrow \infty} \frac{\lambda_{n+1} - \lambda_n}{\lambda_{n+2} - \lambda_{n+1}} \quad \dots (1.22)$$

with λ_n , the value at which the n^{th} bifurcation occurs. For the logistic map, these constants were first evaluated by Feigenbaum as $\alpha = 2.5029$ and $\delta = 4.66920$.

Intermittency or the Pomeau - Manneville Scenario

Pomeau and Manneville [27] suggested that there are certain systems in which for $\lambda < \lambda_c$ stable periodic motion is exhibited but above λ_c , there are chaotic bursts which become more frequent as λ is varied until the motion becomes truly chaotic. Above λ_c , as the stable fixed point becomes unstable, a memory of the fixed point is displayed since the motion of the trajectory slows down and numerous iterations are required to move through the narrow channel between the map and the bisector. This leads to long laminar regions and the motion is chaotic until a new regular phase starts again. This is



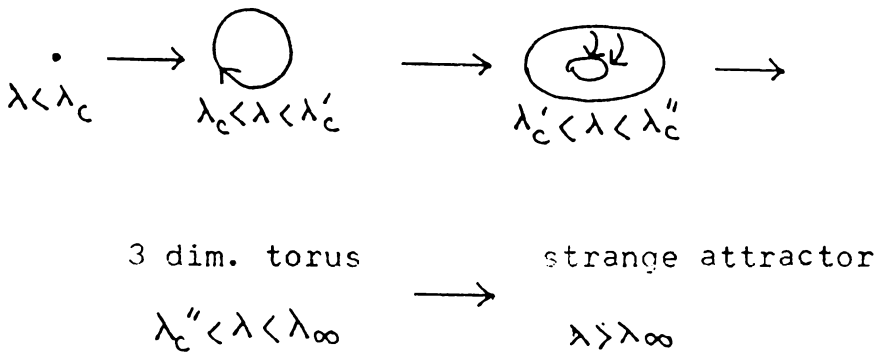
called intermittency and is associated with a saddle-node or tangent bifurcation which occurs due to the collision of stable and unstable fixed points with the disappearance of both. The laminar phases have a mean duration $|\lambda - \lambda_c|^{-1/2}$ [28].

There are three types of intermittency. In type I, the fixed point becomes unstable when a real eigenvalue crosses the unit circle at +1. This is observed in Bénard experiments, nonlinear RCL oscillators etc. In type II, two complex conjugate eigenvalues cross the unit circle simultaneously and in type III, a real eigenvalue crosses the unit circle at -1. Intermittency has been detected in Bénard experiments, Josephson junctions, chemical reactions and lasers.

The Ruelle-Takens-Newhouse scenario

In this scenario, the system undergoes three Hopf bifurcations in succession, before reaching a strange attractor. The power spectrum of such a system will exhibit one, then two and possibly three basic frequencies [29]. When the third

frequency is about to disappear, simultaneously some broad-band noise appears indicating a chaotic state. This route to chaos has been observed in Bénard experiments, Taylor experiments and nonlinear conductors.



1.5 Characterisation of Chaos

We have mentioned that the long-time behaviour of most of the deterministic nonlinear systems generically exhibits chaos. Since this type of motion has stochastic features, its complete description requires statistical methods. This is based on a number of underlying mathematical concepts which are discussed below.

Lyapunov characteristic exponents [4]

The Lyapunov characteristic exponents characterise the mean exponential rate of divergence of trajectories surrounding a point and thus provide a computable quantitative measure of stochasticity. Consider two nearby trajectories in N-dimensional phase space with the initial conditions x_0 and $x_0 + \Delta x_0$. These evolve in time according to (1.1) and the tangent vector Δx has the Euclidean norm.

$$d(x_0, t) = || \Delta x(x_0, t) || \quad \dots \quad (1.23)$$

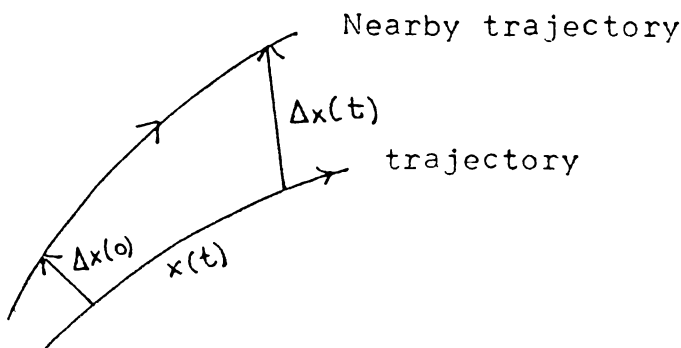
The time evolution of Δx is given by

$$\frac{d}{dt} \Delta x = M(x(t)) \Delta x \quad \dots \quad (1.24)$$

where M is the Jacobian

$$M = \frac{\partial f}{\partial x} \quad \dots \quad (1.25)$$

corresponding to the flow defined by (1.1)



The mean exponential rate of divergence of nearby trajectories is given by

$$\sigma(x_0) = \lim_{\substack{t \rightarrow \infty \\ d(o) \rightarrow 0}} \frac{1}{t} \ln \left[\frac{d(x_0, t)}{d(x_0, 0)} \right] \quad \dots(1.26)$$

Choosing a basis e_i , σ takes values

$$\sigma_i(x_0) = \sigma(x_0, e_i) \quad \dots(1.27)$$

These are the Lyapunov characteristic exponents (LCE) which are usually ordered by size:

$$\sigma_1 > \sigma_2 > \dots > \sigma_N$$

It is clear that at least one of the σ_i 's must vanish since in the direction of flow, Δx grows linearly with time.

The above concept can be generalised to describe the mean rate of exponential growth of a p -dimensional volume in tangent space where $p < N$. Thus the p^{th} order Lyapunov exponents are accordingly defined as,

$$\sigma^p(x_0, V_p) = \lim_{t \rightarrow \infty} \frac{1}{t} \ln \left| \frac{||V_p(x_0, t)||}{||V_p(x_0, 0)||} \right| \dots (1.28)$$

σ^p is the sum of the p largest exponents of order 1.

$$\sigma^p = \sigma_1 + \sigma_2 + \dots + \sigma_p \dots (1.29)$$

For conservative systems this sum is zero, while for dissipative systems, it is negative.

LCEs can be defined for maps as well. Thus if the $m_i(n)$ are the eigenvalues of the matrix A_n defined as

$$A_n = [M(x_n) M(x_{n-1}) \dots M(x_1)]^{1/n} \dots (1.30)$$

where $M = \frac{\partial F}{\partial x}$, corresponding to the F given in (1.2), then the LCEs are given by

$$\sigma_i^{\text{map}} = \lim_{n \rightarrow \infty} \ln [m_i(n)] \dots (1.31)$$

$$\text{Usually } \sigma_i^{\text{map}} = \tau \sigma_i \dots (1.32)$$

where τ is the mean time between successive intersections of the trajectory with the surface of section.

A positive LCE indicates trajectory divergence and chaos while a negative LCE sets the time scale on which transients or perturbations of the state of the system will decay. For a periodic state, there is one LCE equal to zero with all others negative while for a quasi-periodic state with k frequencies, there will be k LCEs equal to zero and others negative.

The Kolmogorov-Sinai entropy [28]

The Kolmogorov-Sinai entropy or K-entropy is the most important measure by which stochastic motion can be characterised. It is defined as follows. The N -dimensional phase space is partitioned into boxes of size l^N . Consider the trajectory $x(t)$ of a system on a strange attractor. The state of the system is measured at time intervals τ . Then P_{i_0, i_1, \dots, i_n} is defined as the joint probability that $x(t=0)$ is in box i_0 , $x(t=\tau)$ is in box i_1 ... and $x(t+n\tau)$ is in box i_n . The quantity

$$K_n = - \sum_{i_0, i_1, \dots, i_n} P_{i_0, i_1, \dots, i_n} \log P_{i_0, i_1, \dots, i_n} \quad (1.33)$$

is proportional to the information needed to locate the system on a special trajectory $i_1^* \dots i_n^*$ with precision l . Therefore $K_{n+1} - K_n$ is the additional information needed to predict in which cell i_{n+1} , the system will be if we know it was previously in the cells i_1^*, \dots, i_n^* . ie. $K_{n+1} - K_n$ measures the loss of information about the system from time n to $n+1$. Then the K entropy is defined as the average rate of loss of information

$$\begin{aligned}
 K &= \lim_{\tau \rightarrow 0} \lim_{l \rightarrow 0} \lim_{n' \rightarrow \infty} \frac{1}{n'\tau} \sum_{n=0}^{n'-1} K_{n+1} - K_n \\
 &= - \lim_{\tau \rightarrow 0} \lim_{l \rightarrow 0} \lim_{n' \rightarrow \infty} \frac{1}{n'\tau} \sum_{i_0, \dots, i_n} P_{i_0, \dots, i_n} \\
 &\quad \times \log P_{i_0, \dots, i_n} \dots (1.34)
 \end{aligned}$$

For regular motion $K = 0$, while for exponential divergence on a strange attractor $K > 0$ and for completely random motion $K \rightarrow \infty$. K is the averaged sum of the LCEs.

For maps with discrete time steps $\tau = 1$ and equation (1.34) is modified as

$$K = - \lim_{n \rightarrow \infty} \frac{1}{n} \sum P_{i_1 \dots i_n} \log P_{i_1 \dots i_n} \dots (1.35)$$

This can be generalied to

$$K_f = - \lim_{n \rightarrow \infty} \frac{1}{n} \cdot \frac{1}{f-1} \log \sum_{i_1 \dots i_n} P_{i_1 \dots i_n}^f \dots (1.36)$$

with $K_1 = K$

The K -entropy is inversely proportional to the time interval over which the state of a chaotic system can be predicted. ie.

$$\tau_m \propto \frac{1}{K} \log \left(\frac{4}{1} \right) \dots (1.37)$$

Invariant measure

The detailed picture of an attractor is given by the probability measure $\rho(x)$ on the attractor which describes how frequently various parts of the strange attractor are visited by the orbit. $\rho(x)$ is defined as the time average of Dirac deltas at the points $x(t)$

$$\rho = \lim_{T \rightarrow \infty} \frac{1}{T} \int_0^T dt \delta x(t) \dots (1.38)$$

The measure is invariant under time evolution. In general there are many distributions invariant to a given map or time evolution. However a unique distribution is singled out by repeated iteration such that time average equals space average for almost all initial conditions x_0 . For a period n -cycle, $\rho(x)$ is discrete having n delta functions at the n stable fixed points. For a one dimensional map, the invariant measure is defined as,

$$\rho(x) = \lim_{N \rightarrow \infty} \frac{1}{N} \sum_{i=0}^N \delta [x - f^i(x_0)] \quad \dots (1.39)$$

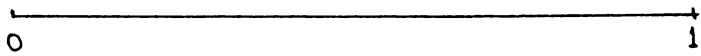
Since $\rho(x)$ has to be stationary, $\rho(x)$ must be independent of time. So we have

$$\rho(y) = \int_0^1 dx \delta [y - f(x)] \rho(x) \quad \dots (1.40)$$

This is the Frobenius-Peron integral equation for $\rho(x)$. If $\rho(x)$ is known, time averages can be replaced by space averages over the invariant measure and this is useful in the computation of LCE and K-entropy. $\rho(x)$ is usually computed numerically [4].

Cantor set and dimensions

The typical geometry of a strange attractor is a set of self similar structures that repeat on finer and finer scales. This can be put in correspondence with the geometry of a Cantor set. A Cantor set is a compact metric space that is totally disconnected, uncountable and of zero measure. It has typically a fractional dimension and displays scale-invariance. As an example we consider the middle-thirds Cantor set constructed as follows [30]. Consider the line of unit length and remove its middle third. Take the remaining two intervals and remove their middle thirds. This process is repeated and in the limit we have a set that has zero net length and an uncountable number of elements.



The definition of fractal or capacity dimension is given by

$$d = \lim_{\epsilon \rightarrow 0} \frac{\ln M(\epsilon)}{\ln (1/\epsilon)} \quad \dots(1.41)$$

where $M(\epsilon)$ is the minimum number of intervals of length ϵ needed to cover the interval $(0,1)$. In the construction of the Cantor set, after the p^{th} repetition of the process, we have $\epsilon = (1/3)^p$ and $M(\epsilon) = 2^p$. Hence

$$d = \lim_{p \rightarrow \infty} \frac{\ln 2^p}{\ln 3^p} = 0.630 \quad \dots(1.42)$$

It is customary to define three important dimensions for a strange attractor.

The capacity dimension D_0

Suppose the strange attractor is embedded in a subset of a p -dimensional Euclidean space \mathbb{R}^p . We take $N(\epsilon)$ as the minimum number of p -dimensional cubes of side ϵ , needed to cover it. Then the capacity dimension D_0 is defined as

$$D_0 = \lim_{\epsilon \rightarrow 0} \frac{\log N(\epsilon)}{\log (1/\epsilon)} \quad \dots(1.43)$$

For small values of ϵ ,

$$\log N (\epsilon) = D_0 \log (1/\epsilon) \quad \dots (1.44)$$

This expression is used in the numerical computation of D_0 by box counting. For this, the space is divided into boxes of size ϵ and the number of boxes containing at least one point of the attractor is counted as M . A graph is plotted with $\log M/\log \epsilon$ vs. $1/\log \epsilon$. D_0 is obtained by fitting a straight line to this graph for several values of ϵ and extrapolating the result to $\epsilon \rightarrow 0$.

The information dimesion D_1

D_1 is a generalisation of D_0 which takes into account the relative probability of the cubes used to cover the attractor. We define [31]

$$I (\epsilon) = \frac{N (\epsilon)}{\sum_{i=1} p_i \log \frac{1}{p_i}} \quad \dots (1.45)$$

where p_i is the probability for one point of the attractor to be contained in the i^{th} cube. It is the amount of information necessary to specify the state of the system to within an accuracy ϵ . Then D_1 is given by,

$$D_1 = \lim_{\epsilon \rightarrow 0} \frac{I(\epsilon)}{\log(1/\epsilon)} \quad \dots (1.46)$$

Since for small ϵ ,

$$I(\epsilon) = D_1 \log(1/\epsilon) \quad \dots (1.47)$$

D_1 tells us how fast the information necessary to specify a point on the attractor increases as ϵ decreases. If all cubes have equal probability, then $I(\epsilon) = \log N(\epsilon)$ and hence $D_1 = D_0$. In all other cases $D_1 < D_0$.

The correlation dimension D_2

D_2 is defined as

$$D_2 = \lim_{\epsilon \rightarrow 0} \frac{\log \left(\frac{N(\epsilon)}{\sum_{i=1}^N P_i^2} \right)}{\log(1/\epsilon)} \quad \dots (1.48)$$

It can be shown that $\sum P_i^2 = C(\epsilon)$ [28], where

$C(\epsilon)$ is the correlation integral given by

$$C(\epsilon) = \lim_{N \rightarrow \infty} \frac{1}{N^2} \sum_{ij} \Theta[\epsilon - (x_i - x_j)] \quad \dots (1.49)$$

Hence

$$D_2 = \lim_{\epsilon \rightarrow 0} \frac{\log C(\epsilon)}{\log(1/\epsilon)} \quad \dots (1.50)$$

This is used in the numerical determination of D_2 from a time series.

Generalised dimensions and f- α spectrum

A complete characterisation of the strange attractor of dynamical systems is now possible by considering the structure of scaling indices α_i on the fractal measure [32]. The concept is most general since it allows different values for the scaling index α and $f(\alpha)$ is defined as the dimension of the set of points on the fractal with the same value of α . The f- α spectrum thus describes the global scaling measure of the strange attractor.

To characterise the inhomogeneous static structure of the strange attractor, an infinite number of dimensions D_q are introduced [33].

$$D_q = \lim_{\epsilon \rightarrow 0} \frac{1}{q-1} \frac{\log \left[\sum_{i=0}^{N(\epsilon)} p_i^q \right]}{\log (1/\epsilon)} \dots (1.51)$$

The first three members of this set correspond to the dimensions introduced earlier; ie., for $q \rightarrow 0$, $D_q \rightarrow D_0$, $q \rightarrow 1$ gives $D_0 \rightarrow D_1$ and if $q = 2$, then

$D_q = D_2$. In general $D_{q'} < D_q$ for $q' > q$; the equality sign holding only if the attractor is uniform. $q \rightarrow \infty$ corresponds to the most concentrated region on the attractor while $q \rightarrow -\infty$ correspond to the most rarefied region.

The generalised partition function for such an attractor is defined as [34].

$$\Gamma = \sum_{i=1}^N \frac{P_i^q}{\epsilon_i^{\tau_i}} \quad \dots(1.52)$$

For large N, this Γ is of order unity only if

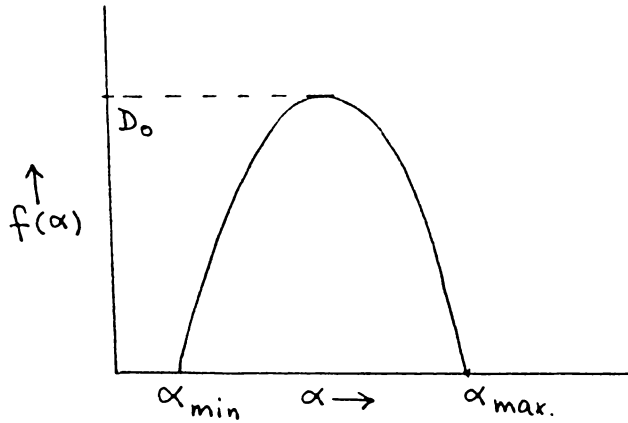
$$\tau = (q-1) D_q \quad \dots(1.53)$$

$\tau(q)$ is obtained by solving (1.52) equated to unity. Then τ is related to $f(\alpha)$ through a Legendre transformation:

$$\tau = \alpha q - f \quad \dots(1.54)$$

where $\alpha = \frac{\partial \tau}{\partial q} \quad \dots(1.55)$

For different values of q , one can thus get the corresponding $f(\alpha)$. The f value at the maximum point gives D_0 .



1.6 Relevance of chaos in related fields

The discovery of chaos has made an enormous impact on atomic physics, nuclear physics, solid state physics, cosmology, fluid mechanics, optics and so on. It has brought out limitations to predictions possible from established laws. However, the realisation that chaos is a common and usual behaviour in nonlinear systems can influence many related fields of science. Chaos has been observed in cardiac cells [35] and neural systems [36]. Although in nonlinear physical systems the presence of chaos is being frowned upon, in biological systems, it is often found to be beneficial.

Chaotic systems can be an information source, since in turbulence information flows from microscopic to macroscopic scales [37]. Chaos is made use of in the human brain and so is applied in the field of artificial intelligence. The richness of a symbolic sequence in a chaotic orbit is of relevance for language theory [38]. Information can be stored in the time series of a system with a chaotic orbit and thus used to create memory. Cellular automata [39] and coupled map lattices can have a large number of attractors which might be useful for storage of information [40]. Tomita pointed out that the soft response in chaotic systems is associated with pattern recognition or learning in brain [41]. Moreover study of dynamical systems with complexity can enhance our understanding of the human brain [42], self-limiting biological reactions, turbulence, complex chemical reactions, meteorological phenomena, fluctuations in the cost of materials and so on.

2. ONE DIMENSIONAL MAPS AND UNIVERSALITY

Dissipative dynamical systems exhibiting complex or chaotic behaviour occur quite commonly in condensed matter physics, fluid physics, accelerator physics, chemical reactions, electrical circuits and so on. For such multidimensional systems, the volume of the phase space contracts in all directions and the trajectory converges to a limit cycle. One direction will have the slowest convergence and hence these systems have asymptotic motions that can be modelled by one dimensional noninvertible maps. The differential equations representing these systems can be reduced to one dimensional maps by means of Poincaré sections, stroboscopic methods or return maps corresponding to the maximum values of the variable. Such maps also arise naturally as simple models of system behaviour as in population studies of certain species. In general, one dimensional maps of the form

$$x_{n+1} = f_{\lambda}(x_n) \quad \dots (2.1)$$

have a tuning parameter λ whose variation drives the system through a series of bifurcations. This period-doubling route, usually called the Feigenbaum Scenario, forms the most common and the most well studied route from periodic to aperiodic behaviour. The sequence of bifurcations exhibits some striking universal features near the infinite bifurcation limit λ_∞ characterised by two scaling constants α and δ . Thus the measurable properties of any system in the aperiodic limit can be described in a way that essentially bypasses the details of the equations governing the system. The universality theory was developed in the context of quadratic maps by Feigenbaum [43]. Soon after this work, several numerical and theoretical studies lent support to the universality picture in a number of models in various dimensions. It was first tested experimentally in 1980 in an actual turbulence experiment [44]. The universality theory was later extended to circle maps [45] and hamiltonian maps [46] and later generalised to include period n -tuplings in complex iterative maps [47]. It also plays an important role in the intermittent route to chaos [48].

2.1 The Universality theory

The key to understanding repeated period-doublings is the introduction of a doubling transformation T which carries a map f to one obtained by

- i) composing f with itself,
- ii) restricting to an appropriate subdomain and
- iii) changing the co-ordinates to magnify the subdomain to the original domain. To account for the universality, one has to show that T has a fixed point and that in the neighbourhood of the fixed point T is expanding in one direction and contracting in all others.

To define the doubling operator T , we consider one-hump maps of the form

$$x_{n+1} = 1 - \lambda |x_n|^z \quad \dots (2.2)$$

where z is the order of the local maximum.

This map has the following general features:

- 1) For $\lambda_{n-1} < \lambda < \lambda_n$, there exists a stable 2^{n-1}

cycle with elements $x_0^*, x_1^*, \dots, x_{2^{n-1}-1}^*$ which is characterised by

$$|\pi f'_{\lambda}(x_i^*)| < 1 \quad \dots (2.3)$$

where the prime denotes differentiation of the function f_{λ} with respect to x_i .

2) At λ_n , all points of the 2^{n-1} cycle become unstable via pitchfork bifurcations leading to a new stable 2^n cycle for $\lambda_n < \lambda < \lambda_{n+1}$.

3) A 2^n superstable cycle is defined by

$$\pi f'_{\lambda_n}(x_i^*) = 0 \quad \dots (2.4)$$

This implies it always contains $x_0^* = 0$ as a cycle element.

4) The distance d_n of the point in a 2^n supercycle which is closest to $x = 0$ is given by

$$d_n = f_{\lambda_n}^{2^{n-1}}(0) \quad \dots (2.5)$$

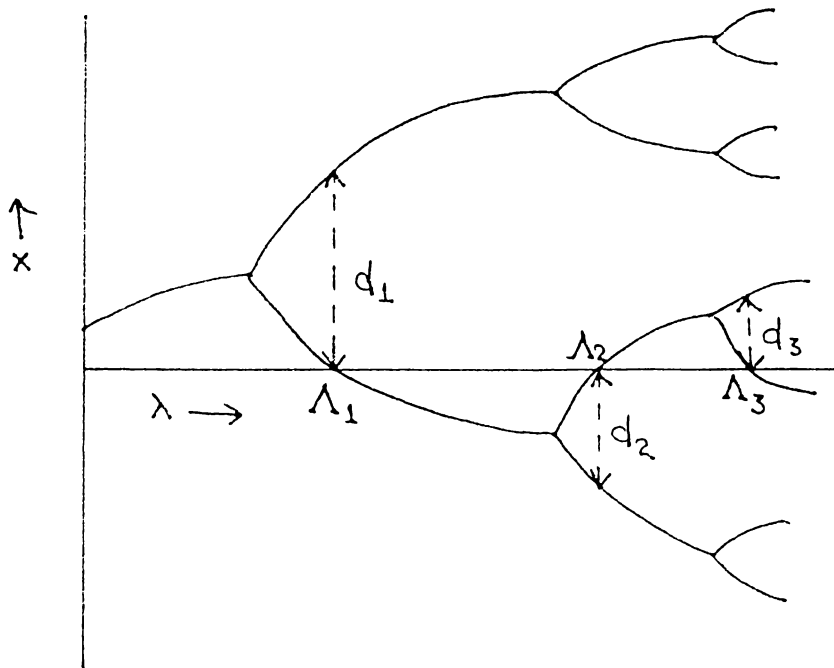
$$\text{We have } \frac{d_n}{d_{n+1}} = -\alpha \quad \dots (2.6)$$

where α is the scale factor introduced in the preceding chapter.

Then

$$\lim_{n \rightarrow \infty} (-\alpha)^n d_{n+1} = d_1 \quad \dots (2.7)$$

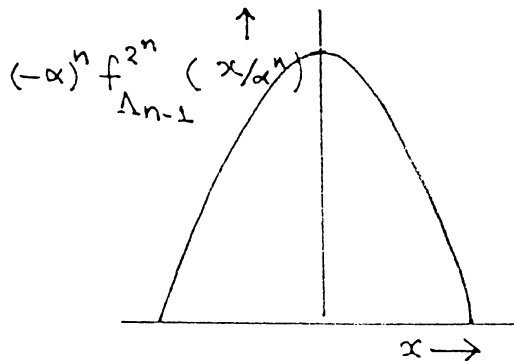
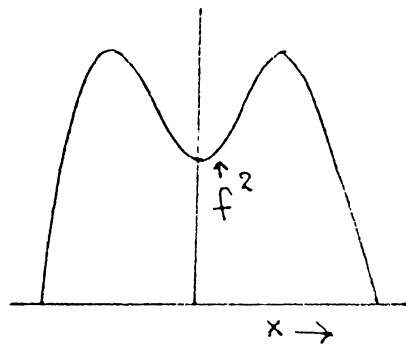
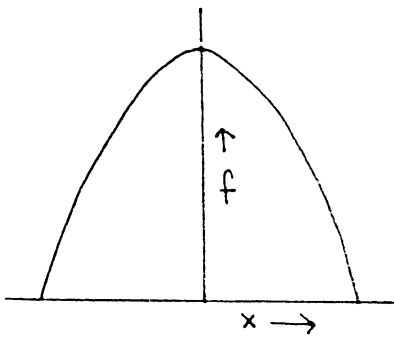
ie.
$$\lim_{n \rightarrow \infty} (-\alpha)^n f_{\Lambda_{n+1}}^{2^n}(o) = d_1 \quad \dots (2.8)$$



This can be generalised to the whole interval $(-1,1)$ and the rescaled functions then converge to a limiting function [28].

$$\lim_{n \rightarrow \infty} (-\alpha)^n f^{\Lambda_{n+1}} \left(\frac{x}{\alpha^n} \right) = g_1(x) \quad \dots (2.9)$$

$g_1(x)$ is determined by the behaviour of $f^{\Lambda_{n+1}}(x)$ around $x = 0$ and should be universal for all f with the same z [49].



We introduce a whole family of functions

$$g_i(x) = \lim_{n \rightarrow \infty} (-\alpha)^n f_{\Lambda_{n+i}}^{2^n} \left(\frac{x}{\alpha^n} \right) \quad \dots (2.10)$$

$$i = 0, 1, 2, \dots$$

where the g_i for $i > 1$ are iterates of g_1 . All such functions are related by

$$g_{i-1}(x) = -\alpha g_i \left(g_i \left(\frac{x}{\alpha} \right) \right) = T g_i(x) \quad \dots (2.11)$$

In the limit $i \rightarrow \infty$, we define

$$g(x) = \lim_{i \rightarrow \infty} g_i(x) \quad \dots (2.12)$$

Clearly $g(x)$ satisfies the equation

$$g(x) = -\alpha g(g(x/\alpha)) \quad \dots (2.13)$$

Thus g is the fixed point function of the doubling transformation T . Since the equation does not fix absolute scales, we introduce a normalisation condition,

$$g(0) = 1 \quad \dots (2.14)$$

Equation (2.13) determines α universally as

$$\alpha = -\frac{1}{g(1)} \quad \dots (2.15)$$

$g(x)$ is obtained as the limit of f^{2^n} 's at the value of Λ_∞ . This is the unique value of Λ at which repeated applications of T will lead to a convergent function.

We define [26, 43]

$$\Delta g_i = g_{i+1}(x) - g_i(x) \quad \dots (2.16)$$

Then equation (2.11) becomes,

$$\begin{aligned} g_i(x) &= -\alpha(g_i + \Delta g_i) [g_i(x/\alpha) + \Delta g_i(x/\alpha)] \\ &= g_{i-1}(x) - \alpha [\Delta g_i(g_i(x/\alpha)) \\ &\quad + g'_i(g_i(x/\alpha)) \Delta g_i(x/\alpha)] + O((\Delta g_i)^2) \\ &\quad \dots (2.17) \end{aligned}$$

$$\begin{aligned} \text{ie. } \Delta g_{i-1}(x) &= -\alpha [\Delta g_i(g_i(x/\alpha)) + g'_i(g_i(x/\alpha)) \\ &\quad \times \Delta g_i(x/\alpha)] + O((\Delta g_i)^2) \quad \dots (2.18) \end{aligned}$$

In the limit $i \rightarrow \infty$, $g_i \rightarrow g$ so that $\Delta g_i \rightarrow 0$.

So we write,

$$\Delta g_i(x) = \eta_i h(x) \quad \dots (2.19)$$

with the condition $\eta_i \rightarrow 0$ as $i \rightarrow \infty$.

Then (2.18) gives a closed equation for $h(x)$ and η_i :

$$\eta_{i-1} = \delta \eta_i, \quad \dots (2.20)$$

$$h(x) = -(\alpha/\delta) [h(g(x/\alpha)) + g'(g(x/\alpha)) \\ \times h(x/\alpha)] \quad \dots (2.21)$$

Equation (2.20) can be trivially solved to give

$$\eta_i = \delta^{-i} \quad \dots (2.22)$$

Then (2.12) is satisfied if $\delta > 1$. It can be shown that [26]

$$\Lambda_{n+1} - \Lambda_n \approx \delta^{-n} \quad \dots (2.23)$$

logarithmically so that the original definition of δ given in Chapter 1 automatically follows.

We observe that universality arises from the fact that bifurcation is a local phenomenon. Here we consider the region near $x = 0$ where distances between points scale as α , while points near $x = 1$ are found to scale as α^2 . It is also possible to consider scaling and universal behaviour centered around points other than these two [50].

2.2 The Renormalisation Group equations and calculation of α and δ

The essence of the renormalisation group (RG) analysis given above is that different maps with the same z value have the same values for α and δ . The RG equations (2.13) and (2.21) can be used to evaluate α and δ for a given z value. However the structure and solutions of these equations are not yet fully studied. Numerical evaluation of α and δ shows that there exists universality classes characterised by α and δ for different z values [51].

Among the available analytic methods, we mention the eigenvalue matching RG method [52] and Helleman's scheme [53]. The former has the drawback that it is difficult to extend it beyond the second or fourth order of renormalisation. Moreover it provides us with the δ values only. There is no direct way of getting α and $g(x)$. The Helleman scheme has been applied to quadratic maps. But for maps with $z > 2$, the algebra involved is very cumbersome.

A method of evaluating α and δ using equations (2.13) and (2.21) was reported by Delbourgo et al which involves the truncation of $g(x)$ to first order in $|x|^z$ [54]. For second or higher order, numerical methods must be resorted to. Moreover the asymptotic expressions in their approach refer to the limit $N \rightarrow \infty$ for N -replication. Even though multifurcations other than bifurcations are usual, we feel that the large N limit is rather unphysical. A computational iterative procedure based on the nested structure of $g(x)$ is used by van der Weele et al and is found to have a rapid convergence for small z values [55].

Perturbative scheme for evaluation of universal parameters

An analytic method based on a perturbative scheme was developed by Singh [56] to solve equation (2.13) for α and $g(x)$. Here $g(x)$ is expanded into an infinite series and the coefficients of expansion are replaced by a perturbative series in inverse powers of α . The method has been applied to quadratic

maps giving good results. We have extended this scheme so that (2.13) and (2.21) can be solved simultaneously for $\alpha, \delta, g(x)$ and $h(x)$ for any general z . Here the functional equations are replaced by infinite dimensional nonlinear vector equations.

To this end we write $g(x)$ as

$$g(x) = 1 + \sum_{n=1}^{\infty} P_n |x|^{nz} \quad \dots (2.24)$$

with the normalisation given in (2.14). In the neighbourhood of the extremum at $x = 0$, $g(x)$ is positive for any z and $g(g(x))$ can be expanded into a similar power series. Thus

$$\begin{aligned} g(g(x)) = & 1 + \sum_{r=1}^{\infty} P_r + (P_1 \sum_{r=1}^{\infty} rzP_r) |x|^z \\ & + (P_2 \sum_{r=1}^{\infty} rP_r + P_1^2 \sum_{r=1}^{\infty} \frac{rz(rz-1)}{2} \\ & \times P_r) |x|^{2z} + \dots \quad \dots (2.25) \end{aligned}$$

We redefine the coefficients of expansion in (2.24) as

$$P_n \alpha^n = S_n |\alpha|^z \quad \dots (2.26)$$

Using (2.24) - (2.26) in (2.13) and equating coefficients of $|x|^{nz}$ we get

$$\frac{1}{\alpha} + 1 + |\alpha|^z \sum_{r=1}^{\infty} \frac{S_r}{\alpha^r} = 0 ; \quad n = 0 \quad \dots (2.27)$$

$$\frac{1}{z} + \sum_{r=1}^{\infty} \frac{r S_r}{\alpha^{r-1}} = 0 ; \quad n = 1 \quad \dots (2.28)$$

$$S_n \left[1 - \frac{1}{|\alpha|^{z(n-1)}} \right] + \sum_{l \geq 2}^n \sum_{r \geq 1}^{\infty} \binom{rz}{l} \frac{S_r}{\alpha^{r-1}}$$

$$\times \sum_{m_1 \geq 1 \dots m_l \geq 1} \frac{S_{m_1} S_{m_2} \dots S_{m_l}}{|\alpha|^{z(n-l)}} \delta_{m_1 + \dots + m_l, n} = 0 ;$$

$$n = 2, 3, 4, \dots \quad \dots (2.29)$$

These form an infinite set of coupled nonlinear equations. To solve these, we expand S_n in inverse powers of α ,

$$S_n(\alpha) = \sum_{m=0}^{\infty} \frac{S_{nm}}{\alpha^m} \quad \dots (2.30)$$

Using this expansion in (2.28) and (2.29), equating coefficients of equal powers of $1/\alpha$ to zero, we obtain

a hierarchy of equations which can be solved successively for the coefficients S_{nm} . These are used in (2.27) to yield the equation for α :

$$\frac{1}{\alpha} + 1 + |\alpha|^z \sum_{r=1}^{\infty} \sum_{m=0}^{\infty} \frac{S_{rm}}{\alpha^{r+m}} = 0 \quad \dots (2.31)$$

The universal function $g(x)$ is given by

$$g(x) = 1 + \sum_{n=1}^{\infty} [|\alpha|^{z-n} \sum_{m=0}^{\infty} \frac{S_{nm}}{\alpha^m}] |x|^{nz}. \quad (2.32)$$

In our work, we have expanded $h(x)$ also into a power series as in (2.24). We substitute this in (2.21) and equate coefficients of $|x|^{nz}$ on both sides to get,

$$- \alpha \sum_{r=1}^{\infty} [1+h_r + |\alpha|^z \frac{rz S_r}{\alpha^r}] = \delta ; \quad n = 0 \quad \dots (2.33)$$

$$- \alpha \sum_{r=1}^{\infty} \left[\binom{rz}{1} \frac{h_r S_1}{\alpha} + 2 \binom{rz}{2} \frac{|\alpha|^{z-1} S_r S_1}{\alpha^r} + h_1 \binom{rz}{1} \frac{S_r}{\alpha^r} \right] = \delta h_1 ; \quad n = 1 \quad \dots (2.34)$$

$$\begin{aligned}
 & - \alpha \sum_{r=1}^{\infty} \left[\left\{ \sum_{l \geq 1}^n \binom{rz}{l} \frac{h_r}{\alpha^r} + (l+1) \binom{rz}{l+1} \frac{S_r}{\alpha^{n-z+r}} \right\} \right. \\
 & \times \sum_{m_1 \geq 1, \dots, m_l \geq 1} \frac{S_{m_1} S_{m_2} \dots S_{m_l}}{\alpha^{z(n-l)}} \delta_{m_1 + \dots + m_l, n} \\
 & + \sum_{n'=1}^{n-1} \sum_{l \geq 1}^{n-n'} \left\{ h_n (l+1) \binom{rz}{l+1} \frac{S_r}{\alpha^{n-n'-z+r}} \right\} \\
 & \times \sum_{m_1 \geq 1, \dots, m_l \geq 1} \frac{S_{m_1} S_{m_2} \dots S_{m_l}}{\alpha^{z(n-l)}} \delta_{m_1 + \dots + m_l, n'} \\
 & \left. + h_n \left[\frac{rz S_r}{\alpha^{r+(n-1)z}} \right] = \delta h_n ; \right. \\
 & \qquad \qquad \qquad n = 2, 3, 4 \dots \qquad \dots (2.35)
 \end{aligned}$$

The expansion given in (2.30) can be used here also and the S_{nm} coefficients determined earlier can be substituted. We have reduced the above set of equations into a matrix eigenvalue equation of the form.

$$D h = \delta h \qquad \dots (2.36)$$

where h is the column $[1, h_1, h_2, \dots, h_n]$. The largest real eigenvalue of D furnishes the relevant δ value.

In practice, we can work only with truncated series of S_r and h_r . We determine the S_{nm} coefficient which are required to retain terms upto a definite power of $1/\alpha$ in the equation for α , (2.31). Then the maximum number of coefficients h_r that can be included are used in the calculation of δ .

However we find that the perturbation series is not highly convergent but shows some of the basic characteristics of asymptotic series. The details of the calculations given in the next chapter indicate that the absolute values of the successive S_{nm} coefficients, for a given n , do not decrease steadily, but decrease for a few m values, then increase, beyond some m value. The corresponding α values calculated using the perturbative series also show some fluctuations about the numerical value, instead of converging to it uniformly. Therefore the selection of the truncation point is rather crucial. It is found that there is definite advantage if we use Padé approximants [57] to sum the series in the expressions for α and δ .

2.4 Universal relations for general z

It is now well established that one-hump maps fall into different universality classes labelled by the order of their extremum z.

For any z value, the first few coefficients S_{nm} using (2.28) and (2.29) work out to be

$$S_{10} = -1/z ; S_{11} = \frac{-(z-1)}{z^2} ; S_{20} = \frac{(z-1)}{2z^2} \dots$$

... (2.37)

The equation for α (2.31) using these coefficients is,

$$\frac{1}{\alpha} + 1 = |\alpha|^z \left[\frac{1}{z\alpha} + \frac{(z-1)}{2z^2\alpha^2} + \dots \right] \quad (2.38)$$

The series in the brackets can be replaced by its Padé approximant. Thus considering the lowest approximation, we use the [1/1] approximant to yield

$$\frac{\alpha^z}{z} = (1+\alpha) \left[1 - \frac{(z-1)}{2z\alpha} \right] \dots \quad (2.39)$$

In the limit $z \rightarrow 1$, we find $\alpha \rightarrow \infty$. For a given $z > 1$, (2.39) can be solved for α . Fig 2.1 shows

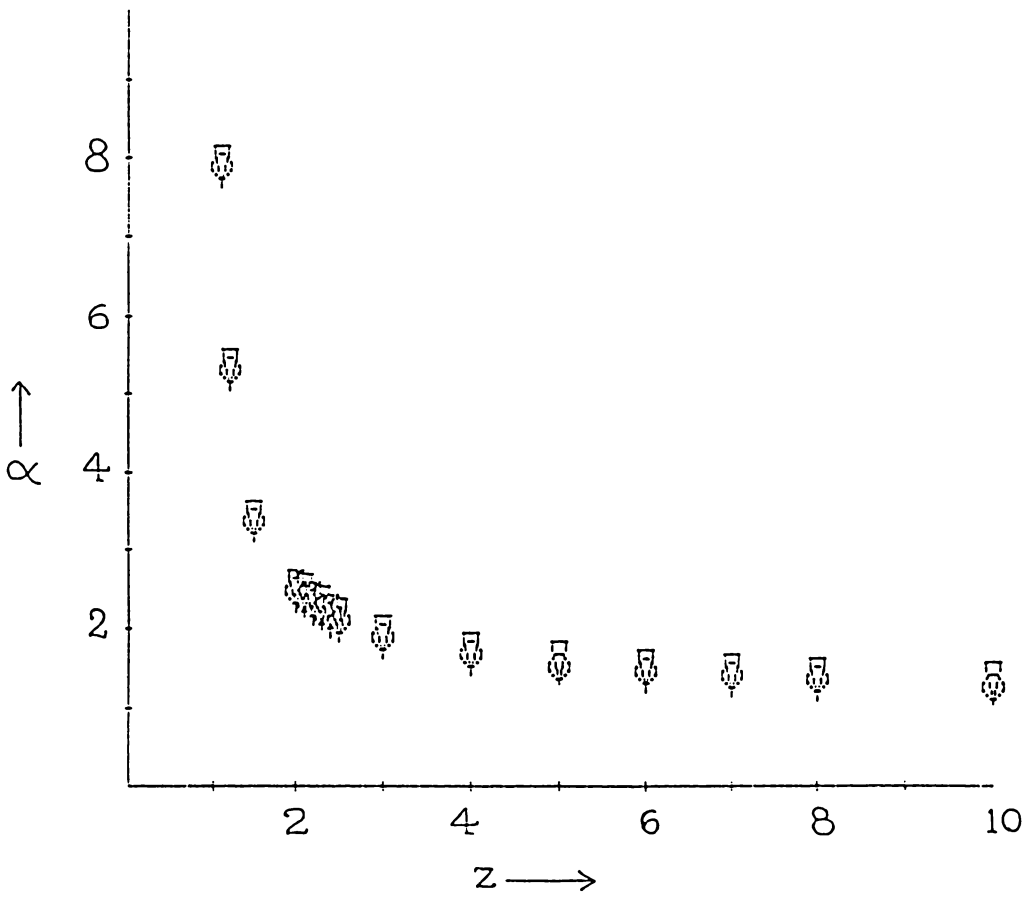


Fig. 2.1 - The values of α for different values of z . The computed values using (2.39) are shown by triangles while numerical values are indicated by circles.

the values of α thus obtained. The numerical values are also plotted. It is clear that the agreement is quite good. The computed values are provided in Table 2.I.

Using the coefficients in (2.37) in the equations for δ (2.33) - (2.35) we get the approximate expression,

$$2\delta = \alpha^{z-\alpha+2} \frac{(z-1)}{z\alpha} + \left[\left\{ \alpha^{z-\alpha-2} - \frac{(z-1)}{z\alpha} \right\}^2 + 4|\alpha|^{z+1} \left\{ \frac{(z-1)}{z\alpha} - \frac{(z-1)}{z^2\alpha^2} - \frac{z(z-1)^2}{z^3\alpha^3} \right\} \right]^{\frac{1}{2}} \dots (2.40)$$

Replacing the series in the last term by its [1/2] Pade approximant, we get

$$2\delta = \alpha^{z-\alpha+2} \frac{(z-1)}{z\alpha} + \left[\left\{ \alpha^{z-\alpha-2} - \frac{(z-1)}{z\alpha} \right\}^2 + \frac{4|\alpha|^{z+2} z(z-1)}{z\alpha(z\alpha+1)+1+z(z-1)} \right]^{\frac{1}{2}} \dots (2.41)$$

As z increases the first term within the square brackets increases faster than the second, so we write

Table 2.I - Computed values of α using (2.39).
 The numerical values are also
 given for comparison [51,55,58].

z	Computed values of α	Numerical α values
1.1	7.978673	7.97
1.2	5.390312	5.37
1.5	3.405767	3.39
2.0	2.517021	2.5029
2.1	2.422142	2.4084
2.2	2.340300	2.3269
2.3	2.268835	2.2557
2.4	2.205783	2.1928
2.5	2.149665	2.1368
3.0	1.940393	1.9277
4.0	1.704310	1.69
5.0	1.571511	1.56
6.0	1.485068	1.467
7.0	1.423759	1.41
8.0	1.377734	1.358
10.0	1.312754	1.2914
100.0	1.047940	1.03373

$$\delta = \alpha^z - \alpha + \frac{|\alpha|^{z+2} z(z-1) \left[\alpha^z - \alpha - 2 - \frac{(z-1)}{z\alpha} \right]^{-1}}{z\alpha(z\alpha+1)+1+z(z-1)} \dots (2.42)$$

When z is large the last term in (2.42) is ≈ 1 .
 So we can recover the universality relation
 derived by Delbourgo [58] from (2.42) i.e.

$$\delta \approx \alpha^z - \alpha + 1 \dots (2.43)$$

For very large values of z , $\delta = \alpha^z - \alpha + c$ where
 $c < 1$. So we can infer the inequality

$$\alpha^z > \delta > \alpha^z - \alpha \dots (2.44)$$

These limiting expressions were derived earlier
 using entirely different arguments [55].

The values of δ for different maps computed
 using equation (2.41) are shown along with numerical
 values in Fig. 2.2. We observe that the computed
 values agree well with numerical values as is evident

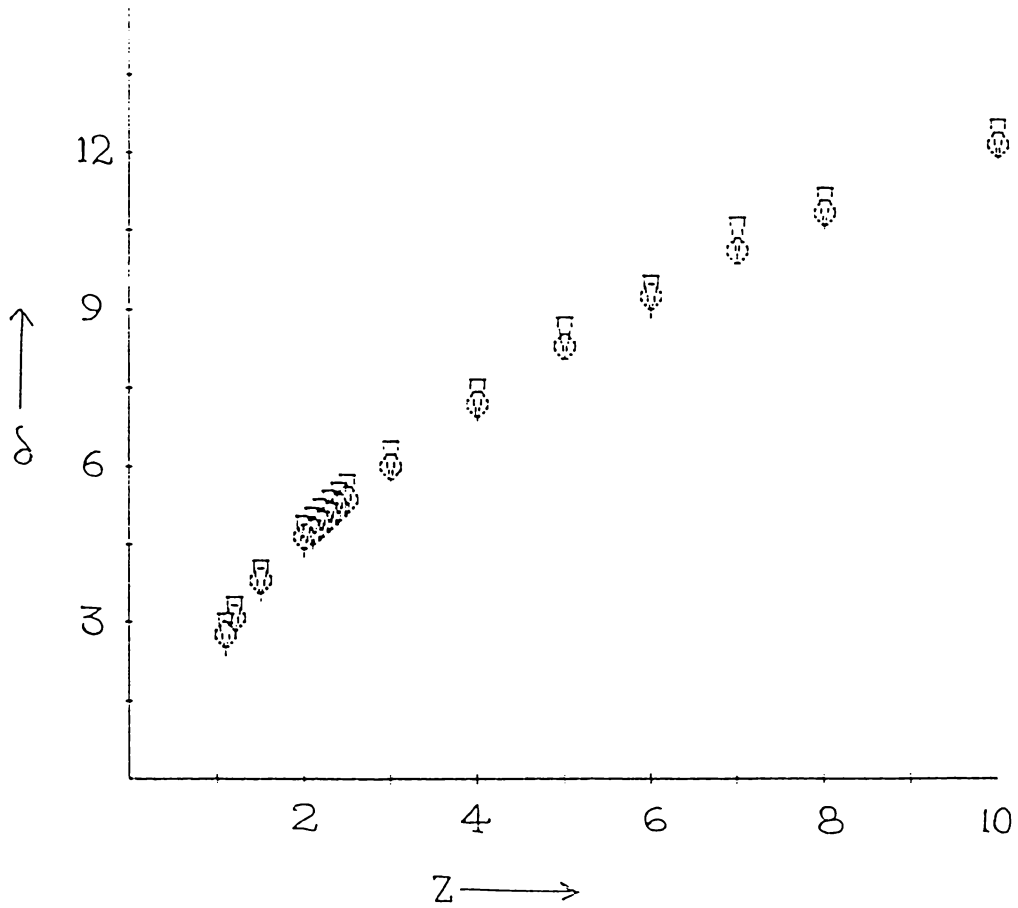


Fig. 2.2 - The δ values of maps with different z values. The triangles correspond to values obtained using (2.41) while circles indicate numerical values.

from Table 2-II.

In the next chapter, we apply the above perturbative scheme to specific cases viz. quadratic, cubic and quartic maps. For non-polynomial maps, we present an expansion in terms of a small parameter ϵ .

Table 2.II - Computed values of δ using (2.41). The numerical values from [51,55,58] are included.

z	Computed values of δ	Numerical δ -values
1.1	2.818065	2.83
1.2	3.118078	3.14
1.5	3.811942	3.80
2.0	4.708019	4.6692
2.1	4.868009	4.8253
2.2	5.023532	4.9773
2.3	5.174898	5.1256
2.4	5.322243	5.2706
2.5	5.466273	5.4127
3.0	6.145081	6.0847
4.0	7.339693	7.29
5.0	8.514767	8.35
6.0	9.313801	9.296
7.0	10.454400	10.2
8.0	10.979350	10.948
10.0	12.350160	12.3
100.0	27.137240	27.75

3. UNIVERSAL PARAMETERS FOR ONE-HUMP MAPS

The perturbative scheme developed in Chapter 2 can be used to obtain the universal constants α and δ as well as the universal function $g(x)$ for any given map. Detailed calculations for different orders of accuracy have been carried out for quadratic, cubic as well as quartic maps and the results are reported. For fractional z values, the general method can be side-stepped and an expansion about the nearest integer value can be performed in the expressions for α and δ . Such an ϵ -expansion does not affect the accuracy of the values much. The results for $1.5 < z < 2.5$ are given.

3.1 The universal constant δ for a quadratic map

The S_{nm} coefficients as well as the value of the scaling constant α for a quadratic map

were first calculated by Singh[56]. We have reproduced his results in Table 3.1 for completeness. We calculate the constant δ for such a map using the perturbative procedure and the elements of the D matrix defined in (2.36) work out to be

$$\begin{aligned}
 D_{11} &= -\alpha - 2\alpha^2 \left[S_{10} + \frac{S_{11}}{\alpha} + \frac{S_{12}}{\alpha^2} + \frac{S_{13}}{\alpha^3} \right] \\
 &\quad - 4\alpha \left[S_{20} + \frac{S_{21}}{\alpha} + \frac{S_{22}}{\alpha^2} \right] - 6 \left[S_{30} + \frac{S_{31}}{\alpha} \right] \\
 &\quad + \frac{8S_{40}}{\alpha} ; \\
 D_{12} &= -\alpha ; \\
 D_{13} &= -\alpha ; \\
 D_{21} &= -2\alpha \left[S_{10}^2 + \frac{2S_{10} S_{11}}{\alpha} + \frac{2S_{10} S_{12}}{\alpha^2} + \frac{S_{11}^2}{\alpha^2} \right] \\
 &\quad - 12 \left[S_{20} S_{10} + \frac{S_{20} S_{11}}{\alpha} + \frac{S_{21} S_{10}}{\alpha} \right] - \frac{30S_{30} S_{10}}{\alpha} ; \\
 D_{22} &= -4\alpha \left[\frac{S_{10}}{\alpha} + \frac{S_{11}}{\alpha^2} \right] - \frac{4S_{20}}{\alpha} ; \\
 D_{23} &= -4\alpha \left[\frac{S_{10}}{\alpha} + \frac{S_{11}}{\alpha^2} \right] ; \\
 D_{31} &= - \frac{12 S_{20} S_{10}^2}{\alpha} ;
 \end{aligned}$$

Table 3.I - The S_{nm} coefficients for the quadratic map [56]

$n \backslash m$	0	1	2	3
1	- 0.5	- 0.25	0	- 0.25
2	0.125	0	0.03125	
3	0	0.0625		
4	0			

$$D_{32} = - \frac{4 S_{10}^2}{\alpha} ;$$

$$D_{33} = - \frac{4 S_{10}^2}{\alpha} \quad \dots (3.1)$$

Using the S_{nm} values given in Table 3.1 and the value of α obtained in [56] as $\alpha = 2.5$, we get

$$D = \begin{bmatrix} 3.75 & -2.5 & -2.5 \\ -0.9 & 2.2 & 2.4 \\ -0.15 & -0.4 & -0.4 \end{bmatrix} \quad \dots (3.2)$$

The largest eigenvalue of D is given by $\delta = 4.66602965$. This is close to the numerical value, 4.6692016 ... [26].

The corresponding h function is

$$h(x) = 1 - 0.3656757x^2 - 0.000736226x^4 \quad . (3.3)$$

3.2 Solutions of RG equations for a cubic map

Next to the logistic or quadratic map, the cubic map is perhaps the most physically interesting system [59,60] and we apply the perturbative scheme to the cubic map. The expansion coefficients

S_{nm} are calculated by substituting $z = 3$ in equations (2.28) and (2.29). The following system of equations give the S_{nm} values:

$$S_{10} = -\frac{1}{3} ;$$

$$S_{20} = -3 S_{10}^3$$

$$S_{11} = -2 S_{20} ;$$

$$S_{21} = -9 S_{10}^2 S_{11} - 15 S_{20} S_{10}^2 ;$$

$$S_{30} = -S_{10}^4 ;$$

$$S_{12} = -2 S_{21} - 3 S_{30} ;$$

$$S_{22} = -9 (S_{10}^2 S_{12} + S_{10}^2 S_{11}^2) - 15 (S_{10}^2 S_{21} + 2 S_{20} S_{11} S_{10}) - 36 S_{30} S_{10}^2 ;$$

$$S_{31} = -4 S_{10}^3 S_{11} - 20 S_{20} S_{10}^3 ;$$

$$S_{40} = 0 ;$$

$$S_{13} = -2 S_{22} - 3 S_{31} - 4 S_{40} ;$$

$$S_{32} = -4 S_{10}^3 S_{12} - 6 S_{10}^2 S_{11}^2 - 20 (3 S_{20} S_{10}^2 + S_{21} S_{10}^3) - 84 S_{30} S_{10}^3 ;$$

: 66 :

$$\begin{aligned}
 S_{23} = & S_{20}^{-3} (3 S_{10}^2 S_{13} + 6 S_{10} S_{11} S_{12} + S_{11}^3) \\
 & - 15 (S_{20} S_{11}^2 + 2 S_{20} S_{10} S_{12} + 2 S_{21} S_{10} S_{11} \\
 & + S_{22} S_{10}^2) - 36 (S_{10}^2 S_{31} + 2 S_{30} S_{10} S_{11}) \\
 & - 66 S_{40} S_{10}^2 ;
 \end{aligned}$$

$$S_{41} = - 15 S_{20} S_{10}^4 ;$$

$$S_{50} = 0 ;$$

$$S_{14} = - 2 S_{23} - 3 S_{32} - 4 S_{41} - 5 S_{50} \quad \dots (3.4)$$

etc.

The coefficients obtained on solving the above set of equations are given in Table 3.II. The equation for α (2.31) works out to be

$$\begin{aligned}
 S_{10} \alpha^4 + (S_{11} + S_{20}) \alpha^3 + (1 + S_{12} + S_{21} + S_{30}) \alpha^2 \\
 + (1 + S_{13} + S_{22} + S_{31} + S_{40}) \alpha + (S_{14} + S_{23} + S_{32} + S_{41} + S_{50}) = 0 \\
 \dots (3.5)
 \end{aligned}$$

Using the S_{nm} values given in Table 3.II, we get

$$\begin{aligned}
 0.333334 \alpha^4 + 0.111111 \alpha^3 - 0.9876542 \alpha^2 \\
 - 0.9753087 \alpha + 0.148148 = 0 \quad \dots (3.6)
 \end{aligned}$$

Table 3.II - The S_{nm} coefficients for the cubic map

$m \backslash n$	0	1	2	3	4
1	-0.33334	-0.222223	-0.0370371	-4.470349×10^{-8}	-0.222218
2	0.1111111	0.0370370	-0.07407406	-0.02057637	
3	-0.02234568	0.04938272	0.1152264		
4	0	-0.2057614			
5	0				

This can be solved for α and the only real and positive root that is greater than 1 is 1.928236. This is the acceptable value of α , very close to the numerical value which is 1.9277 [61].

The equation for the universal function $g(x)$ is found to be

$$g(x) = 1 - 1.763892 |x|^3 + 0.2072627 |x|^6 + 0.0442792 |x|^9 - 0.005537133 |x|^{12} \dots (3.7)$$

δ is the eigenvalue of the D matrix in equation (2.36). Using equations (2.33) - (2.35) for $z=3$, the elements of the matrix are obtained as,

$$\begin{aligned} D_{11} = & -\alpha - 3\alpha^3 \left(S_{10} + \frac{S_{11}}{\alpha} + \frac{S_{12}}{\alpha^2} + \frac{S_{13}}{\alpha^3} + \frac{S_{14}}{\alpha^4} \right) - \\ & - 6\alpha^2 \left(S_{20} + \frac{S_{21}}{\alpha} + \frac{S_{22}}{\alpha^2} + \frac{S_{23}}{\alpha^3} \right) \\ & - 9\alpha \left(S_{30} + \frac{S_{31}}{\alpha} + \frac{S_{32}}{\alpha^2} \right) - 12 \left(S_{40} + \frac{S_{41}}{\alpha} \right) \\ & - \frac{15S_{50}}{\alpha} ; \end{aligned}$$

$$D_{12} = -\alpha ;$$

$$D_{13} = -\alpha ;$$

$$\begin{aligned}
 D_{21} = & -6\alpha^2 \left[S_{10}^2 + \frac{2S_{10} S_{11}}{\alpha} + \frac{1}{\alpha^2} (2S_{10} S_{12} + S_{11}^2) \right. \\
 & + \frac{1}{\alpha^3} (2 S_{10} S_{13} + 2 S_{11} S_{12}) + \frac{1}{\alpha^4} (2 S_{10} S_{14} \\
 & + 2 S_{11} S_{13} + S_{12}^2) \left. \right] - 30\alpha [S_{20} S_{10} + \frac{1}{\alpha} (S_{20} S_{11} \\
 & + S_{10} S_{21}) + \frac{1}{\alpha^2} (S_{12} S_{20} + S_{21} S_{11} + S_{22} S_{10}) \\
 & + \frac{1}{\alpha^3} (S_{20} S_{13} + S_{21} S_{12} + S_{22} S_{11} + S_{23} S_{10})] \\
 & - 72 [S_{30} S_{10} + \frac{1}{\alpha} (S_{30} S_{11} + S_{31} S_{10}) \\
 & + \frac{1}{\alpha^2} (S_{30} S_{12} + S_{31} S_{11} + S_{32} S_{10})] \\
 & - \frac{121}{\alpha} [S_{40} S_{10} + \frac{1}{\alpha} (S_{40} S_{11} + S_{41} S_{10})] \\
 & - \frac{210 S_{50} S_{10}}{\alpha^2} ;
 \end{aligned}$$

$$\begin{aligned}
 D_{22} = & -6 \left[S_{10} + \frac{S_{11}}{\alpha} + \frac{S_{12}}{\alpha^2} \right] - 6 \left[\frac{S_{20}}{\alpha} + \frac{S_{21}}{\alpha^2} \right] \\
 & - \frac{9 S_{30}}{\alpha^2} ;
 \end{aligned}$$

$$D_{23} = -6 \left(S_{10} + \frac{S_{11}}{\alpha} + \frac{S_{12}}{\alpha^2} \right) ;$$

$$D_{32} = -9 \left(\frac{S_{10}^2}{\alpha} + \frac{2S_{10} S_{11}}{\alpha^2} \right) - \frac{30 S_{20} S_{10}}{\alpha^2} ;$$

$$\begin{aligned}
 D_{31} = & - \frac{6 s_{20} s_{10}}{\alpha^2} - 3\alpha [s_{10}^3 + \frac{3s_{10}^2 s_{11}}{\alpha} + \frac{1}{\alpha^2} (3s_{10}^2 s_{12} \\
 & + 3 s_{10} s_{11}^2) + \frac{1}{\alpha^3} (3 s_{10}^2 s_{13} + 6 s_{10} s_{11} s_{12} \\
 & + s_{11}^3)] - 60 [s_{20} s_{10}^2 + \frac{1}{\alpha} (2 s_{20} s_{10} s_{11} + s_{21} s_{10}^2) \\
 & + \frac{1}{\alpha^2} (2 s_{20} s_{10} s_{12} + s_{20} s_{11}^2 + 2 s_{21} s_{10} s_{11} \\
 & + s_{22} s_{10}^2)] - \frac{252}{\alpha} [s_{30} s_{10}^2 + \frac{1}{\alpha} (2 s_{30} s_{10} s_{11} \\
 & + s_{31} s_{10}^2)] - \frac{660 s_{40} s_{10}^2}{\alpha^2} ; \\
 D_{33} = & - 15 (\frac{s_{10}^2}{\alpha} + \frac{2s_{10} s_{11}}{\alpha^2}) \dots (3.8)
 \end{aligned}$$

Taking $[h]$ to be $[1, h_1, h_2]^T$, δ is the largest eigenvalue of the D matrix given in (3.8). This is calculated to be 6.118815, the numerical value being 6.0847 [61].

The eigen function $h(x)$ is given by

$$h(x) = 1 - 0.3640163 |x|^3 - 0.09410955 |x|^6 \dots (3.9)$$

3.3 Universal parameters of a quartic map

The set of equations for S_{nm} coefficients in the case of a quartic map with $z = 4$ is listed below.

$$S_{10} = -\frac{1}{4} ;$$

$$S_{11} + 2S_{20} = 0 ;$$

$$S_{12} + 2S_{21} + 3S_{30} = 0 ;$$

$$S_{13} + 2S_{22} + 3S_{31} + 4S_{40} = 0 ;$$

$$S_{14} + 2S_{23} + 3S_{32} + 4S_{41} + 5S_{50} = 0 ;$$

$$S_{15} + 2S_{24} + 3S_{33} + 4S_{42} + 5S_{51} + 6S_{60} = 0 ;$$

$$S_{16} + 2S_{25} + 3S_{34} + 4S_{43} + 5S_{52} + 6S_{61} + 7S_{70} = 0 ;$$

$$S_{20} + 6S_{10}^3 = 0 ;$$

$$S_{21} + 18S_{10}^2 S_{11} + 28S_{20} S_{10}^2 = 0 ;$$

$$S_{22} + 18 (S_{10}^2 S_{12} + S_{10} S_{11}^2) + 28 (S_{10}^2 S_{21} + 2 S_{20} S_{11} S_{10}) + 66 S_{30} S_{10}^2 = 0 ;$$

: 72 :

$$\begin{aligned} s_{23} + 6 (3 s_{10}^2 s_{13} + 6 s_{10} s_{11} s_{12} + s_{11}^3) \\ + 28 (2 s_{10} s_{20} s_{12} + s_{20} s_{11}^2 + 2 s_{21} s_{10} s_{11} \\ + s_{22} s_{10}^2) + 66 (s_{10}^2 s_{31} + 2 s_{30} s_{10} s_{11}) \\ + 120 s_{40} s_{10}^2 = 0 ; \end{aligned}$$

$$\begin{aligned} s_{24} - s_{20} + 18 (s_{10}^2 s_{14} + 2 s_{10} s_{11} s_{12} + s_{10}^2 s_{12} \\ + s_{11}^2 s_{12}) + 28 (2 s_{20} s_{10} s_{13} + 2 s_{20} s_{11} s_{12} \\ + 2 s_{21} s_{10} s_{12} + s_{20}^2 s_{11} + 2 s_{22} s_{10} s_{11} \\ + s_{23} s_{10}^2) + 66 (2 s_{31} s_{10} s_{11} + s_{30} s_{11}^2 + 2 s_{30} s_{10} s_{12} \\ + s_{32} s_{10}^2) + 120 (2 s_{40} s_{10} s_{11} + s_{41} s_{10}^2) \\ + 190 s_{50} s_{10}^2 = 0 ; \end{aligned}$$

$$\begin{aligned} s_{25} - s_{21} + 18 (s_{10}^2 s_{15} + 2 s_{10} s_{11} s_{14} + s_{11}^2 s_{13} \\ + 2 s_{10} s_{12} s_{13} + s_{11}^2 s_{12}) + 28 (2 s_{20} s_{10} s_{14} \\ + 2 s_{20} s_{11} s_{13} + s_{20}^2 s_{12} + 2 s_{21} s_{10} s_{13} + 2 s_{21} s_{11} s_{12} \\ + 2 s_{22} s_{10} s_{12} + s_{22}^2 s_{11} + 2 s_{23} s_{10} s_{11} + s_{24} s_{10}^2) \\ + 66 (2 s_{30} s_{10} s_{13} + 2 s_{30} s_{11} s_{12} + 2 s_{31} s_{10} s_{12} \\ + s_{31} s_{11}^2 + 2 s_{32} s_{10} s_{11} + s_{33} s_{10}^2) + 120 (s_{40} s_{11}^2) \end{aligned}$$

$$\begin{aligned}
 & + 2s_{40}s_{10} s_{12} + 2s_{41}s_{10}s_{11} + s_{42}s_{10}^2) \\
 & + 190 (2 s_{30}s_{10}s_{11} + s_{51}s_{10}^2) + 276s_{60}s_{10}^2 = 0 ;
 \end{aligned}$$

$$s_{30} + 4 s_{10}^4 = 0 ;$$

$$s_{31} + 16 s_{10}^3 s_{11} + 56 s_{20} s_{10}^3 = 0 ;$$

$$\begin{aligned}
 s_{32} + 4 (4 s_{10}^3 s_{12} + 6 s_{10}^2 s_{11}^2) + 56 (3 s_{20}s_{10}^2 s_{11} \\
 + s_{21}s_{10}^3) + 220 s_{30}s_{10}^3 = 0 ;
 \end{aligned}$$

$$\begin{aligned}
 s_{33} + 16 (s_{10}^3 s_{13} + 3 s_{10}^2 s_{11} s_{12} + s_{10} s_{11}^3) + 56 (s_{22}s_{10}^3 \\
 + 3 s_{20}s_{10}^2 s_{12} + 3 s_{20}s_{10}s_{11}^2 + 3 s_{21}s_{11}) \\
 + 220 (s_{31}s_{10}^3 + 3 s_{30} s_{10}^2 s_{11}) + 560s_{40}s_{10}^3 = 0 ;
 \end{aligned}$$

$$\begin{aligned}
 s_{34} + 4 (4 s_{10}^3 s_{14} + 12 s_{10}^2 s_{11} s_{13} + 12s_{10} s_{11}^2 s_{12} \\
 + 6 s_{10}^2 s_{12}^2 + s_{11}^4) + 56 (3 s_{20}s_{10}^2 s_{13} \\
 + 3 s_{22}s_{10}^2 s_{11} + 3 s_{31}s_{10}^2 s_{11} + s_{30}s_{10}^3) \\
 + 220 (3 s_{40}s_{10}^2 s_{11} + s_{41} s_{10}^3) + 560 s_{50} s_{10}^3 \\
 + 12 s_{20} s_{10}^2 = 0 ;
 \end{aligned}$$

$$s_{40} + s_{10}^5 = 0 ;$$

: 74 :

$$S_{41} + 5 S_{10}^4 S_{11} + 70 S_{20}^4 S_{10} = 0 ;$$

$$S_{42} + 5 (S_{10}^4 S_{12} + 2 S_{10}^3 S_{11}^2) + 70 (4 S_{20}^3 S_{10} S_{11} + S_{21} S_{10}^4) + 495 S_{30}^4 S_{10} = 0 ;$$

$$S_{43} + 5 (S_{10}^4 S_{13} + 4 S_{10}^3 S_{11} S_{12} + 2 S_{10}^2 S_{11}^3) + 70 (4 S_{20}^3 S_{10} S_{12} + 6 S_{20}^2 S_{10}^2 S_{11} + 4 S_{21} S_{10}^3 S_{11} + S_{22} S_{10}^4) + 495 (4 S_{30}^3 S_{10} S_{11} + S_{31} S_{10}^4) + 1820 S_{40}^4 S_{10} = 0 ;$$

$$S_{50} = 0 ;$$

$$S_{51} + 56 S_{20}^5 S_{10} = 0 ;$$

$$S_{52} + 56 (5 S_{10}^4 S_{11} S_{20} + S_{21} S_{10}^5) + 792 S_{30}^5 S_{10} = 0 ;$$

$$S_{60} = 0 ;$$

$$S_{61} + 168 S_{20}^6 S_{10} = 0 ;$$

$$S_{70} = 0 \quad \text{etc.} \quad \dots (3.10)$$

The values of the S_{nm} coefficients calculated using the above equations are given in Table 3-III. Using these, the equation for α (2.31) with terms

Table 3.III - The S_{nm} coefficients for the quartic map

$m \backslash n$	0	1	2	3	4	5	6
1	-0.25	-0.1875	-0.046875	-3.90625×10^{-3}	0	-0.1875	-0.029846191
2	0.09375	0.046875	-0.05273438	-0.1171875	-0.091186523	-0.183563232	
3	-0.015625	0.03515625	0.107421875	0.185546875	0.240356445		
4	9.765625×10^{-4}	-0.021972656	-0.053100585	-0.107116699			
5	0	5.126953×10^{-3}	9.7045898×10^{-3}				
6	0	$-6.40869141 \times 10^{-4}$					
7	0						

upto $1/\alpha^2$ is obtained:

$$\alpha^5 + 0.375\alpha^4 + 0.0625\alpha^3 - 3.91796875\alpha^2 - 3.873046875\alpha + 0.564453125 = 0 \quad \dots (3.11)$$

This equation gives only one real and positive solution greater than one ie.1.690781026. This is in good agreement with the numerical value of α for $z = 4$. viz. 1.69 [61].

The universal function $g(x)$ is,

$$g(x) = 1 - 1.893139806 x^4 + 0.19320775 x^8 + 0.137176782 x^{12} - 0.030593823 x^{16} + 0.001793430346 x^{10} \dots \quad \dots (3.12)$$

The elements of the D matrix in the equation for δ in (2.36) are obtained in this case as,

$$D_{11} = -\alpha - 4\alpha^4 \left[S_{10} + \frac{S_{11}}{\alpha} + \frac{S_{12}}{\alpha^2} + \frac{S_{13}}{\alpha^3} + \frac{S_{14}}{\alpha^4} + \frac{S_{15}}{\alpha^5} + \frac{S_{16}}{\alpha^6} \right] - 8\alpha^3 \left[S_{20} + \frac{S_{21}}{\alpha} + \frac{S_{22}}{\alpha^2} + \frac{S_{23}}{\alpha^3} + \frac{S_{24}}{\alpha^4} + \frac{S_{25}}{\alpha^5} \right] - 12\alpha^2 \left[S_{30} + \frac{S_{31}}{\alpha} + \frac{S_{32}}{\alpha^2} + \frac{S_{33}}{\alpha^3} + \frac{S_{34}}{\alpha^4} \right] - 16\alpha \left(S_{40} + \frac{S_{41}}{\alpha} + \frac{S_{42}}{\alpha^2} + \frac{S_{43}}{\alpha^3} - 20[S_{50} + \frac{S_{51}}{\alpha} + \frac{S_{52}}{\alpha^2}] - \frac{24}{\alpha} (S_{60} + \frac{S_{61}}{\alpha}) - \frac{28}{\alpha^2} S_{10} \right) ;$$

$$D_{12} = -\alpha ;$$

$$D_{13} = -\alpha ;$$

$$D_{14} = -\alpha ;$$

$$\begin{aligned}
 D_{21} = & -12\alpha^3 \left[S_{10}^2 + \frac{2S_{10}S_{11}}{\alpha} + \frac{1}{\alpha^2} (2S_{10}S_{12} + S_{11}^2) \right. \\
 & + \frac{1}{\alpha^3} (2S_{10}S_{13} + 2S_{11}S_{12}) + \frac{1}{\alpha^4} (2S_{10}S_{14} \\
 & + 2S_{11}S_{13} + S_{12}^2) + \frac{1}{\alpha^5} (2S_{10}S_{15} + 2S_{11}S_{14} \\
 & + 2S_{12}S_{13}) \left. \right] - 56\alpha^2 \left[S_{20}S_{10} + \frac{1}{\alpha} (S_{20}S_{11} \right. \\
 & + S_{10}S_{21}) + \frac{1}{\alpha^2} (S_{12}S_{20} + S_{21}S_{11} + S_{22}S_{10}) \\
 & + \frac{1}{\alpha^3} (S_{20}S_{13} + S_{21}S_{12} + S_{22}S_{11} + S_{23}S_{10}) \\
 & + \frac{1}{\alpha^4} (S_{20}S_{14} + S_{21}S_{13} + S_{22}S_{12} + S_{23}S_{11} \\
 & + S_{24}S_{10}) \left. \right] - 121\alpha \left[S_{30}S_{10} + \frac{1}{\alpha} (S_{30}S_{11} + S_{31}S_{10} \right. \\
 & + \frac{1}{\alpha^2} (S_{30}S_{12} + S_{31}S_{11} + S_{32}S_{10}) + \frac{1}{\alpha^3} (S_{30}S_{13} \\
 & + S_{31}S_{12} + S_{32}S_{11} + S_{33}S_{10}) \left. \right] - 240 \left[S_{40}S_{10} \right. \\
 & + \frac{1}{\alpha} (S_{40}S_{11} + S_{41}S_{10}) + \frac{1}{\alpha^2} (S_{40}S_{12} + S_{41}S_{11} \\
 & + S_{42}S_{10}) \left. \right] - \frac{380}{\alpha} \left[S_{50}S_{10} + \frac{1}{\alpha} (S_{50}S_{11} + S_{51}S_{10}) \right] \\
 & - \frac{552 S_{60}S_{10}}{\alpha^2} ;
 \end{aligned}$$

$$D_{22} = -8 \left(s_{10} + \frac{s_{11}}{\alpha} + \frac{s_{12}}{\alpha^2} \right) - 8 \left(\frac{s_{20}}{\alpha} + \frac{s_{21}}{\alpha^2} \right) - \frac{12s_{30}}{\alpha^2} ;$$

$$D_{23} = -8 \left(s_{10} + \frac{s_{11}}{\alpha} + \frac{s_{12}}{\alpha^2} \right) ;$$

$$D_{31} = - \frac{12}{\alpha^2} s_{20} s_{10} - 12 \alpha^2 \left[s_{10}^3 + \frac{3s_{10}^2 s_{11}}{\alpha} + \frac{1}{\alpha^2} (3 s_{10}^2 s_{12} + 3 s_{10} s_{11}^2) + \frac{1}{\alpha^3} (3 s_{10}^2 s_{13} + 6 s_{10} s_{11} s_{12} + s_{11}^3) + \frac{1}{\alpha^4} (3 s_{10}^4 s_{14} + 6 s_{10} s_{11} s_{13} + 3 s_{11}^2 s_{12} + 3 s_{10} s_{12}^2) \right] - 168\alpha \left[s_{20} s_{10}^2 + \frac{1}{\alpha} (2 s_{20} s_{10} s_{11} + s_{21} s_{10}^2) + \frac{1}{\alpha^2} (2s_{20} s_{10} s_{12} + s_{20} s_{11}^2 + 2 s_{21} s_{10} s_{11} + s_{22} s_{10}^2) + \frac{1}{\alpha^3} (2 s_{20} s_{10} s_{13} + 2 s_{20} s_{11} s_{12} + 2 s_{21} s_{10} s_{12} + s_{21} s_{11}^2 + 2 s_{22} s_{10} s_{11} + s_{23} s_{10}^2) \right] - 660 \left[s_{30} s_{10}^2 + \frac{1}{\alpha} (2 s_{30} s_{10} s_{11} + s_{31} s_{10}^2) + \frac{1}{\alpha^2} (2s_{30} s_{10} s_{12} + s_{30} s_{11}^2 + 2 s_{31} s_{10} s_{11} + s_{32} s_{10}^2) \right] - \frac{1680}{\alpha} \left[s_{40} s_{10}^2 + \frac{1}{\alpha} (2 s_{40} s_{10} s_{11} + s_{41} s_{10}^2) \right] - \frac{3420}{\alpha^2} s_{50} s_{10}^2 ;$$

$$D_{32} = - 18 \left(\frac{s_{10}^2}{\alpha} + \frac{2 s_{10} s_{11}}{\alpha^2} \right) - \frac{56}{\alpha^2} s_{20} s_{10} ;$$

$$D_{24} = - 12 \left(s_{10} + \frac{s_{11}}{\alpha} + \frac{s_{12}}{\alpha^2} \right) ;$$

$$D_{33} = - 28 \left(\frac{S_{10}^2}{\alpha} + \frac{2S_{10} S_{11}}{\alpha^2} \right) ;$$

$$D_{34} = - 66 \left(\frac{S_{10}^2}{\alpha} + \frac{2S_{10}S_{11}}{\alpha^2} \right) ;$$

$$\begin{aligned} D_{41} = & - 4\alpha \left[S_{10}^4 + \frac{4S_{10}^3 S_{11}}{\alpha} + \frac{1}{\alpha^2} (4S_{10}^3 S_{12} + 6S_{10}^2 S_{11}^2) \right. \\ & + \frac{1}{\alpha^3} (4 S_{10}^3 S_{13} + 12 S_{10}^2 S_{11} S_{12} + 4 S_{10} S_{11}^3)] \\ & - 280 [S_{20} S_{10}^3 + \frac{1}{\alpha} (3 S_{20} S_{10}^2 S_{11} + S_{21} S_{10}^3) \\ & + \frac{1}{\alpha^2} (3 S_{20} S_{10}^2 S_{12} + 3 S_{20} S_{10} S_{11}^2 + 3 S_{21} S_{10}^2 S_{11} \\ & + S_{22} S_{10}^3)] - \frac{1980}{\alpha} [S_{30} S_{10}^3 + \frac{1}{\alpha} (3S_{30} S_{10}^2 S_{11} \\ & + S_{31} S_{10}^3)] - \frac{7280}{\alpha^2} S_{40} S_{10}^3 ; \end{aligned}$$

$$D_{42} = - \frac{16S_{10}^3}{\alpha^2} ;$$

$$D_{43} = - \frac{56S_{10}^3}{\alpha^2} ;$$

$$D_{44} = - \frac{220S_{10}^3}{\alpha^2} . \quad \dots (3.13)$$

The S_{nm} coefficients given in Table 3.III are used to get the D matrix as,

$$D = \begin{bmatrix} 6.48161599 & -1.690781026 & -1.690781026 & -1.690781026 \\ -0.67462368 & 2.509170305 & 3.018340608 & 4.527510912 \\ -2.93711342 & -0.796549616 & -1.953261165 & -4.604115602 \\ -1.13037874 & 0.08745110 & 0.30607885 & 1.202452628 \\ \dots & \dots & \dots & \dots \end{bmatrix} \quad \dots (3.14)$$

This matrix has only one eigenvalue greater than 1 and it is the acceptable value of δ which is 7.23682924. The numerically obtained value is 7.284 [61].

The corresponding h function in this case reads

$$h(x) = 1 - 0.2290202 x^4 - 0.382212 x^8 + 0.1646167 x^{12} + \dots \quad \dots (3.15)$$

3.4 Universal constants of nonpolynomial maps

Numerically it has been shown that there exists a spectrum of universality classes corresponding to all possible values of z [51]. Thus one can even consider nonpolynomial maps with fractional z values. For some systems due to symmetry or other reasons, the quadratic term may vanish and then maps with higher z values arise as natural reductions. They exhibit interesting phenomena near the onset of chaos [62]. Maps with $z = 1.2$ to 1.4 do occur in chemical turbulence [63].

Kawai and Tye consider maps whose extrema have a logarithmic dependence on x [64]. One dimensional maps of systems with finite degrees of freedom sometimes show nonpolynomial behaviour, a well known example being the Lorenz model [22]. These maps are usually discontinuous at the critical point and the existing method is to approximate them by piecewise linear maps.

For fractional z values, the index m may take fractional as well as integer values and the evaluation of S_{nm} becomes rather difficult. Further, there can arise ambiguities in choosing a cut-off as required by the perturbative procedure. Hence we follow an alternative method that consists in expanding z about z' , where z' is the integer nearest to the fractional z value. Thus we write $z = z' \pm \epsilon$ where $0 < |\epsilon| < 0.5$.

To illustrate the method, we take $z' = 2$. Writing $\alpha = \alpha_0 \mp \delta\alpha$ where α_0 is the value of α for quadratic maps, we find

$$\alpha_0 = 1 + \epsilon \ln \alpha_0 + \frac{\epsilon^2}{2!} (\ln \alpha_0)^2 + \dots \quad \dots(3.16)$$

$$\alpha^{2+\epsilon} = \alpha_0^\epsilon [\alpha_0^2 - (2+\epsilon) \alpha_0 d\alpha] \quad \dots (3.17)$$

where terms containing higher powers of ϵ and $d\alpha$ have been neglected.

Equation (2.31) for $z = 2$ works out to be

$$1+\alpha = |\alpha|^2 \left(\frac{1}{2} + \frac{1}{8\alpha} + \frac{5}{32\alpha^3} + \dots \right) \quad \dots (3.18)$$

Using the expansions given in (3.16) and (3.17), in (3.18), the change in the α value for a given ϵ is,

$$\begin{aligned} d\alpha = & [p_0 + \epsilon(p_1 + p_2 \ln \alpha_0) + \epsilon^2 (p_3 + p_1 \ln \alpha_0 \\ & + \frac{p_2(\ln \alpha_0)^2}{2!})] / [q_0 + \epsilon(q_1 + q_2 \ln \alpha_0) \\ & + \epsilon^2 (q_3 + q_1 \ln \alpha_0 + \frac{q_2(\ln \alpha_0)^2}{2!})] \quad \dots (3.19) \end{aligned}$$

where the coefficients p and q are given in Table 3.IV. For $\epsilon = 0$, $z = 2$ and $d\alpha = 0$ ie. $p_0 = 0$ in (3.19). This gives $\alpha_0 = 2.5$.

Using the same expansion procedure in equation (2.40) we obtain

Table 3.IV - The p and q coefficients in (3.19)

$p_0 = \frac{\alpha_0^2}{2} - \frac{7}{8} \alpha_0 - 1 + \frac{5}{32\alpha_0}$	$q_0 = \alpha_0 - \frac{7}{8} - \frac{5}{32\alpha_0^2}$
$p_1 = -\frac{\alpha_0^2}{4} - \frac{1}{128\alpha_0} + \frac{1}{48}$	$q_1 = \frac{1}{8} - \frac{21}{128\alpha_0^2}$
$p_2 = \frac{\alpha_0^2}{2} + \frac{\alpha_0}{8} + \frac{5}{32\alpha_0}$	$q_2 = \alpha_0 + \frac{1}{8} - \frac{5}{32\alpha_0^2}$
$p_3 = \frac{\alpha_0^2}{8} - \frac{\alpha_0}{32} - \frac{1}{96} - \frac{1}{32\alpha_0}$	$q_3 = -\frac{1}{32} + \frac{1}{48\alpha_0} + \frac{3}{128\alpha_0^2}$

$$\begin{aligned}
 2\delta = & a_0 + \epsilon a_1 + \epsilon^2 a_2 + d\alpha [b_0 + \epsilon b_1 + \epsilon^2 b_2] \\
 & + [c_0 + \epsilon(c_1 + c_1' \ln \alpha_0) + \epsilon^2 (c_2 + c_2' \ln \alpha_0 \\
 & + c_2''(\ln \alpha_0)^2) + d\alpha (d_0 + \epsilon(d_1 + d_1' \ln \alpha_0) \\
 & + \epsilon^2 (d_2 + d_2' \ln \alpha_0 + d_2''(\ln \alpha_0)^2))]^{\frac{1}{2}} \quad \dots (3.20)
 \end{aligned}$$

The coefficients a_0, a_1, \dots are given in Table 3.V.

For $\epsilon = 0$ and $d\alpha = 0$, the value of δ_0 is given by

$$\begin{aligned}
 \delta_0 = & \frac{1}{2} \left[\alpha_0^2 - \alpha_0 + 2 + \frac{1}{2\alpha_0} + (\alpha_0^4 + 2\alpha_0^3 - \alpha_0^2 + 2\alpha_0 \right. \\
 & \left. + 4 + \frac{2}{\alpha_0})^{\frac{1}{2}} \right] \quad \dots (3.21)
 \end{aligned}$$

For $\alpha_0 = 2.5$, we get $\delta_0 = 4.660415379$.

The values of α and δ for different values of ϵ are given in Tables 3.VI and 3.VII. We find the values are sufficiently accurate for small values of ϵ . The error in δ is more due to the accumulation of errors from α_0, δ_0 and $d\alpha$.

Table 3.V - The coefficients $a_0, a_1 \dots$ occurring in (3.20)

$a_0 = \alpha_0^2 - \alpha_0 + 2 + \frac{1}{2\alpha_0}$ $a_1 = \alpha_0^2 \ln \alpha_0 + \frac{1}{4\alpha_0}$ $a_2 = \frac{\alpha_0^2 (\ln \alpha_0)^2}{2!} - \frac{1}{8\alpha_0}$	$b_0 = 1 - 2\alpha_0 + \frac{1}{2\alpha_0^2}$ $b_1 = -\alpha_0 - 2\alpha_0 \ln \alpha_0 + \frac{1}{4\alpha_0^2}$ $b_2 = -\alpha_0 \ln \alpha_0 - \alpha_0 (\ln \alpha_0)^2 - \frac{1}{8\alpha_0^2}$
$c_0 = \alpha_0^4 - 2\alpha_0^3 - \alpha_0^2 + 2\alpha_0 + 4 + \frac{2}{\alpha_0}$ $c_1 = \alpha_0^2 - \frac{\alpha_0}{2} + \frac{1}{\alpha_0} - \frac{1}{2}$ $c_1' = 2\alpha_0^4 - 2\alpha_0^3 - 2\alpha_0^2 - 2\alpha_0 - 1$ $c_2 = -\frac{\alpha_0^2}{2} + \frac{\alpha_0}{2} - \frac{1}{2\alpha_0}$ $c_2' = \alpha_0^2 - \frac{\alpha_0}{2} - 1$ $c_2'' = 2\alpha_0^4 - \alpha_0^3 - \alpha_0^2 - \alpha_0 - \frac{1}{2}$	$d_0 = -4\alpha_0^3 + 6\alpha_0^2 + 2\alpha_0 + \frac{2}{\alpha_0^2} - 2$ $d_1 = -2\alpha_0^3 + 2\alpha_0^2 + \frac{1}{\alpha_0} + \frac{1}{\alpha_0^2} + \frac{5}{2}$ $d_1' = -8\alpha_0^3 + 6\alpha_0^2 + 4\alpha_0 + 2$ $d_2 = -\frac{1}{2\alpha_0^2} + \frac{1}{\alpha_0}$ $d_2' = -4\alpha_0^3 + 2\alpha_0^2 + \frac{1}{\alpha_0} + \frac{5}{2}$ $d_2'' = -8\alpha_0^3 + 3\alpha_0^2 + 2\alpha_0 + 1$

Table 3.VI - Values of α for different values of ϵ

z	ϵ	α	z	ϵ	α
2.01	0.01	2.48972863	1.99	-0.01	2.51050864
2.02	0.02	2.47968810	1.98	-0.02	2.52126123
2.03	0.03	2.46987213	1.97	-0.03	2.53226461
2.04	0.04	2.46027465	1.96	-0.04	2.54352586
2.05	0.05	2.45088977	1.95	-0.05	2.55505228
2.06	0.06	2.44171178	1.94	-0.06	2.56685137
2.07	0.07	2.43273514	1.93	-0.07	2.57893088
2.08	0.08	2.42395446	1.92	-0.08	2.59129880
2.09	0.09	2.41536454	1.91	-0.09	2.60396334
2.1	0.10	2.40696031	1.90	-0.10	2.61693298
2.2	0.20	2.33212098	1.80	-0.20	2.76546462
2.3	0.30	2.27127801	1.70	-0.30	2.95590441
2.4	0.40	2.22131078	1.40	-0.40	3.20158779
2.5	0.50	2.17988403	1.50	-0.50	3.51838508

Table 3.VII - Values of δ for different values of ϵ

z	ϵ	δ	z	ϵ	δ
2.01	0.01	4.675260170	1.99	-0.01	4.645299095
2.02	0.02	4.689811193	1.98	-0.02	4.629933778
2.03	0.03	4.704047684	1.97	-0.03	4.61434967
2.04	0.04	4.717950242	1.96	-0.04	4.598569856
2.05	0.05	4.723840994	1.95	-0.05	4.582625646
2.06	0.06	4.744680047	1.94	-0.06	4.566548998
2.07	0.07	4.757478773	1.93	-0.07	4.550374359
2.08	0.08	4.769875397	1.92	-0.08	4.53413879
2.09	0.09	4.781858018	1.99	-0.09	4.517882072
2.1	0.10	4.793413203	1.90	-0.10	4.501647019
2.2	0.20	4.882918566	1.80	-0.20	4.352394078
2.3	0.30	4.917969637	1.70	-0.30	4.280301067

3.5 Comments and discussion

The perturbative expansion procedure discussed in this chapter and the preceding one has certain advantages over existing methods of evaluating universal parameters. Although some amount of computation cannot be avoided in the final steps, the method is an analytic procedure. This approach is algebraically much simpler even when z is large. Thus for the quartic map, we note that the δ values we obtained for the three successive approximations of $[h]$ are, 6.757592744, 7.48537771 and 7.23682924, the last value being the closest to the numerically computed one. It would be interesting to compare this behaviour with that found in an eigenvalue matching RG calculation [65], where in the values 9.31426, 8.08956, and 6.99948 are obtained corresponding to 1-2 cycles, 1-4 cycles and 2-4 cycles renormalisation. We find that the perturbative method yields the best value in a sufficiently small number of steps.

4. FRACTAL DIMENSIONS OF THE FEIGENBAUM ATTRACTOR

For one dimensional maps of the form considered in the previous chapters, the period doubling cascade accumulates at λ_∞ , where the system possesses a 2^∞ orbit. The associated universal behaviour is characterised by the function $g(x)$ that satisfies (2.13). The iterates of $g(x)$ form a nearly self-similar Cantor set, called the Feigenbaum attractor. The nature of the self-similarity of such an attractor for one hump maps was studied in detail by Hu [66]. He derives analytic approximations for the first three dimensions D_0 , D_1 and D_2 . But in the actual calculations, an approximate $g(x)$ is used. We discuss the analytic expressions obtained using the $g(x)$ obtained by solving (2.13) by the perturbative scheme and given in (2.32). The generalised dimensions D_q for quadratic maps have been studied in detail by Jensen et al [67], and the D_0 and D_1 for attractors obtained by

period multiplications other than period doublings were calculated by Chang and McCown [68].

4.1 Self-similarity of the Feigenbaum attractor

The attractor consists of a set of points $(x_i)^k$ generated by the map

$$x_{i+1} = g(x_i), \quad \dots (4.1)$$

Starting from $x_0 = 0$. This set consists of two subsets, the even subset $(x_i)_{\text{even}}^k$ and the odd subset $(x_i)_{\text{odd}}^k$

$$(x_i)^k = (x_i)_{\text{even}}^k \cup (x_i)_{\text{odd}}^k \quad \dots (4.2)$$

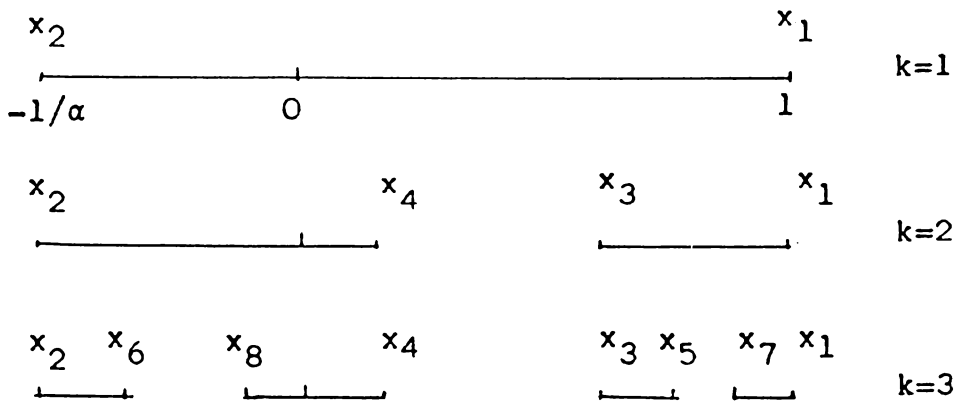
with

$$(x_i)_{\text{even}}^k = (x_i, i = 2, 4, \dots, 2^k) \quad \dots (4.3)$$

and

$$(x_i)_{\text{odd}}^k = (x_i, i = 1, 3, 5, \dots, 2^k - 1) \quad \dots (4.4)$$

Thus for $k = 1, 2, 3 \dots$ the set is shown in the figure



From the normalisation condition $g(0) = 1$ and from (2.13) we find,

$$\begin{aligned}
 x_1 &= 1 ; & x_2 &= -\frac{1}{\alpha} ; & x_3 &= g\left(\frac{1}{\alpha}\right) ; & x_4 &= \frac{1}{\alpha^2} \\
 x_5 &= g\left(\frac{1}{\alpha^2}\right) ; & x_6 &= -\frac{1}{\alpha} g\left(\frac{1}{\alpha}\right) ; & x_7 &= g\left(\frac{1}{\alpha}\left(g\left(\frac{1}{\alpha}\right)\right)\right) \\
 x_8 &= -\frac{1}{\alpha^3} \dots & & & & & \dots & (4.5)
 \end{aligned}$$

The whole set lies in the interval $(-\frac{1}{\alpha}, 1)$. It is possible to rescale the set such that the new set

$(x'_i)^k$ lies in the interval $(0,1)$; using the transformation [66]

$$x'_i = \frac{1}{(1+1/\alpha)} (x_i + \frac{1}{\alpha}) \quad \dots (4.6)$$

It is proved in [66] that the even subset is exactly similar to the whole set while the odd subset is only approximately so and we have the relation

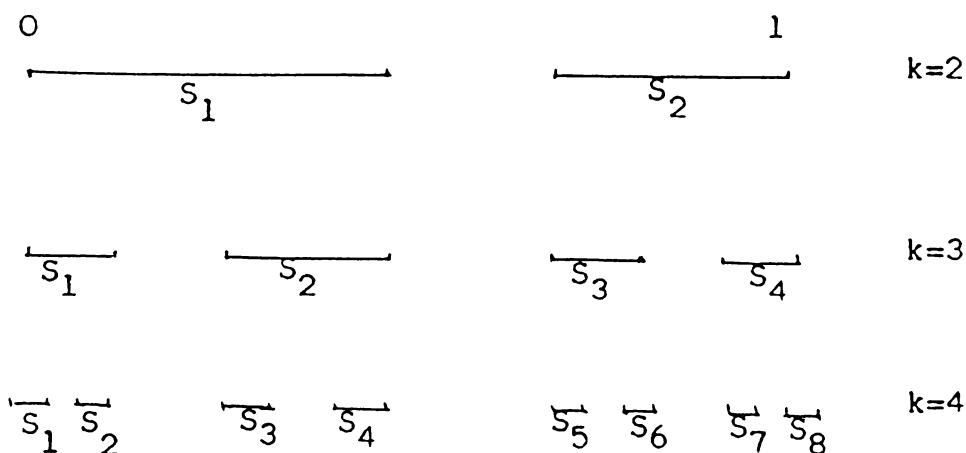
$$(x_i)^k \approx -\frac{1}{\alpha} (x_i)_{\text{even}}^{k-1} \cup \frac{1}{\alpha'} (x_i)_{\text{odd}}^{k-1} \quad \dots (4.7)$$

where $\alpha' = -\alpha g'(1)$. Each subset can be further divided into two subsets similar to it and so on. Thus the Feigenbaum attractor can be divided into 2^{m-1} subsets with $m > k$, as $S_1, S_2, \dots, S_{2^{m-1}}$ each having the same structure but rescaled by a different factor $1/S_j$, Here

$$S_j = \frac{1}{x'_{2^j} - x'_{2^{j-1}}} \quad \dots (4.8)$$

with the (x'_i) ordered such that

$$0 = x'_1 < x'_2 < x'_3 < \dots < x'_{2^{m-1}} = 1 \quad \dots (4.9)$$



The iterates given in (4.5) after the rescaling using equation (4.6) and the ordering mentioned in (4.9) become

$$x'_1 = 0 ; \quad x'_2 = \frac{1}{\alpha} \quad ; \quad x'_3 = \frac{1}{(1 + \frac{1}{\alpha})} [g(\frac{1}{\alpha}) + \frac{1}{\alpha}] ;$$

$$x'_4 = 1 \dots \dots (4.10)$$

The universal function $g(x)$ is obtained by solving (2.13). This has been done in Chapter 2 using the perturbative expansion method. Using the first few coefficients S_{nm} given in (2.37) in the expression for $g(x)$ in (2.32), we find the universal function for any general z in the form,

$$g(x) = 1 - |\alpha|^z \left[\frac{1}{z\alpha} + \frac{(z-1)}{z^2\alpha^2} \right] |x|^z + \frac{\alpha^z(z-1)}{2z^2\alpha^2} |x|^{2z} + \dots \quad \dots (4.11)$$

The behaviour of $g(x)$ for some typical values of z is shown in Fig. 4.1.

4.2 The Capacity dimension D_0

Considering the first four iterates given in (4.10) we find the set consists of two subsets, that are scaled by S_1 and S_2 respectively. From (4.8) we get

$$S_1 = \frac{1}{x'_2 - x'_1} = \alpha \quad \dots (4.12)$$

and

$$\begin{aligned} S_2 &= \frac{1}{x'_4 - x'_3} \\ &= \frac{(1 + \frac{1}{\alpha})}{(1 - g(\frac{1}{\alpha}))} \quad \dots (4.13) \end{aligned}$$

If it takes $N(\epsilon)$ steps of width ϵ to cover the whole set, then

$$N(\epsilon) = N(S_1\epsilon) + N(S_2\epsilon) \quad \dots (4.14)$$

For small ϵ ,

$$N(\epsilon) \propto \epsilon^{-D_0} \quad \dots (4.15)$$

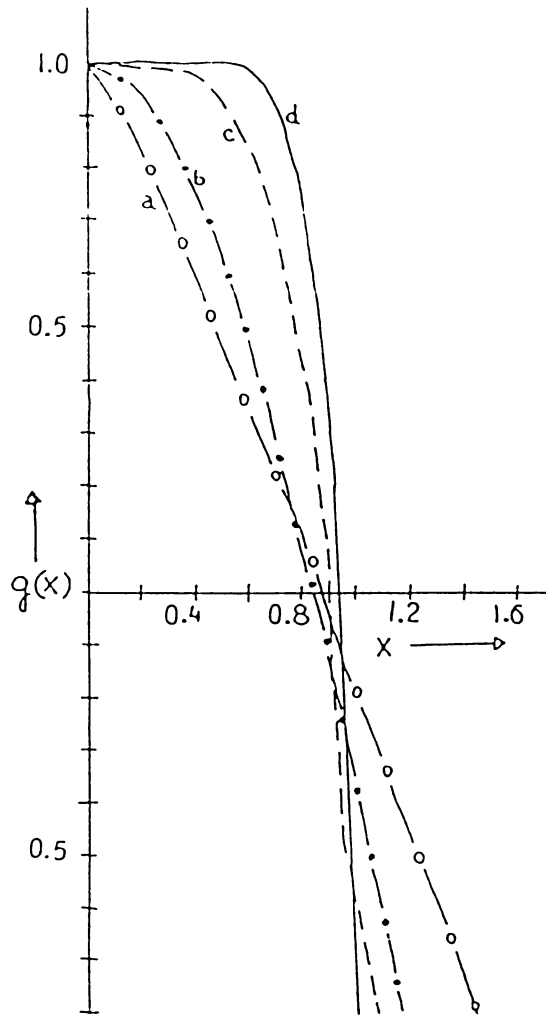


Fig. 4.1 - The universal function $g(x)$ computed using (4.11) for a) $z=1.2$, b) $z=2$, c) $z=5$, d) $z=10$

from the definition D_0 given in (1.44). Substituting (4.15) in (4.14)

$$\begin{aligned} \epsilon^{-D_0} &= (S_1 \epsilon)^{-D_0} + (S_2 \epsilon)^{-D_0} \\ \text{ie } 1 &= S_1^{-D_0} + S_2^{-D_0} \end{aligned} \quad \dots (4.16)$$

If we consider the set after m iterations, there will be $R = 2^{m-1}$ subsets and then (4.16) can be generalised to [66]' :

$$\sum_{j=1}^R (S_j)^{-D_0} = 1 \quad \dots (4.17)$$

As a first approximation, we use (4.16) to derive an expression for D_0 . Substituting for S_1 and S_2 from (4.12) and (4.13)

$$\left(\frac{1}{\alpha}\right)^{D_0} + \left[\frac{1 - g\left(\frac{1}{\alpha}\right)}{1 + \frac{1}{\alpha}} \right]^{D_0} = 1 \quad \dots (4.18)$$

From (2.39) we have

$$\frac{1}{\alpha} + 1 = \frac{|\alpha|^z}{z\alpha} \left[1 - \frac{(z-1)}{2z\alpha} \right]^{-1} \quad \dots (4.19)$$

Using (4.11)

$$g\left(\frac{1}{\alpha}\right) = 1 - \left[\frac{1}{z\alpha} + \frac{(z-1)}{z^2\alpha^2}\right] + \frac{(z-1)}{2\alpha^{z+2}z^2} \dots (4.20)$$

Then (4.18) can be simplified as,

$$\frac{1}{\alpha^{D_0}} + \frac{\left[1 + \frac{(z-1)}{2z\alpha}\right]^{D_0}}{\alpha^z D_0} = 1 \dots (4.21)$$

This is a transcendental equation for D_0 . For a given z , α is computed using (4.19) and (4.21) is solved by the successive bisection method [80] to get D_0 . The results are given in Table 4.I. The variation of D_0 with z is given in Fig. 4.2. The numerical values for $z = 2, 3, 4$ and 5 [66] are also shown for comparison. Our calculations give $D_0 = 0.5366545$ for $z = 2$, very close to the numerical value 0.538 [67].

We find that the expression (4.18) has been recently derived by Bhattacharjee [69]. He derives an interpolation formula for D_0 . The values of D_0 calculated using his equation do not agree with our computed values for higher values of z .

4.3 The information dimension D_1

Using similar scaling arguments, we derive an expression for D_1 . The information entropy defined

Table 4.I - The values of the capacity dimension D_0 for different z values. Available numerical values are also given [66].

z	α	D_0 (computed)	D_0 (numerical)
1.1	7.978673	0.3185205	
1.2	5.390312	0.3766027	
1.5	3.405767	0.4653759	
2.0	2.517021	0.5366545	0.538 ± 0.01
2.5	2.149665	6.5774682	
3.0	1.940393	0.6050853	0.601 ± 0.01
3.5	1.802739	0.6253683	
4.0	1.704310	0.6410400	0.640 ± 0.09
4.5	1.629944	0.6535812	
5.0	1.571511	0.6638768	0.661 ± 0.08
5.5	1.524224	0.6725070	
6.0	1.485068	0.6798533	
6.5	1.452041	0.6861959	
7.0	1.423759	0.6917333	
7.5	1.399233	0.6966110	
8.0	1.377734	0.7009468	
8.5	1.358715	0.7048263	
9.0	1.341753	0.7083248	
9.5	1.326520	0.7114913	
10.0	1.312754	0.7143796	
100.0	1.047940	0.7759078	

G3799

: 99 :

7
517.928.4
#MB

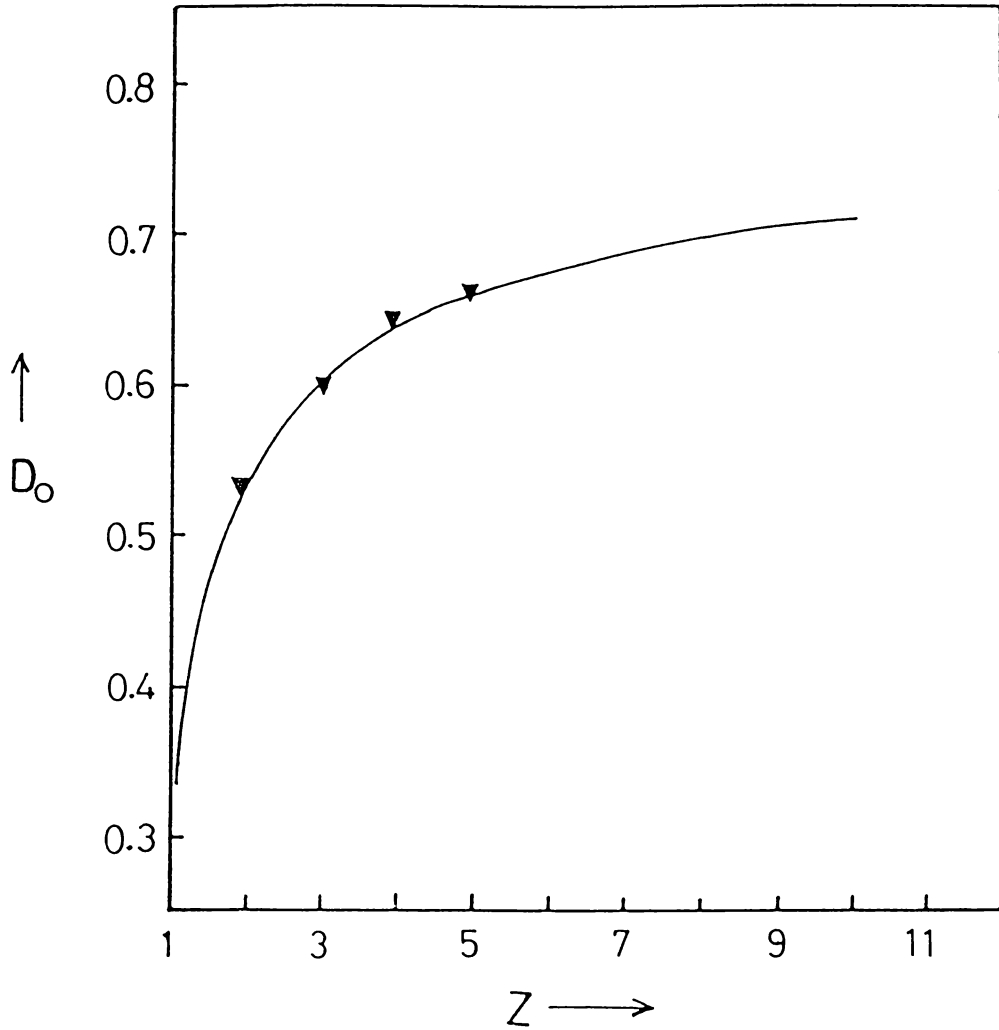


Fig. 4.2 - The values of the capacity dimension D_0 calculated using (4.21) for different z values. The triangles indicate the numerical values [66].

in (1.45) can be expressed as the sum of the contributions from the subsets S_1 and S_2 ie.

$$I(\epsilon) = I_1(\epsilon) + I_2(\epsilon) \quad \dots(4.22)$$

If the probability for the iterates to be in S_1 is p_1 and that to be in S_2 is p_2 we have $p_1+p_2 = 1$. Taking $N(\epsilon)$ to be the number of steps of width ϵ to cover the whole set, we require the same number to cover the subset S_1 at resolution ϵ/S_1 . Thus [31],

$$I_1(\epsilon) = p_1 \ln \frac{1}{p_1} + p_1 I(\epsilon S_1) \quad \dots(4.23)$$

$$I_2(\epsilon) = p_2 \ln \frac{1}{p_2} + p_2 I(\epsilon S_2) \quad \dots(4.24)$$

Then (4.22) gives,

$$I(\epsilon) = p_1 \ln \frac{1}{p_1} + p_2 \ln \frac{1}{p_2} + p_1 I(\epsilon S_1) + p_2 I(\epsilon S_2) \quad \dots(4.25)$$

For small ϵ , we have from (1.47)

$$I(\epsilon) \propto D_1 \ln \left(\frac{1}{\epsilon} \right) \quad \dots(4.26)$$

Then (4.25) can be written as,

$$D_1 \ln \left(\frac{1}{\epsilon} \right) = p_1 \ln \frac{1}{p_1} + p_2 \ln \frac{1}{p_2} + p_1 D_1 \ln \left(\frac{1}{\epsilon S_1} \right) + p_2 D_1 \ln \left(\frac{1}{\epsilon S_2} \right) \quad \dots(4.27)$$

Since p_1 and p_2 are equal in the present context,

$$p_1 = p_2 = \frac{1}{2}$$

Thus (4.27) gives,

$$D_1 \ln \left(\frac{1}{\epsilon} \right) = \ln 2 + \frac{1}{2} D_1 \left[\ln \left(\frac{1}{\epsilon S_1} \right) + \ln \left(\frac{1}{\epsilon S_2} \right) \right] \dots (4.28)$$

$$\text{ie. } D_1 = \frac{2 \ln 2}{\ln(S_1 S_2)} \dots (4.29)$$

In general if we are considering R subsets we get, [66]

$$D_1 = \frac{R \ln R}{\sum_{j=1}^R \ln S_j} \dots (4.30)$$

Using (4.12), (4.13), (4.19) and (4.20) in (4.29) and simplifying,

$$D_1 = \frac{2 \ln 2}{(z+1) \ln \alpha - \ln \left[1 + \frac{(z-1)}{2z\alpha} \right]} \dots (4.31)$$

Thus D_1 can be computed for a given z . For $z = 2$, the value is 0.5183, while the numerical value is 0.5171. The variation of D_1 with z is shown in Fig.4.3 while the computed values are given in Table 4.II. The computed values given in [66] are also plotted in Fig. 4.3 for comparison.

Table 4.II - The values of the information dimensions D_1 calculated using (4.31). Available numerical values are included for comparison [66].

z	D_1 (computed values)	D_1 (numerical values)
1.1	0.3182830	
1.2	0.3756095	
1.5	0.4596621	
2.0	0.5183313	0.517 ± 0.08
2.5	0.5440816	
3.0	0.5560675	0.557 ± 0.01
3.5	0.5609948	
4.0	0.5619522	0.556 ± 0.04
4.5	0.5605657	
5.0	0.5577611	
5.5	0.5540956	0.558 ± 0.02
6.0	0.5499165	
6.5	0.5454470	
7.0	0.5408324	
7.5	0.5361673	
8.0	0.5315165	
8.5	0.5269203	
9.0	0.5224089	
9.5	0.5179980	
10.0	0.5136993	
100.0	0.3192317	

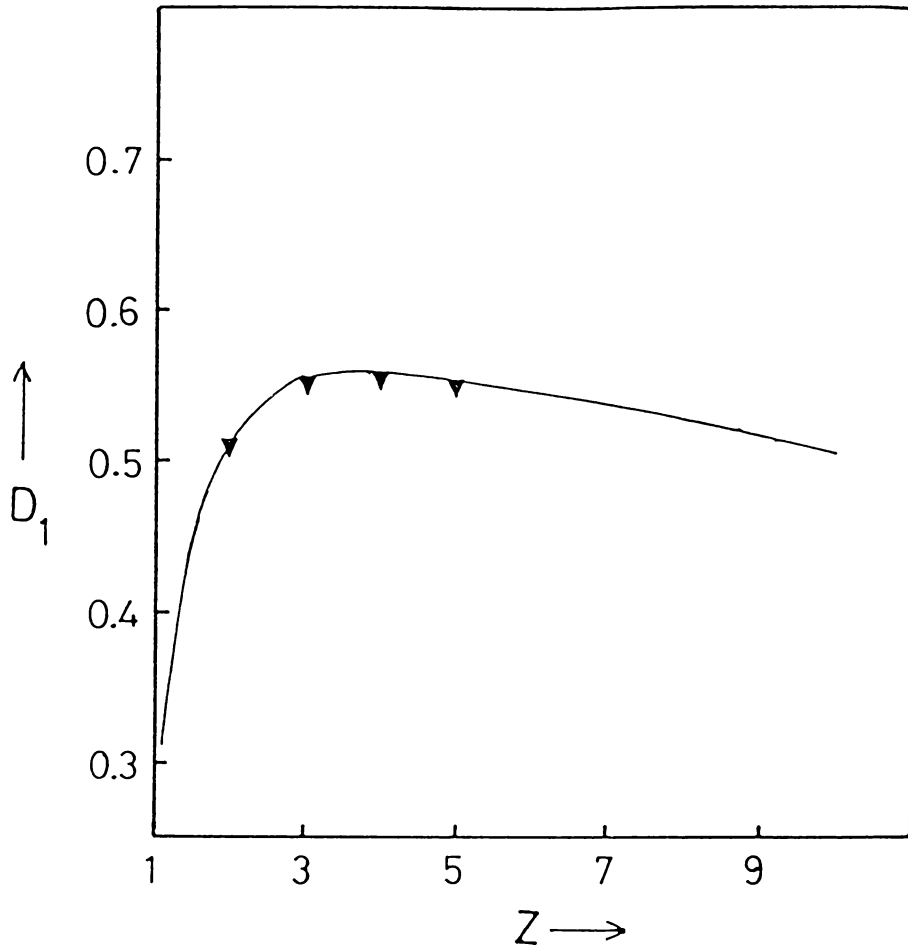


Fig. 4.3 - The information dimension D_1 vs z as given by (4.31). The available numerical values are shown by triangles.

4.4 The correlation dimension D_2

The generalised dimensions D_q , other than D_0 and D_1 can be computed by defining the partition function discussed in Chapter 1. From (1.52) we have the partition function

$$\Gamma = \frac{p_1^q}{l_1^\tau} + \frac{p_2^q}{l_2^\tau} \quad \dots(4.32)$$

Equation (1.53) gives

$$D_q = \frac{\tau}{(q - 1)} \quad \dots(4.33)$$

It is clear from (4.8) that

$$l_1 = \frac{1}{S_1} \quad \text{and} \quad l_2 = \frac{1}{S_2}$$

and in this case $p_1 = p_2 = \frac{1}{2}$. Thus (4.32) can be modified as,

$$S_1^\tau + S_2^\tau = 2^q \quad \dots (4.34)$$

If we consider in general R subsets for greater accuracy, we write

$$\sum_{j=1}^R S_j^c = R^q \quad \dots(4.35)$$

The correlation dimension is given by $q = 2$ and so (4.33) gives $\tau = D_2$. Thus (4.34) implies

$$S_1^{D_2} + S_2^{D_2} = 4 \quad \dots (4.36)$$

The explicit expressions for S_1 and S_2 given in (4.12) and (4.13) modify (4.36) as

$$\alpha^{D_2} + \left[\frac{(1 + \frac{1}{\alpha})}{1 - g(\frac{1}{\alpha})} \right]^{D_2} = 4 \quad \dots (4.37)$$

This can be simplified further using (4.19) and (4.20) to yield

$$\alpha^{D_2} + \frac{\alpha^{zD_2}}{\left[1 + \frac{(z-1)}{2z\alpha} \right]^{D_2}} = 4 \quad \dots (4.38)$$

This equation can be solved by the successive bisection method to get D_2 for different values of z . The results are tabulated in Table 4.III. The D_2 vs z relationship is plotted in Fig. 4.4.

4.5 Discussion

It is found that the variation with z is significantly different for the three dimensions studied

Table 4.III - The values of the correlation dimension D_2 for different values of z . The numerical values available in [66] are also given.

z	D_2 (computed values)	D_2 (numerical values)
1.1	0.3180460	
1.2	0.3746270	
1.5	0.4542183	
2.0	0.5022655	0.501 ± 0.02
2.5	0.5172233	
3.0	0.5197161	0.509 ± 0.02
3.5	0.5166886	
4.0	0.5110947	0.498 ± 0.05
4.5	0.5043395	
5.0	0.4971327	0.483 ± 0.03
5.5	0.4898491	
6.0	0.4826857	
6.5	0.4757461	
7.0	0.4690801	
7.5	0.4627077	
8.0	0.4566326	
8.5	0.4508471	
9.0	0.4453420	
9.5	0.4401018	
10.0	0.4351122	
100.0	0.2548094	

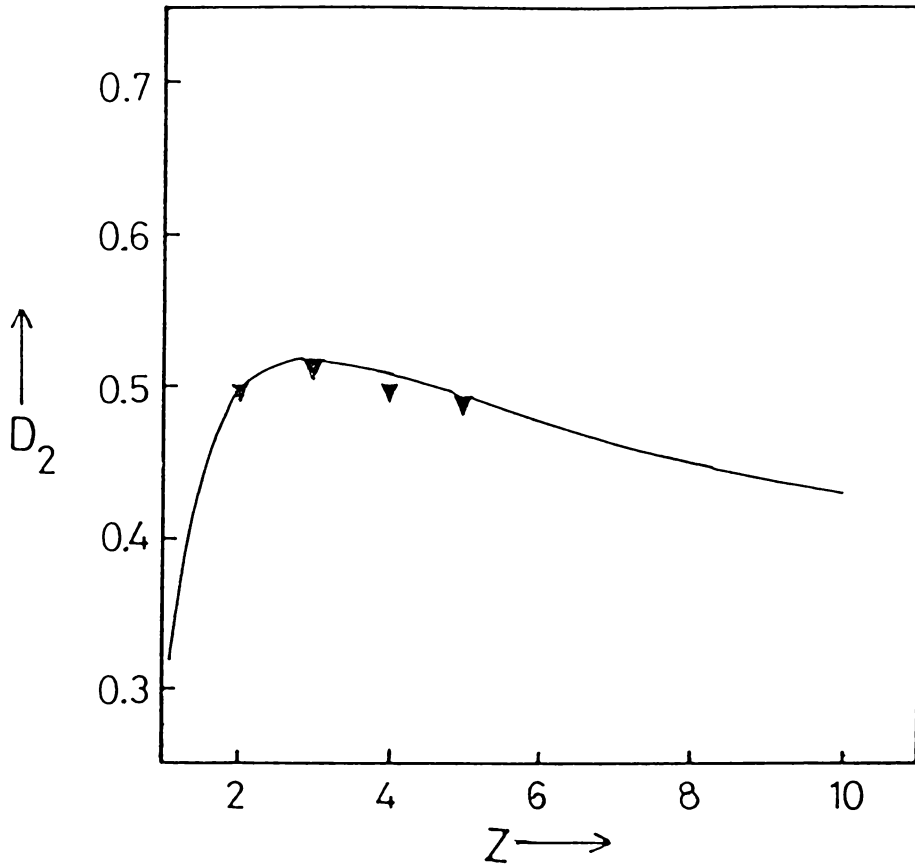


Fig. 4.4 - The variation of the correlation dimension as a function of z expressed in (4.38). The numerical values [66] are indicated by triangles.

here. Thus D_0 increases with z and shows almost saturation for very large z values, while D_1 increases first and then shows a dip at larger values of z . D_2 also decreases, as z increases beyond a certain value. Thus the asymptotic values of the three dimensions are well separated while for small z values, they are very close. For each z value we have $D_0 > D_1 > D_2$. The available numerical values agree well with the values computed here.

Our method has the advantage that an analytic $g(x)$ is used and the accuracy of the values can be improved by including more terms in $g(x)$. The dimensions for any z , including fractions, can be calculated in a straight-forward manner.

5. ONSET OF CHAOS IN DISSIPATIVE SYSTEMS

Methods for establishing chaos in dissipative systems have special significance since such systems, unlike conservative systems, need not necessarily show stochastic behaviour. Therefore it is important to predict under what conditions chaos first appears in nonintegrable systems with dissipative perturbation. The origin of chaos in such systems can be traced to the motion of the system near its unperturbed homoclinic orbit or separatrix. Melnikov's method [70] introduces an integral function which measures the separation between the perturbed stable and unstable manifolds of a separatrix, using calculations involving the unperturbed orbits. If this function has a simple zero, then the two manifolds intersect transversally. This implies that the structure of a horseshoe is

embedded in their neighbourhood [71]. Holmes and Marsden developed this method for a two degree of freedom hamiltonian system [1]. They further extended it to higher dimensional systems where Arnold diffusion occurs [72].

5.1 The Melnikov-Holmes method

We consider a two dimensional autonomous system that has a single hyperbolic fixed point and is perturbed by a periodic function of time. Such a system is described by

$$\dot{x} = f_0(x) + \epsilon f_1(x, t) \quad \dots (5.1)$$

where $x = \begin{pmatrix} x_1 \\ x_2 \end{pmatrix} \in \mathbb{R}^2$ and

$$f_0 = \begin{pmatrix} f_{01}(x_1, x_2) \\ f_{02}(x_1, x_2) \end{pmatrix} \quad \text{and}$$

$$f_1 = \begin{pmatrix} f_{11}(x_1, x_2, t) \\ f_{12}(x_1, x_2, t) \end{pmatrix}$$

f_0 and f_1 are sufficiently smooth functions and f_1 is T -periodic in t .

The unperturbed system corresponding to $\epsilon=0$ in (5.1), is hamiltonian and integrable so that

a real valued function H exists and

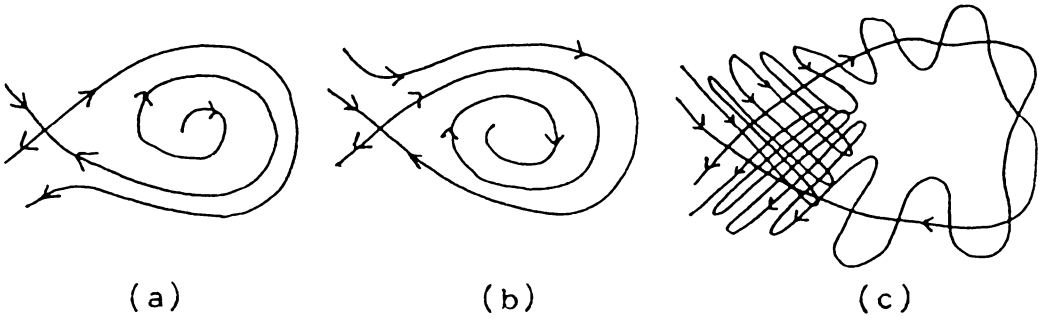
$$f_{01} = \frac{\partial H}{\partial x_2} ; \quad f_{02} = - \frac{\partial H}{\partial x_1} \quad \dots (5.2)$$

The system is assumed to possess a hyperbolic fixed point X_0 and an integrable separatrix orbit $x_0(t) = \chi_0$ such that

$$\lim_{t \rightarrow +\infty} x_0(t) = \lim_{t \rightarrow -\infty} x_0(t) = X_0 \quad \dots (5.3)$$

The stable and unstable branches $x_0^s(t)$ and $x_0^u(t)$ join smoothly and in general, there is an elliptic fixed point within the separatrix.

When the system is perturbed, the phase space may be extended to three dimensions (x_1, x_2, t) , and we view the motion in a surface of section $t = \text{constant (mod. } T)$. The stable and unstable orbits in the surface of section do not join smoothly. For a dissipative perturbation, three possibilities arise and these are indicated below in diagrammatic form:



It is only in the last case that chaotic motion appears. To obtain the conditions for the intersections, we write the stable and unstable orbits as,

$$x^{s,u}(t, t_0) = x_0(t-t_0) + \epsilon x_1^{s,u}(t, t_0) \quad \dots (5.4)$$

where t_0 is an arbitrary initial time, which fixes the particular Poincaré section chosen. From equation (5.1)

$$\dot{x}_0(t-t_0) = f_0(x_0(t-t_0)) \quad \dots (5.5)$$

The total time derivate of (5.4) is thus,

$$\dot{x}^{s,u} = f_0(x_0(t-t_0)) + \epsilon \dot{x}_1^{s,u} \quad \dots (5.6)$$

From (5.1),

$$\begin{aligned} \dot{x}^{s,u} &= f_0(x) + \epsilon f_1(x,t) \\ &= f_0(x_0(t-t_0)) + \epsilon x_1(t,t_0) + \epsilon f_1(x_0(t-t_0) \\ &\quad + \epsilon x_1(t-t_0),t) \end{aligned} \quad \dots (5.7)$$

The right hand side can be expanded to first order in ϵ . Then

$$\begin{aligned} \dot{x}_1^{s,u} &= f_0(x_0(t-t_0)) + \epsilon J(x_0) x_1^{s,u} \\ &\quad + \epsilon f_1(x_0(t-t_0),t) \end{aligned} \quad \dots (5.8)$$

Comparing (5.8) with (5.6) we get [4],

$$\dot{x}_1^{s,u} = J(x_0) x_1^{s,u} + f_1(x_0(t-t_0),t) \quad \dots (5.9)$$

Here $J(x_0)$ is the Jacobian matrix of f_0 evaluated at $x_0(t-t_0)$. Thus

$$J(x_0) = \begin{pmatrix} \frac{\partial f_{01}}{\partial x_{01}} & \frac{\partial f_{01}}{\partial x_{02}} \\ \frac{\partial f_{02}}{\partial x_{01}} & \frac{\partial f_{02}}{\partial x_{02}} \end{pmatrix} \quad \dots (5.10)$$

Equation (5.9) can be solved for x^s for $t > t_0$ and for x^u for $t < t_0$ with the condition that

$$x^S(t \rightarrow \infty) = x^U(t \rightarrow -\infty) = X_p \quad \dots (5.11)$$

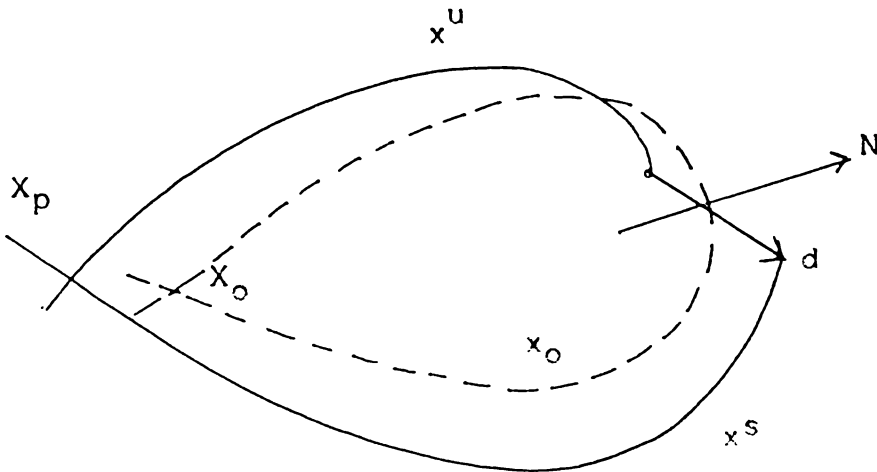
where X_p denotes the position of the hyperbolic fixed point in the perturbed system.

The distance between the two solutions is,

$$d(t, t_0) = x_1^S(t, t_0) - x_1^U(t, t_0) \quad \dots (5.12)$$

The Melnikov function $M(t, t_0)$ is defined as the projection of d along a normal N to the unperturbed orbit x_0 at t .

$$\text{ie. } M(t, t_0) = N \cdot d \quad \dots (5.13)$$



From (5.5)

$$N = \begin{pmatrix} -f_{02}(x_0) \\ f_{01}(x_0) \end{pmatrix}$$

Therefore (5.13) becomes

$$\begin{aligned} M(t, t_0) &= f_{01}d_2 - f_{02}d_1 \\ &= f_0 \wedge d \end{aligned} \quad \dots (5.14)$$

where \wedge denotes the antisymmetric wedge product defined by,

$$x_1 \wedge x_2 = x_{10}x_{21} - x_{11}x_{20}$$

We write

$$M(t, t_0) = M^S - M^U \quad \dots (5.15)$$

where

$$M^{S,U}(t-t_0) = f_0 \wedge x_1^{S,U} \quad \dots (5.16)$$

$$\begin{aligned} \dot{M}^S &= \dot{f}_0 \wedge x_1^S + f_0 \wedge \dot{x}_1^S \\ &= J(x_0) \dot{x}_0 \wedge x_1^S + f_0 \wedge \dot{x}_1^S \\ &= J(x_0) f_0 \wedge x_1^S + f_0 \wedge J(x_0) x_1^S + f_0 \wedge f_1 \\ &= \text{Tr } J(x_0) f_0 \wedge x_1^S + f_0 \wedge f_1 \end{aligned} \quad \dots (5.17)$$

Since the unperturbed system is assumed to be hamiltonian, $\text{Tr } J = 0$. This gives,

$$\dot{M}^S = f_0 \wedge f_1$$

By integrating this, it can be shown that

$$M^S(t_0) = - \int_{t_0}^{\infty} (f_0 \wedge f_1) dt \quad \dots (5.18)$$

Similarly for the unstable orbit, we have

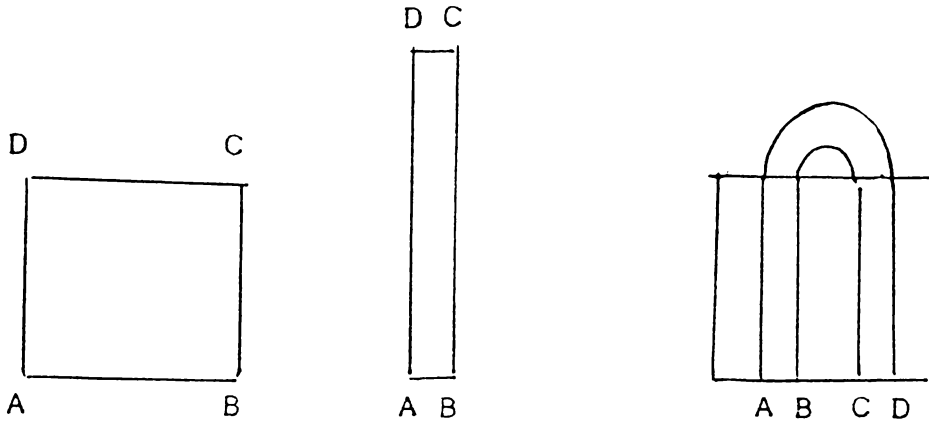
$$M^U(t_0) = - \int_{-\infty}^{t_0} (f_0 \wedge f_1) dt \quad \dots (5.19)$$

Combining (5.18) and (5.19), we get

$$M(t_0) = - \int_{-\infty}^{\infty} (f_0 \wedge f_1) dt \quad \dots (5.20)$$

The behaviour of $M(t_0)$ is crucial in determining the possibility of chaotic motion near the separatrix.

If $M(t_0)$ has a simple zero ie. $\frac{\partial M}{\partial t_0} \neq 0$ and is independent of ϵ , then the local stable and unstable manifolds intersect transversally [73]. This implies the Poincaré section has Smale-horseshoe chaos[74]. A Smale-horseshoe, shown in the figure, though not an attractor, can influence the behaviour of orbits



which pass close to it. These orbits therefore display an extremely sensitive dependence on initial conditions and exhibit a chaotic transient before stabilising to orbits of all periods, including a strange attractor. Thus Melnikov's method predicts the lowest boundary of chaotic threshold [75].

The boundary of the horseshoe region is given by $M(t_0) = 0$ and $\frac{\partial M}{\partial t_0} = 0$ while $\frac{\partial^2 M}{\partial t_0^2} \neq 0$. Then if

$\frac{\partial M}{\partial \lambda} \Big|_{\lambda_B} \neq 0$, then λ_B is the bifurcation value at

which quadratic homoclinic tangencies occur.

In general one cannot always get explicit expressions exactly for $x_0(t)$. So a numerical calculation of $x_0(t)$ is inevitable [76]. We note that the

Melnikov method is the only analytic method available for predicting the appearance of chaos in a dynamical system. The method has been extended to predict the appearance of a heteroclinic tangency by Ling [77] and generalised to deal with regions of chaos in the parameter space of quasiperiodically forced two degree of freedom dissipative systems by Wiggins [78].

5.2 Transition to chaos in a driven pendulum with nonlinear dissipation

A driven pendulum with dissipation is known to have phase locked states as well as chaotic behaviour [79]. If the pendulum is moving through an inhomogeneous medium, the damping may be x -dependent. Here we consider one such situation where the damping is nonlinear and of the van der Pol type . The equation of motion of such a pendulum is,

$$\ddot{x} + \sin x = A \sin \omega t - \beta \dot{x}(x^2 - 1) \quad \dots (5.21)$$

where A and ω are the amplitude and frequency of the driving term while β is the damping constant. In the spirit of the previous section, this equation can be written as,

$$\begin{aligned} \dot{x} &= v \\ \dot{v} &= -\sin x + \epsilon[\beta(1-x^2)\dot{x} + A \sin \omega t] \end{aligned} \quad \dots (5.22)$$

where ϵ is a small parameter.

The Melnikov analysis described in § 5.1 is used to analyse the onset of chaos in this pendulum. The unperturbed system corresponding to $\epsilon = 0$ is integrable and its hamiltonian is

$$H_0 = \frac{v^2}{2} - \cos x \quad \dots (5.23)$$

The unperturbed homoclinic orbits are given by [1]

$$x_0(t) = 2 \tan^{-1}(\sinh t) \quad \dots (5.24)$$

$$v_0(t) = 2 \operatorname{sech} t \quad \dots (5.25)$$

The Melnikov function $M(t_0)$ defined in (5.20), for the system given in (5.22) is then,

$$\begin{aligned} M(t_0) &= - \int_{-\infty}^{\infty} \left[\beta \{1-x_0^2(t-t_0)\} v_0^2(t-t_0) \right. \\ &\quad \left. + A v_0(t-t_0) \sin \omega t \right] dt \end{aligned} \quad \dots (5.26)$$

Changing the variables to $\tau = t-t_0$ and using the explicit forms for x_0 and v_0 from (5.24) and (5.25), $M(t_0)$ can be split into four integrals as

$$\begin{aligned}
 M(t_0) = & - 4\beta \int_{-\infty}^{\infty} \operatorname{sech}^2 \tau \, d\tau \\
 & + 16\beta \int_{-\infty}^{\infty} \operatorname{sech}^2 \tau [\tan^{-1}(\sinh \tau)]^2 \, d\tau \\
 & - 2A \cos \omega t_0 \int_{-\infty}^{\infty} \operatorname{sech} \tau \sin \omega \tau \, d\tau \\
 & + 2A \sin \omega t_0 \int_{-\infty}^{\infty} \operatorname{sech} \tau \cos \omega \tau \, d\tau \quad \dots (5.27)
 \end{aligned}$$

The first integral is easily evaluated while the third vanishes and we get

$$\int_{-\infty}^{\infty} \operatorname{sech}^2 \tau [\tan^{-1}(\sinh \tau)]^2 \, d\tau = \frac{\pi^2}{2} - 4 \quad \dots (5.28)$$

$$\int_{-\infty}^{\infty} \operatorname{sech} \tau \cos \omega \tau \, d\tau = \pi \operatorname{sech} \left(\frac{\pi\omega}{2} \right) \quad \dots (5.29)$$

Using these in (5.27)

$$M(t_0) = - (72 - 8\pi^2) \beta + 2\pi A \operatorname{sech} \left(\frac{\pi\omega}{2} \right) \sin \omega t_0 \quad (5.30)$$

We define a function $R(\omega)$ as

$$R(\omega) = \frac{(8\pi^2 - 72)}{2\pi} \operatorname{cosh} \left(\frac{\pi\omega}{2} \right) \quad \dots (5.31)$$

Thus for $\frac{A}{\beta} > R(\omega)$, equation (5.30) shows that $M(t_0)$

oscillates between positive and negative values.

This indicates transverse intersections of the stable and unstable manifolds resulting in local stochasticity. Fig. 5.1 shows the variation of $R(\omega)$ with ω . For values of A and β lying above the curve, the system can exhibit chaotic behaviour.

It is clear from (5.30) that at $A = A_c$ given by

$$A_c = R(\omega)\beta = \frac{(8\pi^2 - 72)}{2\pi} \cosh\left(\frac{\pi\omega}{2}\right) \quad \dots (5.32)$$

$M(t_0, A_c)$ has a quadratic zero, in the surface of section.

$$\text{ie. } M(t_0, A_c) = \frac{\partial M(t_0, A_c)}{\partial t_0} = 0$$

$$\text{while } \left. \frac{\partial M}{\partial A} \right|_{A_c} \neq 0 \quad \dots (5.33)$$

Then A_c corresponds to a bifurcation value at which homoclinic tangency occurs. It has been shown by Holmes that the homoclinic bifurcation is the limit of a countable sequence of subharmonic bifurcations that take place inside the separatrix [74].

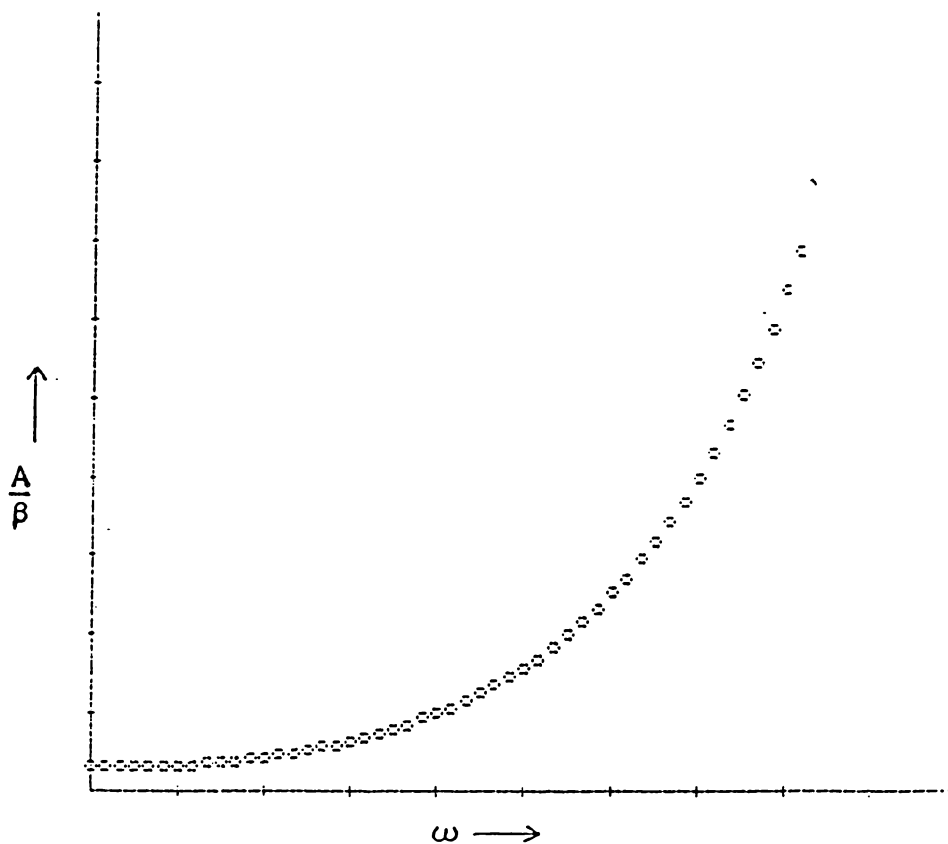


Fig. 5.1 - The threshold for chaos in the parameter plane as predicted by the Melnikov-Holmes criterion (5.31). Chaos can exist for parameter values corresponding to points above the curve.

However it is found that in many situations, the numerically observed threshold lies above the Melnikov prediction [75]. This is because, the Melnikov criterion does not imply that the trajectories will be asymptotically chaotic. In some cases there can be transient chaos followed by asymptotically periodic trajectories [80]. So we carried out a detailed numerical analysis of the above system.

5.3 Numerical Analysis

To investigate the occurrence of chaotic attractors in the van der Pol pendulum, we have to rely heavily on numerical studies involving phase portraits, Poincaré maps, power spectra and computation of maximum Lyapunov exponent. We carried out a numerical integration of (5.22) using fourth order Runge-Kutta-Gills Scheme [81]. The integration was carried out in general at time steps of $\frac{1}{100}$ th of a drive period and the trajectory watched for 20 to 30 periods. There are three control parameters for the problem, namely the damping constant β , the driving frequency ω and the driving amplitude A .

In our studies we kept β mostly at 0.2. A plot of the output values of x and \dot{x} gives the phase portraits corresponding to the chosen values of A, ω and β . To observe the Poincare' map, we plot the outputs obtained after an interval of time equal to the period of the driving force.

To explore the chaotic region in its complexity and variety, we analysed the power spectra using the Fast Fourier Transform (FFT) technique [82]. These help to distinguish chaotic bands from periodic orbits and observe the fine structure of periodic orbits embedded in bands. In the algorithm for FFT we write the x_k values which are the outputs of the numerical integration of (5.22) as

$$x_k = \sum_{l=0}^{N-1} a_l e^{-2\pi i k l / N} \quad \dots (5.34)$$

There is a lot of redundancy involved in the evaluation of (5.34) and FFT takes advantage of these to reduce substantially the number of operations required. To eliminate spurious frequency components, a cosine bell or some other tapering function is

applied to the output before FFT is applied [83].

The computation of the maximum Lyapunov exponent σ_{\max} can be used as a test for chaos. To compute σ_{\max} , we write (5.21) as an autonomous system of first order differential equations as

$$\begin{aligned} \dot{x}_1 &= x_2 \\ \dot{x}_2 &= -\sin x_1 + \beta (1-x_1^2) x_2 + A \sin x_3 \\ \dot{x}_3 &= \omega \end{aligned} \quad \dots (5.35)$$

The variational system of equations for the tangent vector w is given by

$$\begin{aligned} \dot{w}_1 &= w_2 \\ \dot{w}_2 &= -(\cos x_1 + 2\beta x_2 x_1) w_1 + \beta(1-x_1^2) w_2 \\ &\quad + (A \cos x_3) w_3 \\ \dot{w}_3 &= 0 \end{aligned} \quad \dots (5.36)$$

We take $w_3 = 1$ and for an initial w_0 and x_0 solve the above two sets of equations. w is normalised to a norm of unity every τ seconds [84,30]. Thus

$$\begin{aligned} d_k &= ||w_{k-1}(\tau)|| \\ \text{with } w_k(0) &= \frac{||w_{k-1}(\tau)||}{d_k} \end{aligned} \quad \dots (5.31)$$

Then from (1.26),

$$\sigma_{\max} = \lim_{n \rightarrow \infty} \frac{1}{nC} \sum_{j=1}^n \ln d_i \quad \dots (5.38)$$

A positive value for σ_{\max} is the signature of chaos.

The prominent features of our numerical studies are summarised below.

Chaotic attractor at low frequencies

Because of the nonlinear dissipative term, the system in (5.22) would always enter into a limit cycle behaviour, which makes it difficult to trace the region near the separatrix. For small values of ω , the phase portraits below the Melnikov threshold A_c , show periodic orbits near the separatrix. For $\omega=0.04$ and $\beta = 0.2$, $A_c = 0.22$. Fig. 5.2 shows the phase portrait for $A = 0.1$. The Poincare' map corresponding to this value reveals a periodic 5 cycle. The system becomes chaotic for $A > 0.25$. The chaotic attractor for $A = 0.6$ and the corresponding FFT are given in Fig. 5.3. We computed σ_{\max} at this frequency and found it to be equal to -2.5×10^{-2} for $A = 0.1$,

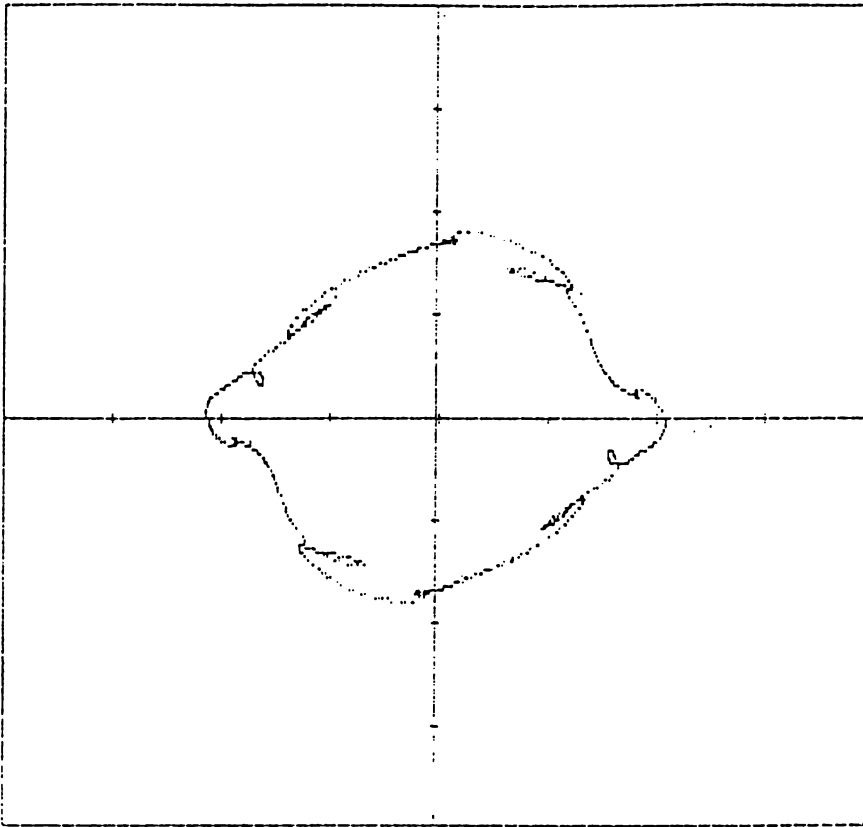


Fig. 5.2 - Phase portrait of the van der Pol pendulum
for $\omega = 0.04$, $\beta = 0.2$ and $A = 0.1$.

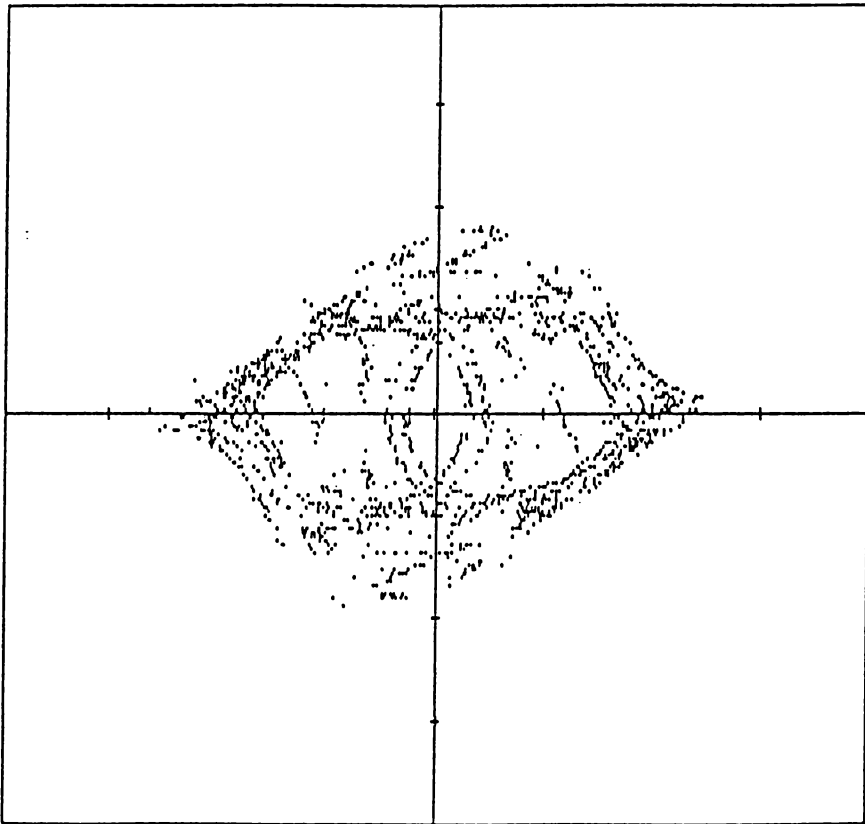


Fig. 5.3.a. - Phase portrait of the chaotic attractor of the system corresponding to $\omega = 0.04$, $\beta = 0.2$ and $A = 0.6$.

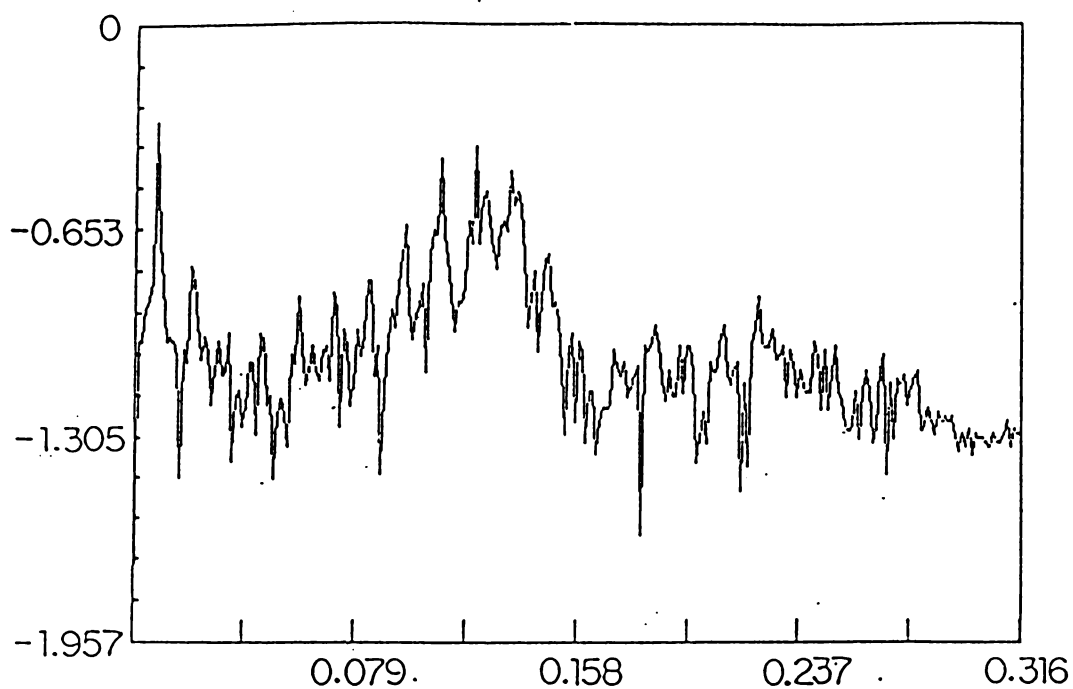


Fig. 5.3.b. - The power spectrum using FFT for the chaotic attractor given in Fig.5.3.a. Log (power) is plotted along the Y-axis with frequency along the X-axis.

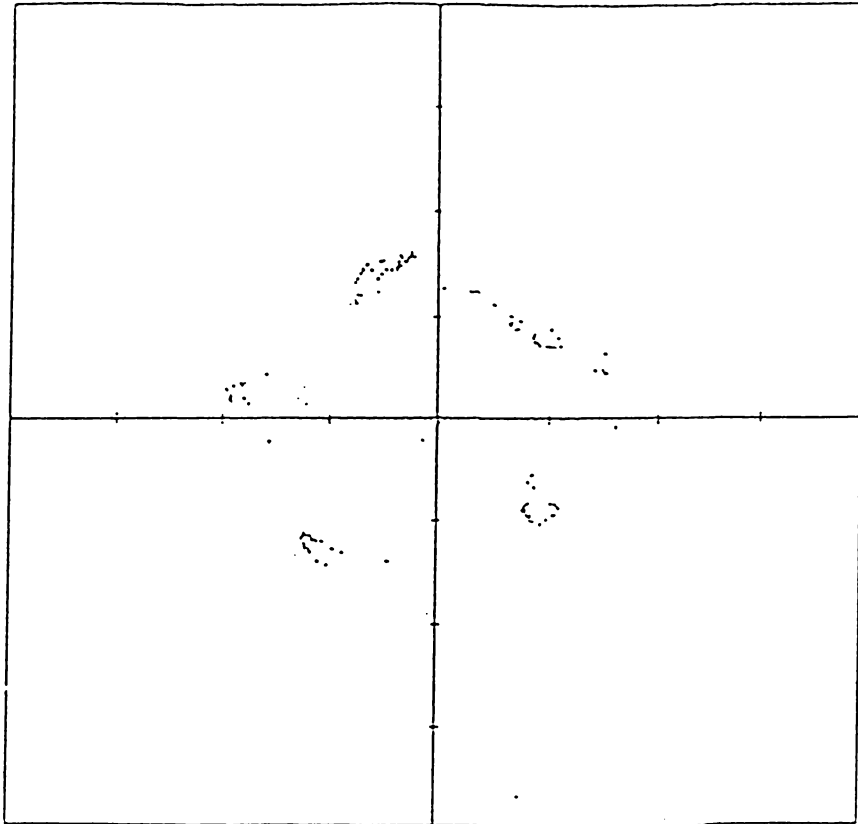


Fig. 5.3.c. - The Poincaré map of the chaotic attractor for parameter values $\beta = 0.2$, $\omega = 0.04$ and $A = 0.6$.

while it is 9.8×10^{-2} for $A = 0.6$. This confirms the existence of a chaotic attractor for $A = 0.6$. Qualitatively the same type of behaviour exists for frequencies upto $\omega = 0.06$.

Band formation and period-doubling sequence inside the band

For values of ω lying in the range $0.08 < \omega < 1$, the system shows a tendency towards the formation of a thick or band-like limit cycle. For a pendulum with a dissipation of the usual type ie. $\beta \dot{x}$, the limit cycle forms the stable attractor of the system. However, here because the dissipation has a quadratic dependence on x , the system has to adjust continuously as x changes along the trajectory and this repeated attempt to approach a limit cycle leads to a thick band like limit cycle. We observe that this occurs below the Melnikov criterion, but near escape from the potential well. Thus for $\omega = 0.4$, the band exists for A lying between 0.1 to 0.28. Fig. 5.4 shows such a band for $A = 0.2$.

The FFT analysis for these values reveals some hidden periodicity inside the band. For $A < 0.2$, FFT

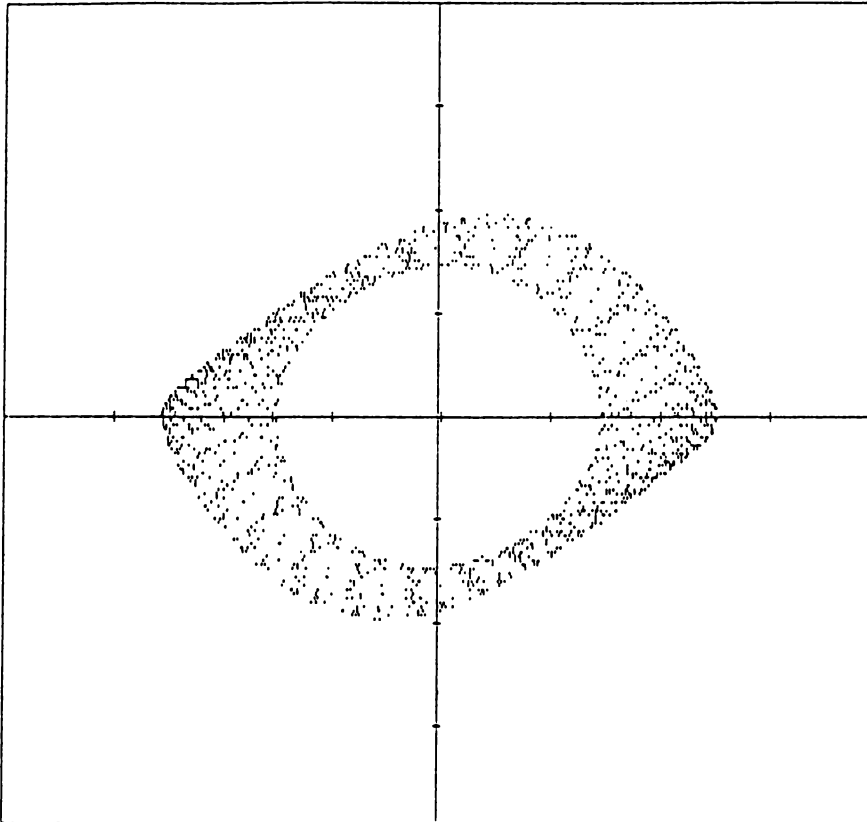


Fig. 5.4 - The band-like limit cycle in the phase space for $\omega = 0.4$, $\beta = 0.2$ and $A = 0.2$.

shows only four fundamental modes while at $A = 0.21$, a period-doubling takes place producing peaks on either side of the original modes. The next two period doublings occur at $A = 0.217$ and 0.218 . This sequence of period-doublings are clear from the FFT given in Fig. 5.5. These, we presume, are subharmonic bifurcations that take place inside the separatrix. The sequence is found to accumulate near $A \approx 0.27$. This accumulation point should correspond to the homoclinic bifurcation value. Using (5.32) this works out to be $A_c \approx 0.2667$, very close to the value obtained using the FFT analysis.

For slightly higher values of A , ie $A > 0.27$, the trajectory extends from $-\pi$ to $+\pi$ spending most of the time near $\pm \pi$. When A increases beyond 0.29 , the system either jumps to a nearby fixed point or diverges to ∞ . This type of behaviour usually coincides with a homoclinic tangency of the separatrix [85].

The maximum Lyapunov exponent computed for different values of A corresponding to the band are given in Table 5.I. We find that σ_{\max} is small but negative for low values of A . However just before

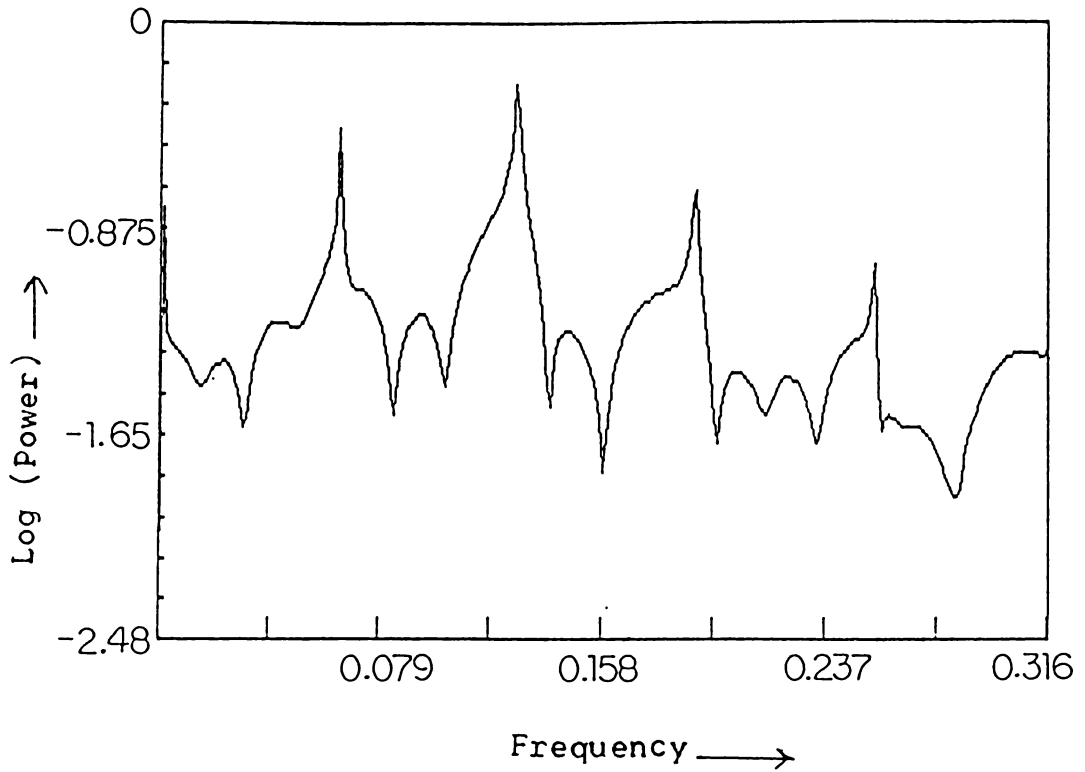


Fig. 5.5.a. - The FFT of the band shown in Fig. 5.4 for $\beta = 0.2$, $\omega = 0.4$ and $A = 0.2$, revealing four fundamental modes.

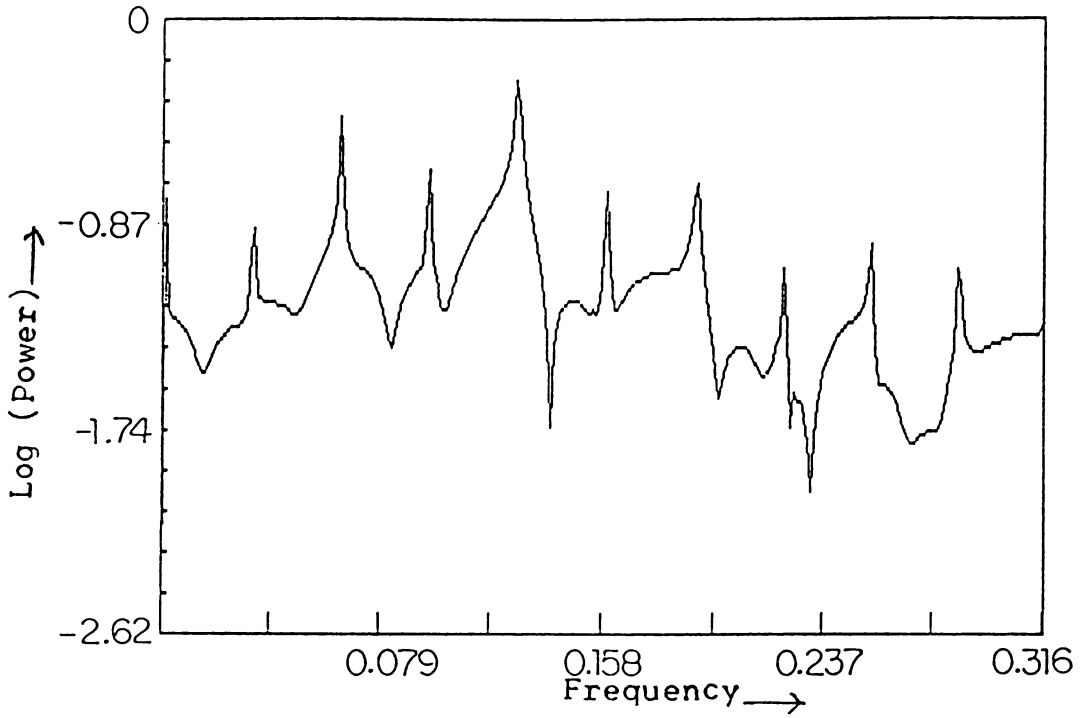


Fig. 5.5.b. - The FFT at $A = 0.21$. The additional peaks on either side of the four fundamental modes, indicate a period-doubling has taken place inside the band

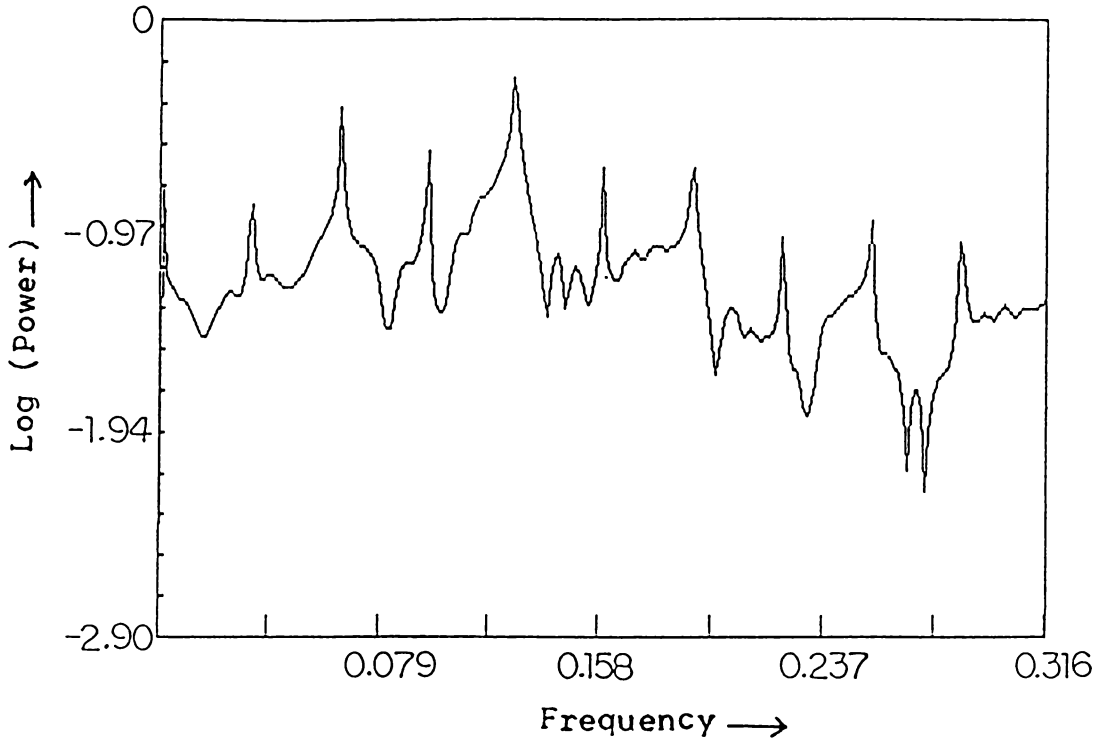


Fig. 5.5.c. - The FFT corresponding to $A = 0.217$, when a second period-doubling takes place.

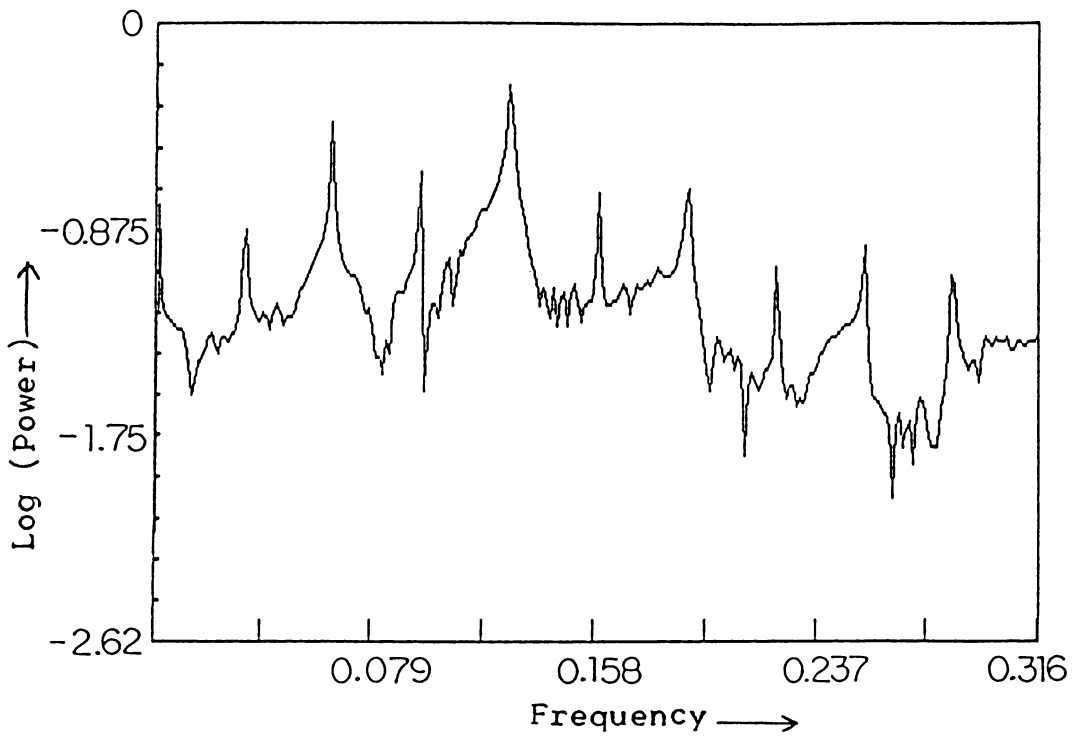


Fig. 5.5.d. - The FFT for $A = 0.218$, after the third period-doubling.

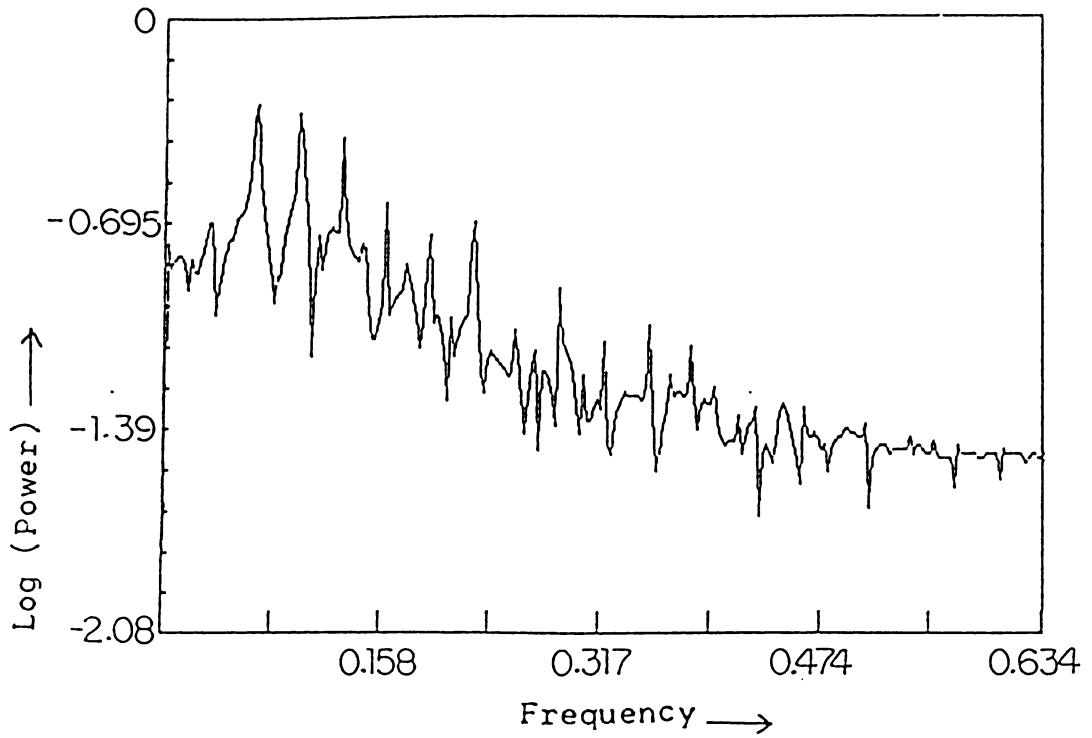


Fig. 5.5.e. - The FFT corresponding to $A = 0.27$, at the accumulation point of the period-doubling bifurcations.

Table 5.I - The maximum Lyapunov exponent
computed for $\omega = 0.4$, $\beta = 0.2$

A	σ_{\max}
0.18	$- 6.14 \times 10^{-6}$
0.2	$- 5.73 \times 10^{-6}$
0.26	$+ 3.88 \times 10^{-7}$
0.3	$+ 1.61 \times 10^{-5}$
0.35	$+ 1.79 \times 10^{-5}$

escape from the well, σ_{\max} acquires small positive values.

For higher values of ω , the same type of behaviour is generally observed. However at $\omega = 1$, the band which exists for $A < 0.3$, splits into periodic trajectories. Thus at $A = 0.3$, we observe asymptotically a periodic 4 cycle, as given in Fig. 5.6. When A is increased further, the driving force predominates and the system tends to a one-cycle having the same periodicity as the external force. However we observe some transient chaos in this region before the trajectory settles down to the one-cycle (Fig. 5.7).

Instability of the centre

For the unperturbed system, the centre $(0,0)$ is an elliptic fixed point. But for sufficiently large values of the perturbation, the centre is unstable and trajectories starting near it, spiral away. We find that the stability of the centre is determined by the parameter β and that the stability is lost through a bifurcation. Fig. 5.8 shows a two-cycle at $\beta = 0.0005$.

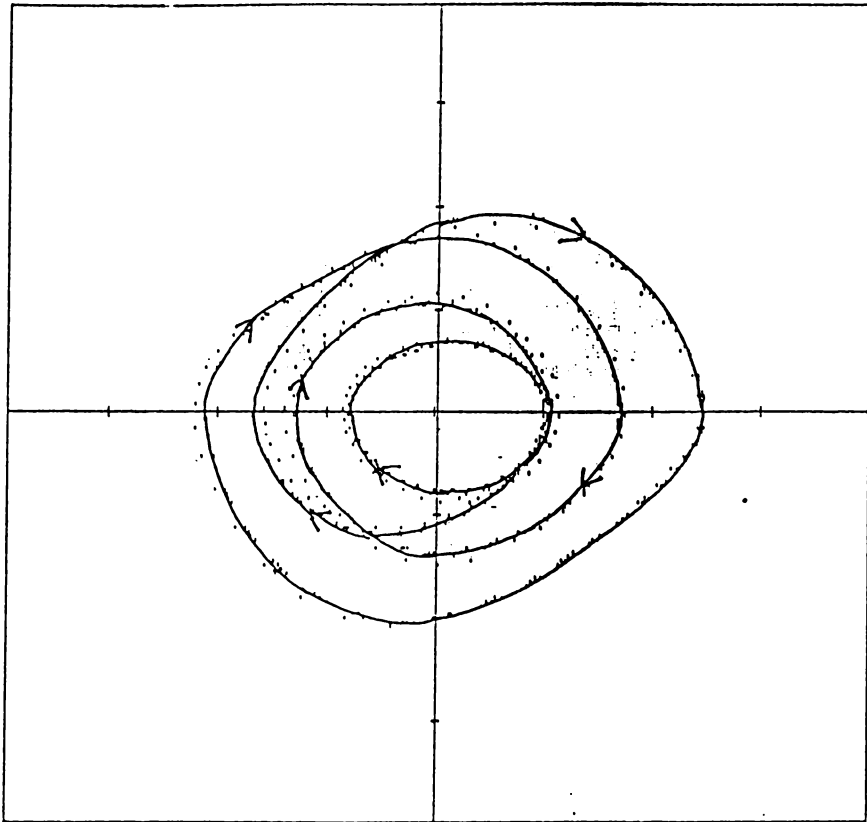


Fig. 5.6.a. - The periodic four cycle observed at $\beta = 0.2$, $\omega = 1$ and $A = 0.3$.

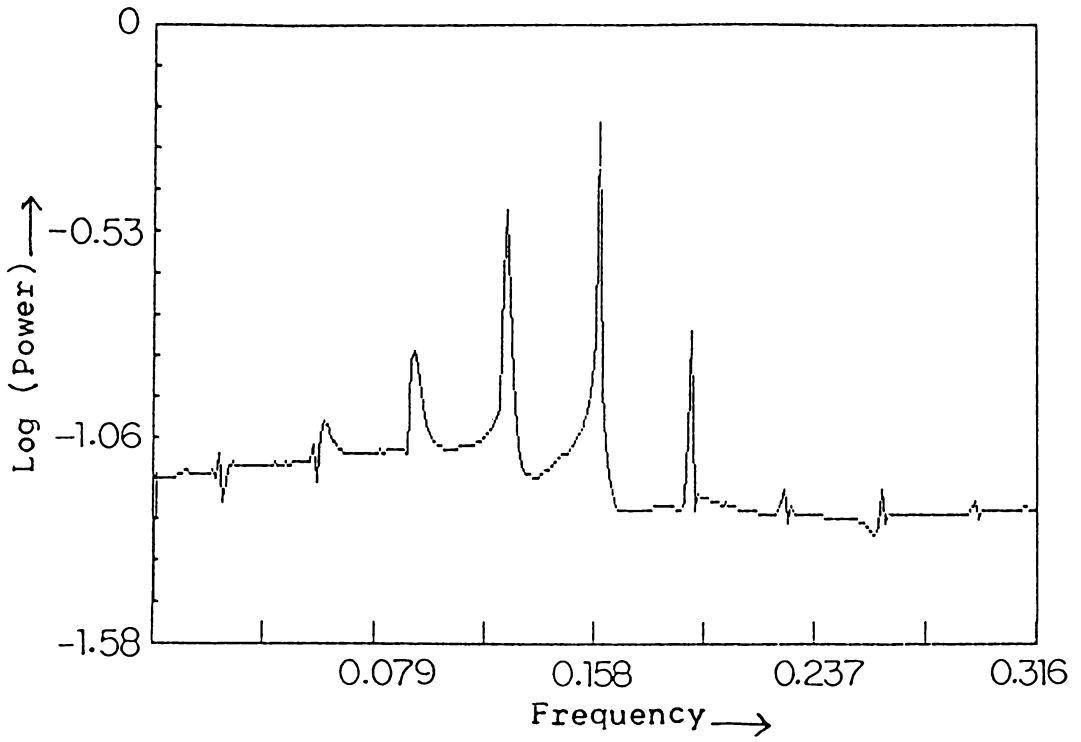


Fig. 5.6.b. - The FFT of the trajectory given in Fig. 5.6.a. revealing a periodic four cycle.

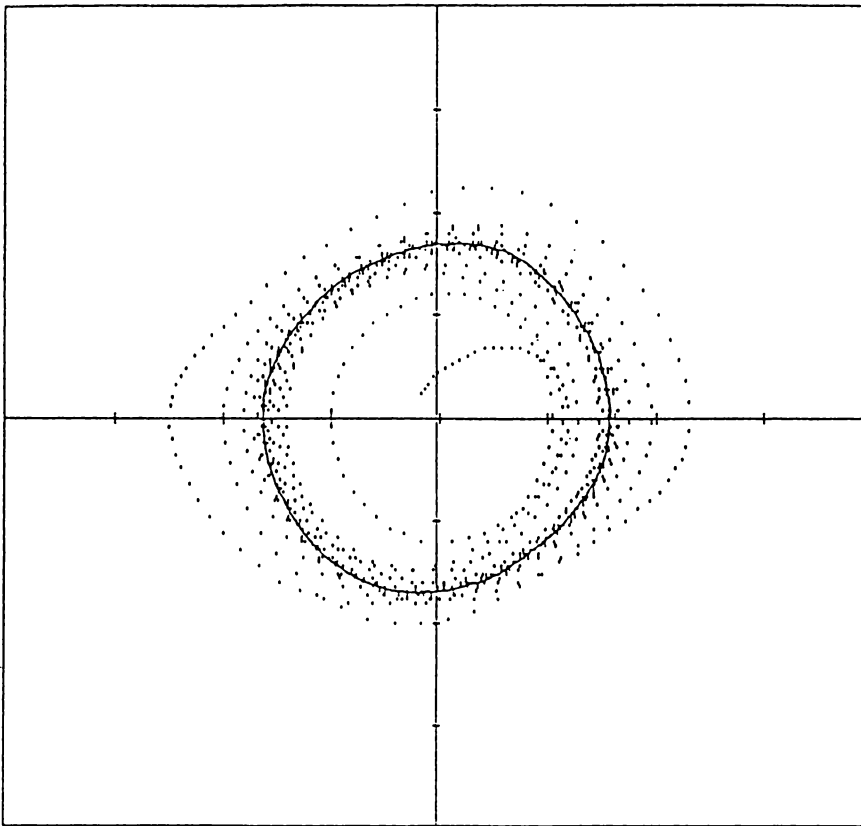


Fig. 5.7. - The asymptotic one cycle observed with the periodicity of the driving term, at $A = 0.5$, $\beta = 0.2$ and $\omega = 1$.

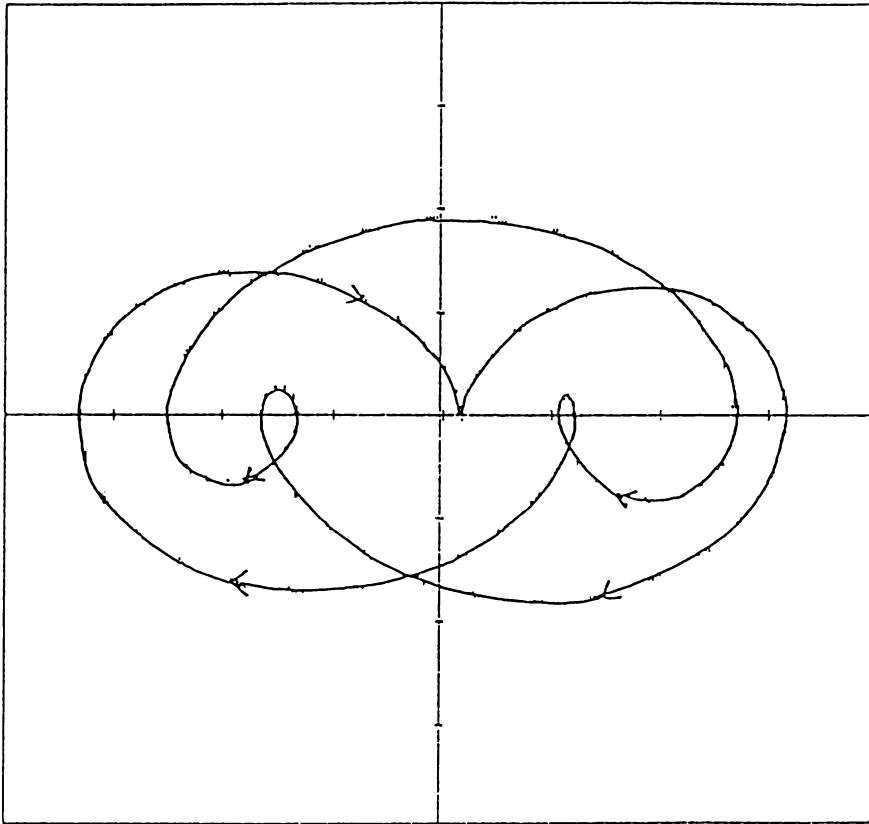


Fig. 5.8. - The periodic two cycle existing near the centre $(0,0)$ just before it becomes unstable corresponding to $\beta = .0005$, $\omega = 0.4$ and $A = 0.01$.

5.4 Effect of external noise

External noise is an unavoidable factor in actual experiments. So a full understanding of a physical system necessitates the inclusion of external noise in the theory. Though chaotic behaviour is possible and quite common in non-linear dynamical systems without external noise, the response of the system to noise is interesting especially near bifurcation points. In general, noise plays a rather constructive role in the theory of chaotic phenomena [86]. In the case of one dimensional maps, it is found that external noise will wash out all details in higher order bifurcation sequences [87]. This results in a truncation of the infinite sequence and chaos sets in earlier at $\lambda_{\infty}(\epsilon) < \lambda_{\infty}(0)$, where ϵ is the noise strength. Thus noise acts as a disordering field here [88]. There are situations where noise destabilises the chaos and produces some kind of order. The transition to order is characterised by a sharpening of the power spectrum, abrupt decrease of entropy and

appearance of negative Lyapunov exponent etc [89].

It is of considerable interest to study how the presence of noisy perturbations can affect the variety of dynamical behaviour observed in the system, discussed in § 5.3. Noise is usually modelled by the addition of a random term to the deterministic dynamical equations. The equations of motion (5.22) modify as

$$\begin{aligned} \dot{x} &= v \\ \dot{v} &= -\sin x + [\beta(1-x^2)\dot{x} + A \sin \omega t] \\ &\quad + \Gamma(t) \end{aligned} \quad \dots (5.39)$$

We take $\Gamma(t)$ to be amplitude limited or rectangular noise with amplitude Γ_0 . This corresponds to finite power fluctuations in an actual system.

For small values of ω , we find noise levels upto 0.01 have no significant effect on the trajectories. But for $\Gamma_0 \approx 0.1$, the onset of chaos is earlier. For $A = 0.6$ we study the effect of noise for various levels of noise amplitudes. The number of frequencies N within a power range, is plotted against the noise level Γ_0 in Fig. 5.9. It is clear that noise reduces N considerably thus

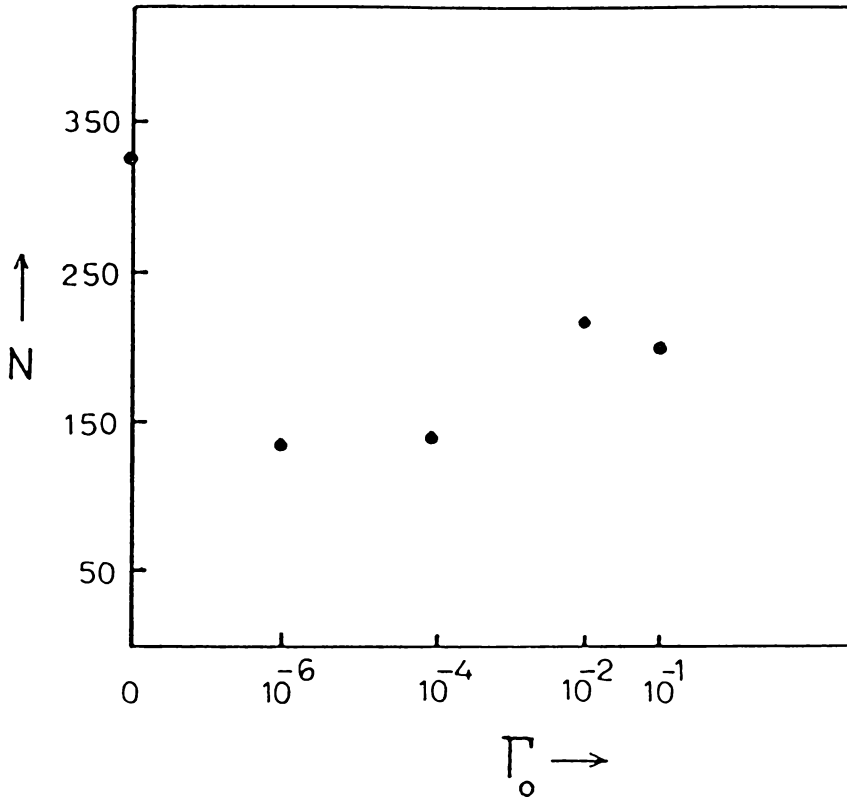


Fig. 5.9. - The number of peaks N lying within a definite power range is plotted against noise level Γ_0 . It is clear that N is reduced considerably for non zero values of Γ_0 .

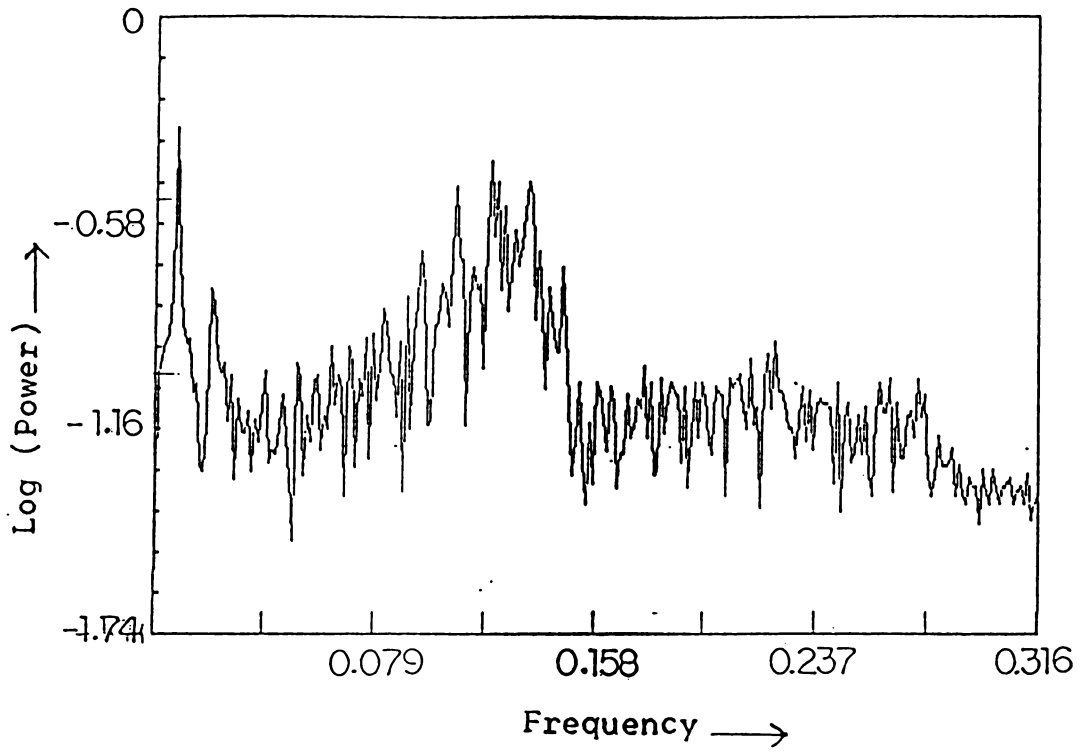


Fig. 5.10. - The FFT for $\omega = 0.4$, $\beta = 0.2$ and $A = 0.6$, in the presence of an external noise of amplitude $\Gamma_0 = 10^{-6}$.

indicating a tendency towards order. This is also evident from the peaking of the whole spectrum about a definite frequency (Fig. 5.10). Such noise-induced order was observed earlier by Matsumoto and Tsuda [89].

The period-doubling inside the band takes place earlier in the presence of noise. Thus when $\Gamma_0 = 0.01$, even at $A = 0.2$, the FFT looks like that at $A = 0.218$ with $\Gamma_0 = 0$. This is given in Fig. 5.11. At higher frequencies, the introduction of noise clears away the transient chaos observed earlier. So the periodic nature of the trajectory is established quite early in time, whereas without noise the periodicity is observed only asymptotically (Fig. 5.12).

Thus we find external noise reduces the randomness of the strange attractor at low frequencies and speeds up the bifurcation sequence inside the band while at higher frequencies, it wipes out the transient chaos.

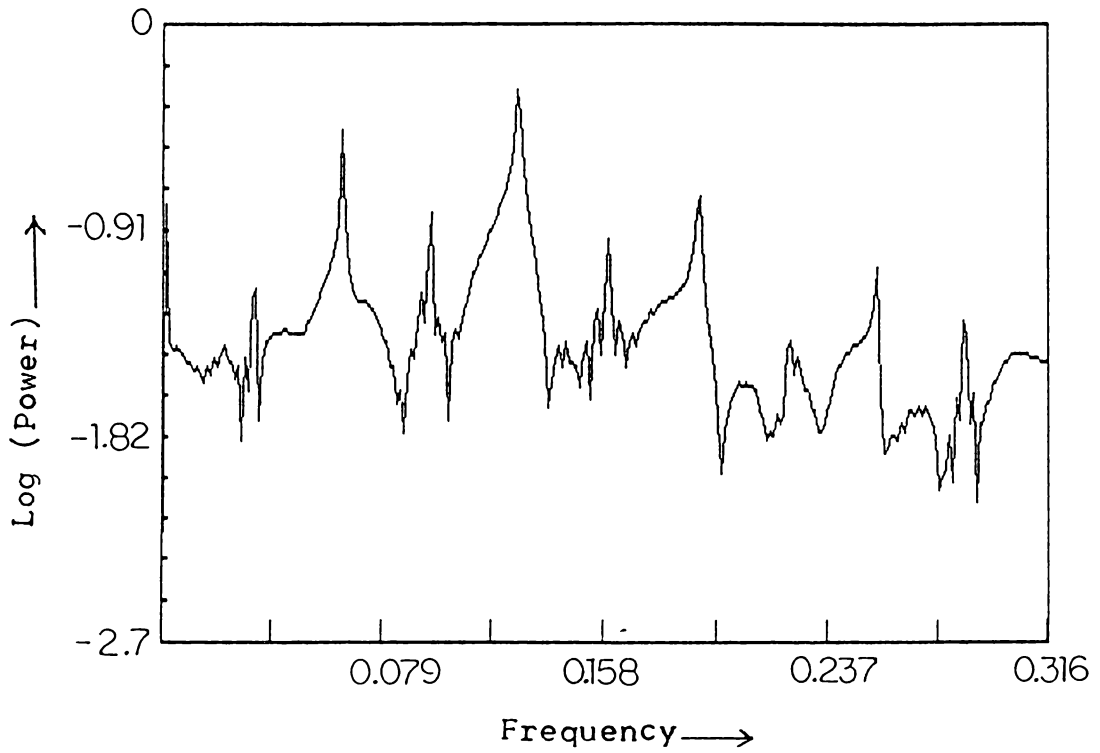


Fig. 5.11.a. - The FFT in the presence of a noise of amplitude $\Gamma_0 = 0.01$, for $\omega = 0.4$, $\beta = 0.2$ and $A = 0.2$. This is to be compared with the FFT given in Fig. 5.5.d. with $\Gamma_0 = 0$ and $A = 0.217$.

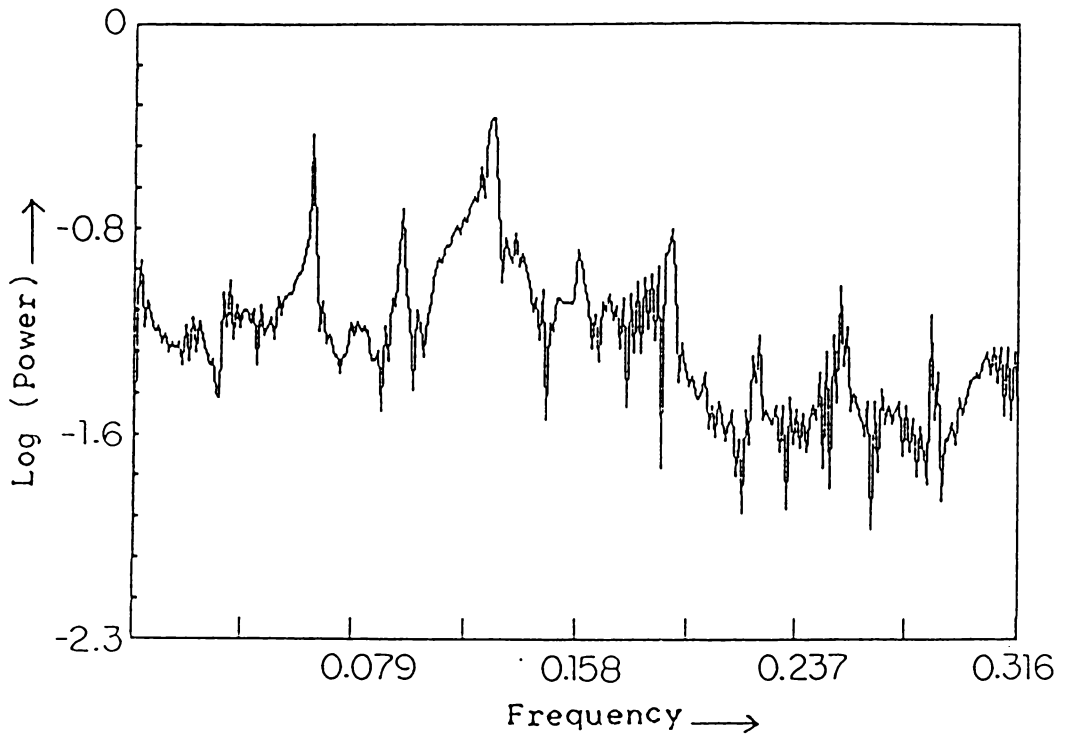


Fig. 5.11.b. - The FFT with noise of amplitude $\Gamma_0 = 0.01$ at $\omega = 0.4$, $\beta = 0.2$ and $A = 0.22$.

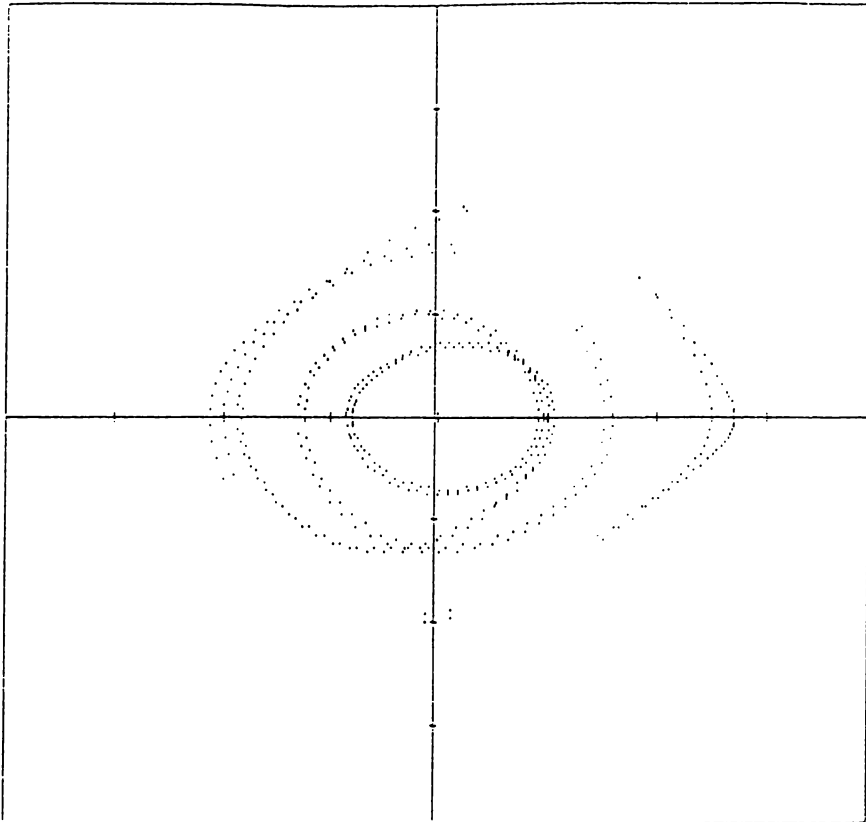


Fig. 5.12 - The phase portrait for $\omega = 1$, $\beta = 0.2$, $A = 0.3$ and $\Gamma_0 = 0.01$. The periodic four cycle is established very soon in the presence of noise while without noise, the periodicity is evident only asymptotically.

REFERENCES

- [1] J Guckenheimer and P J Holmes .. 'Nonlinear oscillations, dynamical systems and bifurcations of vector fields' (Springer, Berlin, 1983).
- [2] N Minorsky .. 'Nonlinear oscillations' - (van Nostrand Co Inc. New York 1969) 390.
- [3] M V Berry .. in Topics in Nonlinear Dynamics ed. S Jorna, Am. Inst. Phys. Conf. Proc. 46 (1978) 16.
- [4] A J Lichtenberg and M A Lieberman .. 'Regular and Stochastic motion' (Springer, New York, 1983).
- [5] J Ford .. in Fundamental Problems in Statistical Mechanics' Vol. 3. ed. E G D Cohen (North Holland, Amsterdam 1975) 215.
- [6] C.S Gardner, J M Greene, M D Kruskal and R M Miura .. Phys. Rev. Lett. 19 (1974) 1095.
- [7] M A Olshanetzky and A N Perelomov .. Lett. Nuovo. Cimento 16 (1976) 33.
- [8] R H G Helleman .. in Fundamental Problems in Statistical Mechanics, Vol. 5, ed. E G D Cohen (North Holland, Amsterdam 1980) 165.
- [9] M Henon and C Heiles .. Astron. J. 69 (1964) 73.
- [10] C Horton, L Reichl and V Szebehely eds. .. 'Longtime Predictions in Dynamics' (John Wiley Pub. New York, 1982).

- [11] C L Siegel
and J K Moser .. Lectures on Celestial
Mechanics (Springer
Heidelberg 1971).
- [12] G R Smith
and A N Kaufman .. Phys. Rev. Lett. 34
(1975) 1613.
- [13] E Fermi .. Phys. Rev. 75 (1949)
1169.
- [14] J Moser .. Nachr. Akad. Wiss.
Gottingen Math. Phys.
K1 (1962) 1.
- [15] V I Arnold .. Sov. Math. Dok. 2 (1961)
501, 3 (1962) 136;
Russian Math. Surveys.
18 (1964) 85.
- [16] J Greene .. J. Math. Phys. 20 (1979)
1183.
- [17] V I Arnold .. Sov. Math. Dok. 5 (1964)
581.
- [18] M A Lieberman
and A J Lichtenberg .. Phys. Rev. A5 (1972)
1852.
- [19] H Froehling,
J D Crutchfield,
D Farmer,
N H Packard and
R Shaw .. Physica D3 (1981) 605.
- [20] M J Feigenbaum .. Los Alamos Science 1
(1980) 4.
- [21] R May .. Nature 261 (1976) 459.
- [22] E N Lorenz .. J. Atmos. Sci. 20 (1963)
130.

- [23] H Haken .. Phys. Lett. A53 (1975)
77.
- [24] O E Rossler .. Phys. Lett. A57 (1976)
397.
- [25] M Henon .. Comm. Math. Phys. 50
(1976) 69.
- [26] M J Feigenbaum .. J. Stat. Phys. 19 (1978)
25.
- [27] Y Pomean .. Comm. Math. Phys. 74
and P Manneville (1980) 189.
- [28] H G Schuster .. 'Deterministic Chaos'
(Physik Verlag, Weinheim)
1984.
- [29] J P Eckmann .. Rev. Mod. Phys. 53 (1981)
643.
- [30] W H Steeb .. 'Chaos and Quantum Chaos'
and J A Louw (World Scientific,
Singapore 1986) 42.
- [31] J D Farmer .. Physica D7 (1983) 153.
E Ott and J A Yorke
- [32] T C Halsey,
M. H Jensen,
L. P Kadanoff, .. Phys. Rev. A33 (1986)
I Procaccia and 1141.
B I Shraiman
- [33] H G E Hentschel .. Physica D8 (1983) 435.
and I Procaccia
- [34] A Arneodo, .. Phys. Lett. A124 (1987)
G Grasseau and 426.
E J Kostelich

- [35] M R Guevara, .. Science 214 (1981)
L Glass and 1350.
A Shrier
- [36] H Hayashi, .. Phys. Lett A98
S Ish'zuka, (1983) 474.
K Hirakava
- [37] R Shaw .. Zeit. fur Nat. A36
(1981) 80.
- [38] N Chomsky .. 'Reflections on
language (Pantheon
Books New York 1975).
- [39] B A Huberman .. Phys. Rev. Lett. 52
and T Hogg (1984) 1048.
- [40] J J Hopfield .. Proc. Natt. Acad.
Sci. 79 (1982) 2554;
81 (1984) 3088.
- [41] K Tomita .. Prog. Theor. Phys.
79 (1984) 1.
- [42] K Tomita .. Phys. Lett. A111,
(1985) 152.
- [43] M J Feigenbaum .. J. Stat. Phys. 21
(1979) 669.
- [44] A Libchaber .. J. Phys. (Paris)
and J Maurer Colloq. 41 C₃ (1980)
51.
- [45] M J Feigenbaum, .. Physica D5(1982)
L P Kadanoff and 370.
S J Shenker
- [46] G Benettin, .. Lett. Nuovo Cimento
C Cercignani, 28 (1980) 1.
L Galgani and
A Giorgitti

- [47] P Cvitanovic and J Myrheim .. Phys. Lett A94 (1983) 329.
- [48] B Hu and J Rudnick .. Phys. Rev. A34 (1986) 2453.
- [49] M J Feigenbaum .. Physica D7 (1983) 16.
- [50] S J Chang and P R Fendley .. Phys. Rev. A33 (1986) 4092.
- [51] B Hu and I I Satija .. Phys. Lett A98 (1983) 143.
- [52] B Hu and J M Mao .. Phys. Rev. A25 (1982) 3259.
- [53] R H G Helleman .. in Proc. of the 93rd E. Fermi Inst. School of Physics on Nonlinear Acoustics ed. D. Sette (North Holland Amsterdam 1984).
- [54] R Delbourgo, W Hart and B G Kenney .. Phys. Rev. A31 (1985) 514.
- [55] J P van der Weele, H W Capel and K Kluiving .. Phys. Lett. A119 (1986) 15.
- [56] V Singh .. Pramana (J. Phys) 24 (1985) 31.
- [57] G A Baker Jr .. 'Essentials of Pade Approximants (Academic Press, New 1975).
- [58] R Delbourgo and B G Kenny .. Phys. Rev. A33 (1986) 3292.

- [59] S Fraser and R Kapral .. Phys. Rev. A25 (1982) 3223.
- [60] S Fraser, E Celarier and R Kapral .. J. Stat. Phys. 33 (1983) 341.
- [61] R V Mendes .. Phys. Lett. A84 (1981) 1.
- [62] I Procaccia, S Thomae and C Tresser .. Phys. Rev. A35 (1987) 1884.
- [63] Y Kuramoto and S Koga .. Phys. Lett. A92 (1982) 1.
- [64] H Kawai and S H H Tye .. Phys. Rev. A30 (1984) 2005.
- [65] P R Hauser, E M F Curado and C Tsallis .. Phys. Rev. A30 (1984) 2074.
- [66] B Hu and J M Mao .. J. Phys. A20 (1987) 1809.
- [67] T C Halsey and M H Jensen .. Physica D23 (1983) 112.
- [68] S J Chang and J Mc Cown .. Phys. Rev. A31 (1985) 3791.
- [69] J K Bhattacharjee .. Phys. Lett. A117 (1986) 339.
- [70] V K Melnikov .. Trans. Moscow. Math. Soc. 12 (1963) 1.
- [71] S Smale .. Bull. Amer. Math. Soc. 73 (1967) 747.

- [72] P J Holmes and J E Marsden .. J. Math. Phys. 23 (1982) 669.
- [73] J E Marsden .. in 'Chaos in Nonlinear dynamical systems' ed. J. Chandra (Siam, Philadelphia 1984) 19.
- [74] B Greenspan and P J Holmes .. in 'Nonlinear Dynamics and Turbulence' eds. Barenblatt, G Iooss and D D Joseph (Pitman, London 1981)
- [75] M Bartuccelli, P L Christiansen, N F Pedersen and M P Soerensen .. Phys. Rev. B33 (1986) 4686.
- [76] F H Ling and G W Bao .. Phys. Lett. A122 (1987) 413.
- [77] F H Ling .. Phys. Lett. A119 (1987) 447.
- [78] S Wiggins .. Phys. Lett. A124 (1987) 138.
- [79] D D'Humieres, M R Beasley, B A Huberman, and A Libchaber .. Phys. Rev. A26 (1982) 3483.
- [80] R L Kautz and R Monaco .. J. Appl. Phys. 57 (1985) 875.
- [81] E V Krishnamoorthy and S K Sen .. 'Computer-based Numerical Algorithms' (Affiliated East-West Press Pvt. Ltd. New Delhi 1976) 333.

- [82] E O Brigham .. 'The Fast Fousier Transform' (Prentice Hall Inc. Englewood Cliffs 1974)
- [83] P W Milonni,
M L Shih
and J R Ackerhalt .. 'Chaos in laser-matter interactions' - (World Scientific Pub. Co. Pte. Ltd. Singapore 1987)
- [84] A Wolf,
J B Swift,
H L Swinney and
J A Vastano .. Physica D16 (1985) 285.
- [85] R H Abraham
and H B Stewart .. Physica, D21 (1986) 394.
- [86] J P Crutchfield,
J D Farmer and
B A Huberman .. Phys. Rep. 92 (1982) 45.
- [87] G Mayerkress
and H Haken .. J. Stat. Phys. 26 (1981) 149.
- [88] J P Crutchfield
and B A Huberman .. Phys. Lett. A77 (1980) 407.
- [89] K Hatsumoto
and I Tsuda .. J. Stat. Phys. 31 (1983) 87; 34 (1984) 111.
- [90] A B Rechester
and R B White .. Phys. Rev. A27 (1983) 1203.